AD-A055 442 TRANSPORTATION SYSTEMS CENTER CAMBRIDGE MASS F/G 17/2.1
MARITIME COMMUNICATION EXPERIMENTS AND SEARCH-AND-RESCUE EVALUA--ETC(U)
MAY 78 P D ENGELS, C B DUNCOMBE, A E FOLEY
UNCLASSIFIED TSC-USCG-78-9-VOL-2 USCG-D-69-77-2 NL

2 OF 3
AD A055 442

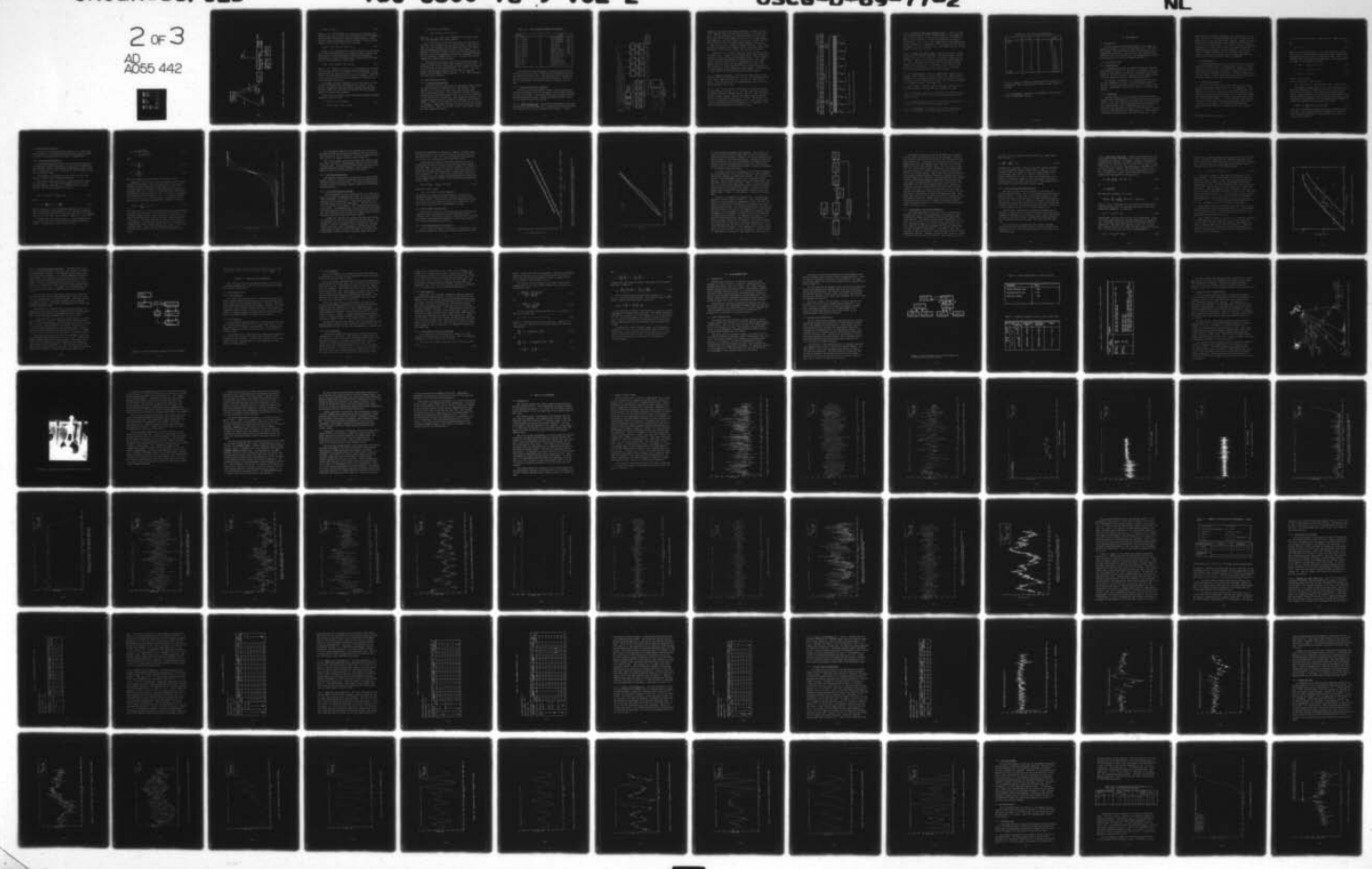

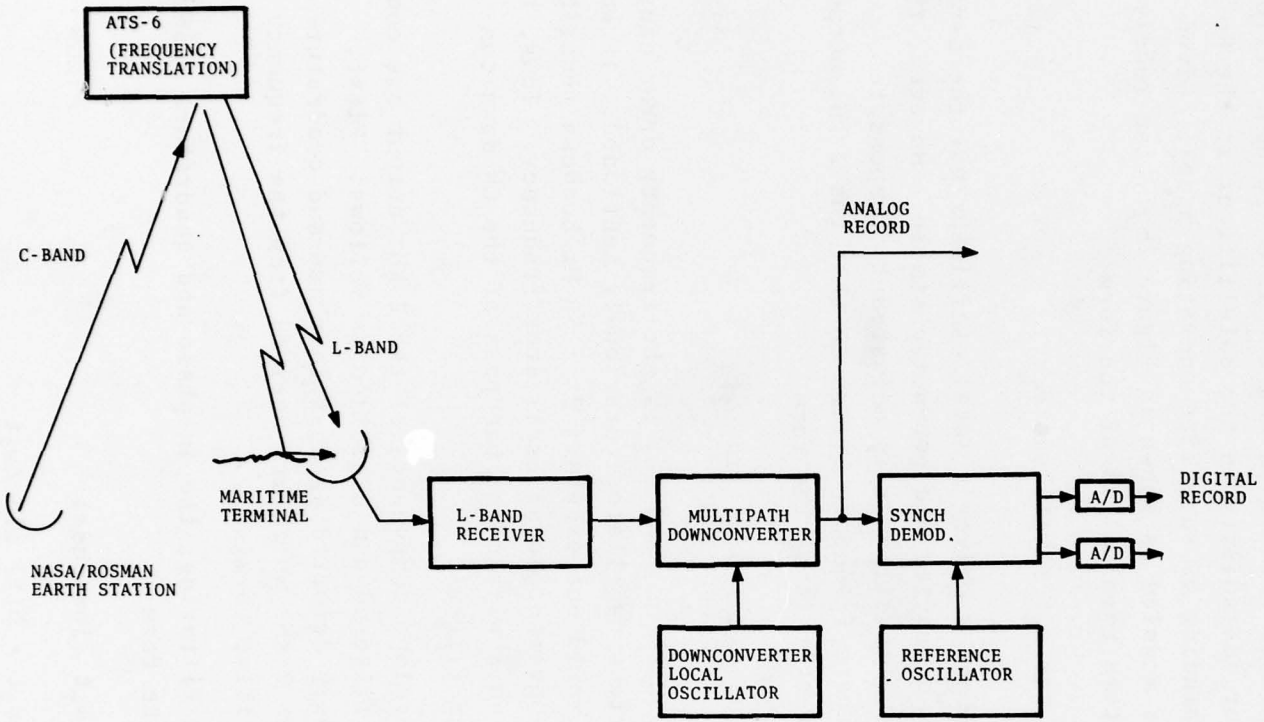

FIGURE 2-38. PICTORIAL DIAGRAM OF THE CONTINUOUS WAVE MULTIPATH MEASUREMENT SYSTEM

$$S_L(t) = \sin \omega_L t \tag{2-1}$$

where $\omega_L = 2\pi \cdot 1550.075$ MHz + $\Delta\omega_L$, and $\Delta\omega_L$ is a frequency error caused by oscillator instability in the satellite or at the Rosman Earth Terminal (depending on satellite operating mode). Given that the channel is modeled as shown in Figure 2-37, the received signal at the maritime terminal is of the form

$$S_{LR}(t) = a(t) \cos \omega_L t + b(t) \sin \omega_L t \tag{2-2}$$

Neither the L-band receiver's local oscillator nor the oscillators in the CW down-converter are perfectly stable. However, the down-converter's local oscillator is adjusted to compensate approximately for these frequency errors so that the 2 kHz output of the CW down-converter is of the form

$$S_2(t) = a(t) \cos \omega_2 t + b(t) \sin \omega_2 t \tag{2-3}$$

where $\omega_2 = 2\pi \cdot 200$ Hz + $\Delta\omega_2$ and $\Delta\omega_2$ is the frequency error caused by all of the imperfect oscillators previously mentioned. It was estimated that $\Delta\omega_2$ would not exceed $\pm 2\pi \cdot 50$ Hz between recalibrations of the down-converter local oscillator frequency. Thus, the 2 kHz output was always within the bandpass of the CW down-converter and digitizer filters.

The complex envelope components of the 2 kHz output are converted to baseband filtered and digitized as follows: First, $S_2(t)$ is synchronously detected against in-phase and quadrature reference signals at 2 kHz which are derived from the frequency standard in the maritime terminal.

After low pass filtering, the in-phase and quadrature baseband components are of the form

$$\begin{aligned} I &= S_2(t) \cos \omega_r t \text{ (low-pass)} \\ &= a(t) \cos \Delta\omega_2 t + b(t) \sin \Delta\omega_2 t \end{aligned} \tag{2-4}$$

$$Q = S_2(t) \sin \omega_r t \text{ (low-pass)}$$
$$= - a(t) \sin \Delta\omega_2 t + b(t) \cos \Delta\omega_2 t \qquad (2\text{-}5)$$

where $\Delta\omega_2 = \omega_2 - \omega_r$. The I and Q components are sampled, digitized, and recorded at 200 complex samples.

It is interesting to note that the effects of oscillator instability, $\Delta\omega_2$, are mixed with the channel effects, a(t) and b(t). Thus, the I and Q samples (and the analog recorded 2 kHz signal) contain information pertaining to both of these effects. It is desirable to include oscillator effects with the pure channel data because, in fact, the transmitter and receiver component characteristics (filtering, component drift, etc.) constitute part of the communication channel characteristics.

The recorded I and Q data contain the information necessary to extract the narrow-band channel model parameters defined above. In particular, the relative multipath power can be derived by analysis of the envelope of the baseband process, $[I^2 + Q^2]^{1/2}$. The bandwidth of the multipath process can be derived by a spectral analysis of the complex baseband process, I + jQ. These techniques are discussed in Section 3.

2.3 DATA ACQUISITION SYSTEM

2.3.1 Analog Recording System

The analog recording system for the equipment terminal onboard the cutter utilized a Sangamo Sabre II tape recorder. This machine is a 14-track (plus edge track) tape recorder which uses 1-inch magnetic tape. It has a full set of input electronics for both direct and FM recording as well as a full set of electronics for FM and direct reproducing. Thus, during an experiment the equipment operator was able to monitor continuously all pertinent signals to insure signal continuity and to be aware of any electronics problems. Spare input and output electronic cards were stocked in the shelter. Table 2-13 contains a list of the signals recorded and their channel allocation.

TABLE 2-13. TAPE RECORDER PATCHING CONFIGURATION

CHANNEL	SIGNAL
CH 1 (direct)	Bell ANBFM/DPSK Voice
CH 2 (direct)	Bell ANBFM/DPSK Data
CH 3 (direct)	Bell ANBFM/DPSK Clock
CH 4 (direct)	Bell Hybrid Voice
CH 5 (direct)	Bell Hybrid Data
CH 6 (direct)	Bell Hybrid Clock
CH 7 (direct)	Magnavox Hybrid Voice
CH 8 (direct)	Magnavox Hybrid Data
CH 9 (direct)	Magnavox Hybrid Clock
CH 10 (direct)	Time Code IRIG B
CH 11 (FM)	Ranging Data
CH 12 (direct)	CW Multipath Data
CH 13 (FM)	Bell Hybrid C/N_o
CH 14 (FM)	Magnavox Hybrid C/N_o

All signals to be recorded went to a patch panel as did each of the tape recorder inputs. Signals were then patched easily to the given tape recorder input. The patch panel also provided for easy reconfiguration of the analog recording format. Failure of one recording channel thus did not result in extensive loss of data.

2.3.2 Digital Data Acquisition Module

The digital acquisition module (Figure 2-39) was designed to operate in conjunction with the equipment in the shipboard terminal and steerable antenna. The module provides the necessary interface between the measured analog, synchro, and digital signals and an 9-track Kennedy digital tape recorder.

2.3.2.1 Module Description - The module time multiplexes, digitizes, and encodes 15 parallel inputs into a sequences of 8-bit bytes which are recorded directly onto the Kennedy tape recorder. A block

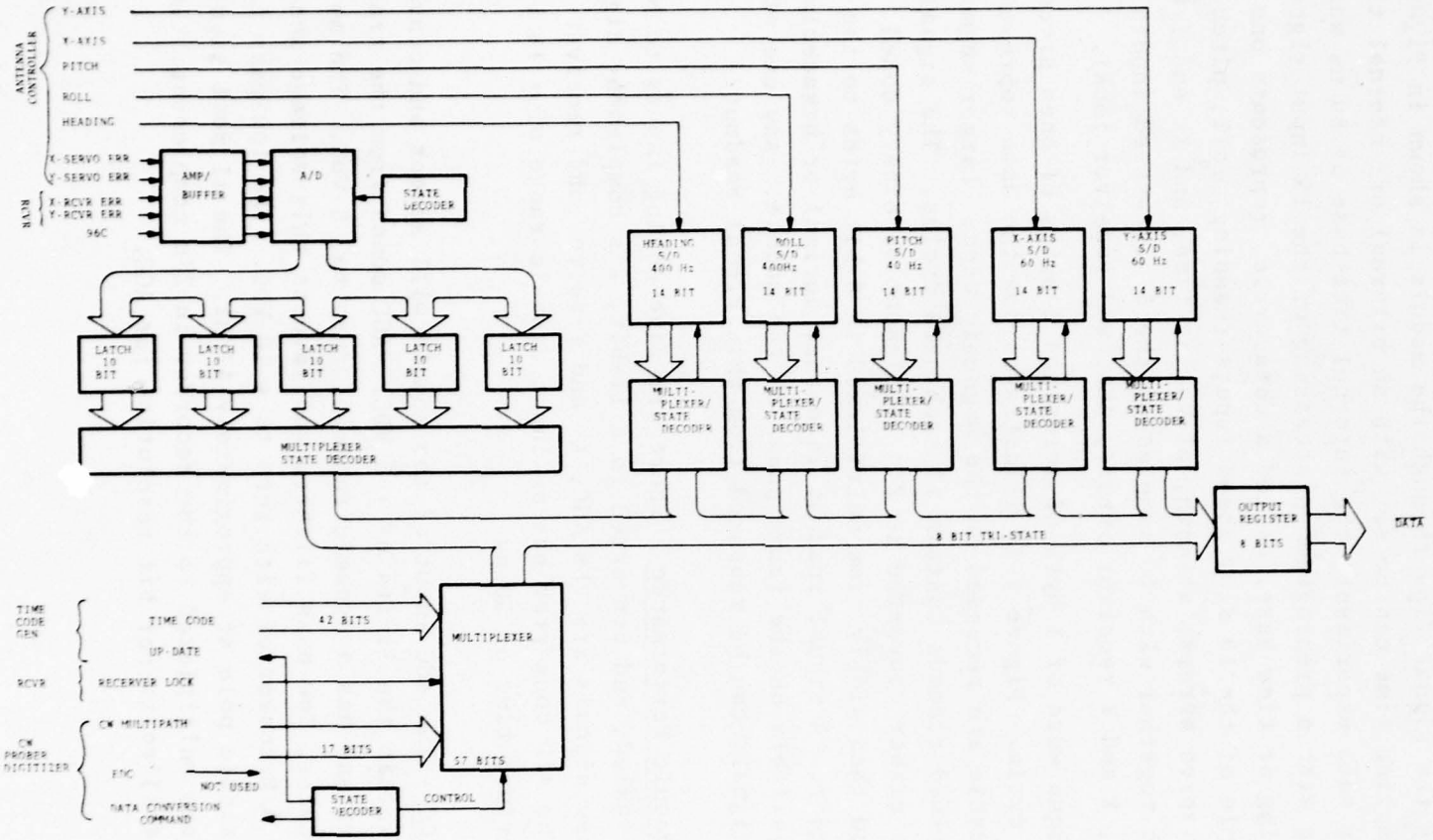

FIGURE 2-39. BLOCK DIAGRAM OF THE DATA ACQUISITION MODULE - 1

diagram of the signal flow through the module is shown in Figure 2-40. Sampling time can be set with an external or internal time base. For this experiment, the internal time base of 50 ns was used along with a preprogrammed accessing of the 15 input signals. The sampling or time base, called a data cycle, represents one complete sample of the 10 slow speed inputs (heading, roll, pitch, X- and Y- servo errors, azimuth, elevating time, and X- and Y-axis positions) together with 10 samples of the 5 high-speed inputs (CW multipath, X and Y receiver errors, AGC, and receiver lock).

A unique word of 1 byte of zeros and 5 bytes of ones preceed each data cycle. Figure 2-40 illustrates how the data representing one data cycle are recorded on the magnetic tape. Larger segments of data termed records contain 11 such data cycles. The signal inputs are either converted to 2's complement or binary coded decimal and then simply time multiplexed in 8-bit bytes to the tape recorder. A visual readout in either decimal or hexadecimal is also available on the front panel of the module. Any one of the 15 input signals can be measured from this visual readout.

2.3.2.2 Module Performance - There are five analog inputs to be buffered, scaled, and converted to a 12-bit, 2's complement digital word. These signals are the AGC, X- and Y-servo, and receiver errors. The A/D converter has an input dynamic range of ± 10 VDC and an aperture time of 50 ns

2.3.2.3 AGC - The AGC input of the module will accept and convert a voltage within the limits of ± 5 VDC. AGC comes from the tracking receiver and has a dynamic range of zero to -5 VDC. The module buffers, scales, low-pass filters, and inverts this voltage and drives the A/D converter with zero to + 10 VDC. The low-pass filter has a single pole at approximately 47 Hz. The 11 most significant bits are multiplexed to the recorder in 2's complement. This yields 0.04883 volts per bit resolution for AGC.

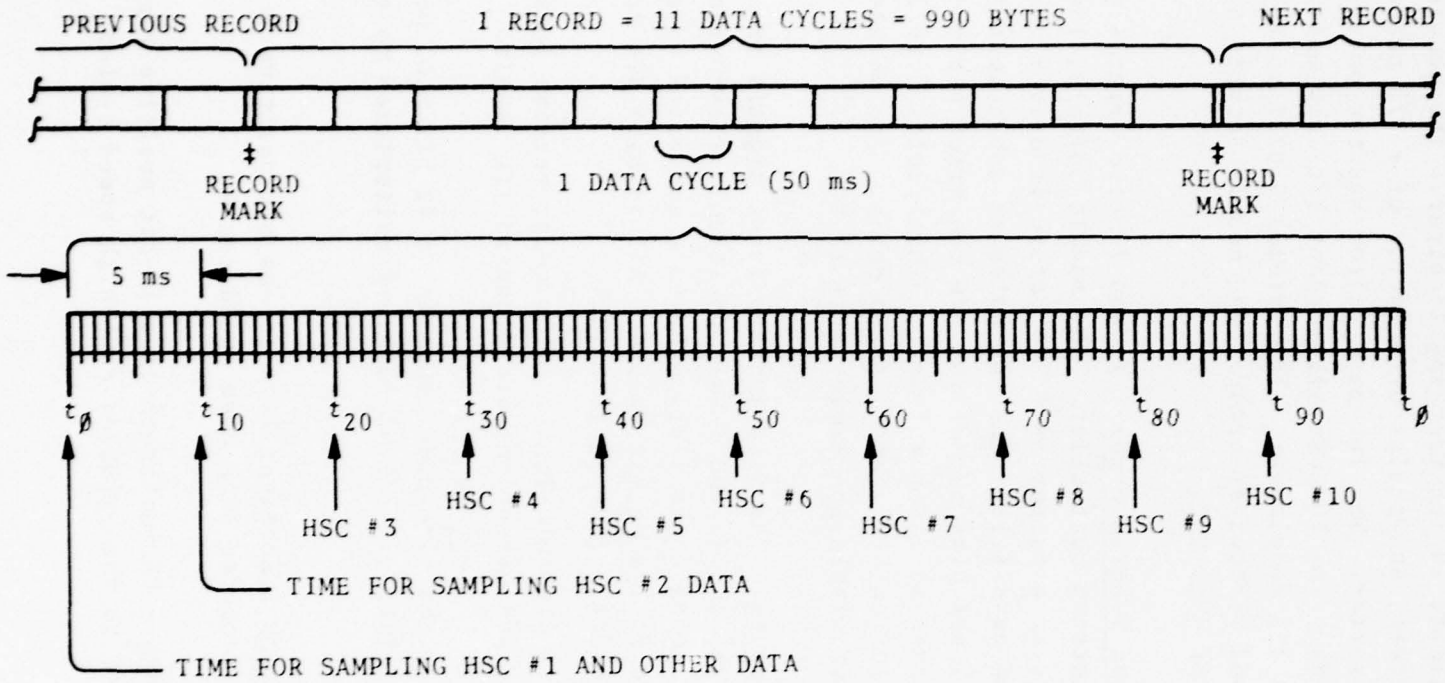

FIGURE 2-40. GENERAL TIMING DIAGRAM OF THE DATA ACQUISITION MODULE

2.3.2.4 X-Receiver Error and Y-Receiver Error - X- and Y-receiver error signals originate in the tracking receiver. The module buffers, low-pass filters, and scales by a factor of + 2/3 before it drives the A/D converter. The low pass filter has two poles at approximately 2.5 Hz. The 10 most significant bits are multiplexed to the recorder in 2's complement. This yields 0.0293 volts per bit resolution of X- and Y-receiver error. The module accepts a voltage within the limits of ± 13 VDC.

2.3.2.5 X-Servo and Y-Servo Error - X- and Y-Servo error signals originate in the antenna controller. The module buffers, low-pass filters, and scales by a factor of + 2/3 before it drives the A/D converter. The low-pass filter has two poles at approximately 10 Hz. All 12 significant bits out of the A/D converter are multiplexed to the recorder in 2's complement. This yields 0.007324 volts per bit resolution of X- and Y-servo error. The module accepts a voltage of within the limits of ± 13 VDC.

2.3.2.6 Synchro Inputs - The five synchro input signals are the heading, roll, pitch, and X- and Y-axis position. These signals originate in the antenna controller. They are converted to a digital format with the following bit values. All 14 bits are recorded on the Kennedy recorder. (See Table 2-14.)

The remaining 5 digital signals (time code, receive lock, CW mulitpath, azimuth, and elevation) are standard TTL levels.

2.3.2.7 Time Code - The time code consists of 42 bit BCD, positive logic with 1 ms resolution. All 42 bits are multiplexed to the Kennedy recorder.

2.3.2.8 Receiver Lock - Receiver Lock is one bit positive logic, is multiplexed to the recorder each high speed cycle.

2.3.2.9 CW Multipath - CW multipath is a 16-bit positive logic word, is multiplexed to the recorder each high speed cycle.

TABLE 2-14. BIT VALUES FOR SYNCHRO DATA

	BIT	VALUE
MSB	1	180°
	2	90°
	3	45°
	4	22.5°
	5	11.25°
	6	5.625°
	7	2.813°
	8	1.406°
	9	0.7031
	10	0.3516°
	11	0.1758°
	12	0.08799°
	13	0.04395°
LSB	14	0.02197°

2.3.2.10 Azimuth - Azimuth is multiplexed to the recorder as a 10-bit BCD word. This is sufficient for 0.359° with one degree resolution.

2.3.2.11 Elevation - Elevation is multiplexed to the recorder as a 9-bit BCD word with sign bit.

3. DATA ANALYSIS

3.1 INTRODUCTION

The data analysis procedures performed in this report are designed to support the basic technical objectives of the ATS-6 test program. These objectives include the evaluation of the experimental antenna in its autotrack and slave modes; the performance of the voice, digital data, and ranging modems, and the characterization of the marine propagation channel.

3.2 DISCUSSION OF TESTS

3.2.1 Antenna Tests

The antenna was designed such that the boresight pointing error would not exceed 12°. This angle corresponds to the 1-dB contour of the antenna's sum pattern. The antenna data analysis therefore consists in part of computing the boresight pointing error and comparing it against the design specification.

The antenna's performance in the autotrack and slave modes are also compared on the basis of a defined figure of merit. Section 3.2 defines the figure of merit, which is simply a comparison of performance in each mode to that of a fixed position antenna.

3.2.2 Modem Tests

The data analysis is also concerned with the evaluation of the operational performance of the voice, digital data, and ranging modems. Tests were conducted to determine the voice intelligibility, bit error rates, and ranging precision at given carrier-to-noise power density ratios established during the testing. Typically, the data analysis consists of the following: The word lists recorded from the voice modem outputs on 1-inch instrumentation tape are transferred to 1/4-inch tape and sent to CBS

Laboratories* in Stamford, Connecticut, for intelligibility evaluation. The 1200 b/s data were decoded from the 1-in tape and the number of bit errors and block errors computed. Ranging precision was measured by computing the standard deviation of the time-of-arrival of the ranging signal. As a result of various experimental uncertainties, it was rather difficult to predict how well the modems would perform under different conditions. To overcome this problem a channel simulator was used to generate preliminary curves of bit error rates versus carrier-to-noise power density ratios, with relative multipath level as a parameter.

3.2.3 Multipath Tests

The CW multipath data were analyzed to determine the received carrier-to-multipath ratios, multipath Doppler spread, and other parameters. The C/M ratio was estimated by a graphical technique which consisted of fitting a theoretical cumulative Rician distribution to the histogram of the data. A second techniques which used the method of moments and estimated the ratio from the second and fourth moments of the sampled data was also used.

3.2.4 Antenna Pointing Error

One of the objectives of the ATS-6 testing was to evaluate the steerable antenna under various sea state conditions. This antenna is described in AMI (1974, 75). To accomplish this, the antenna's X- and Y-servo positions and the ship's heading, roll, and pitch were digitized and recorded on a 14-track tape recorder. These data were subsequently stripped off the tapes and processed by a PDP-10 digital computer. A set of equations relating the recorded data to the actual antenna elevation and azimuth to the satellite was developed. These equations established the measured antenna azimuth and elevation and have the following form:

*Subsequently EPSCO Laboratories.

$$\alpha = \sin^{-1}(\cos R \cos\theta \cos\phi \cos P - \cos R \sin P \sin\theta - \sin R \cos\theta \sin\phi) \quad (3\text{-}1)$$

and

$$A_Z = H + \beta' \quad (3\text{-}2)$$

where H is the ship's heading, β' the satellite bearing from the ship, α and A_Z the measured elevation and azimuth, respectively. The quantities P, R, ϕ, and θ are the ship's pitch, roll, X-servo position, and Y-servo position, respectively. The measured bearing angle β' was computed as follows:

$$\beta' = 360 - \beta \quad \text{if } X_o \geq 0 \quad y_o > 0 \quad (3\text{-}3)$$

$$\beta' = -\beta \quad \text{if } X_o \geq 0 \quad y_o \leq 0 \quad (3\text{-}4)$$

$$\beta' = 180 - \beta \quad \text{if } X_o < 0 \quad (3\text{-}5)$$

where $\beta = \tan^{-1}(y_o/X_o)$

and $X_o = \cos P \sin\theta + \sin P \cos\phi \cos\theta$

$y_o = \cos R \cos\theta \sin\phi + \sin R \cos P \cos\theta \cos\phi - \sin P \sin R \sin\theta$

The computer program subtracts the correct azimuth and elevation from the measured azimuth and elevation to the satellite. The differences represent the azimuth and elevation pointing errors. An expression for the boresight error was computed, since with a symmetric antenna pattern the received signal level is proportional to this parameter. This pointing error was computed as follows and termed the total pointing error TPERR.

$$TPERR = \cos^{-1}\left[\left(\cos(\Delta\alpha)\ \cos(\Delta A \cos\alpha)\right)\right] \quad (3\text{-}6)$$

where ΔA is the measured azimuth error and $\Delta\alpha$ the measured elevation error. These expressions were programmed on a PDP-10 computer so that the variables could be plotted versus time and statistically analyzed.

3.3 MULTIPATH DATA ANALYSIS

The object of the multipath data analysis is to derive parameters relevant to the channel model and to verify that this model is valid for anticipated maritime satellite communications.

3.3.1 Narrow-Band Data Analysis

The narrow-band multipath data are in the form of samples of the in-phase and quadrature outputs I and Q of the CW down-converter subsystem. These can be analyzed to determine the direct path power-to-multipath power ratio, denoted C/M, and the Doppler spread of the multipath fading.

Two techniques were employed to derive the C/M ratio: the method-of-moments and the histogram techniques.

The received signal consists of a steady direct-path component with power, C, and a multipath component of power, M. The received composite amplitude, A, is characterized as a Rician variate. The Rician distribution is given by

$$p(v) = v \exp\left[-\frac{v^2 + a^2}{2}\right] I_o(av) \qquad (3\text{-}7)$$

where

$$v = \sqrt{2}\,\alpha\sqrt{\frac{C}{M}} \text{ and } a = \sqrt{2}\sqrt{\frac{C}{M}} \qquad (3\text{-}8)$$

and α is the ratio of the instantaneous amplitude, A, in the presence of multipath to the amplitude of the direct path component, $\sqrt{2C}$. The received composite instantaneous amplitude, A, is directly related to the recorded I and Q samples. Namely, $A_i = [I_i^2 + Q_i^2]^{1/2}$.

Assuming that the received signal is a Rician fading process, then the C/M ratio can be derived directly from the amplitude samples. In particular, from Liv et al. (1973):

$$\frac{C}{M} = \frac{\left[2-\overline{x^4}/\left(\overline{x^2}\right)^2\right]^{1/2}}{1-\left[2-\overline{x^4}/\left(\overline{x^2}\right)^2\right]^{1/2}} \tag{3-9}$$

where

$$\overline{x^2} = \frac{1}{n}\sum_{i=1}^{n} A_i^2 \tag{3-10}$$

$$\overline{x^4} = \frac{1}{n}\sum_{i=1}^{n} A_i^4 \tag{3-11}$$

and A_i are samples of the envelope of the fading carrier.

Cumulative distributions of the instantaneous received amplitude were also plotted. These histograms can be used to derive estimates of C/M by comparing the experimental results with similarly plotted histograms of a pure theoretical Rician process at various C/M ratios. Figure 3-1 illustrates these theoretical histograms for different values of C/M. The curves were generated by integrating the Rician density $\rho(v)$; i.e., relative frequency $= Q(x) = \int_0^x r \exp\left(-(v^2+a^2)/2\right) I_0(av)dv$. The modified Bessel function $I_0(av)$ was approximated with the asymptotic expression,

$$I_0(av) \simeq \frac{e^{av}}{\sqrt{2\pi av}} \quad \text{for } av > 10 \tag{3-12}$$

For values of $av \leq 10$ its series expression was used and terminated when the ratio of the nth to (n-1)th term was less than 10^{-2}. The program to compute and plot these curves also shifted each curve along the horizontal axis so that 0 dB always coincided with the 50 percentile. This made comparison of their slopes, the histogram technique for determining C/M, much easier. The comparison is made based on the histogram slope in the vicinity of the median amplitude point. In this way, the experimental data can be associated with theoretical Rician processes with specific C/M ratios.

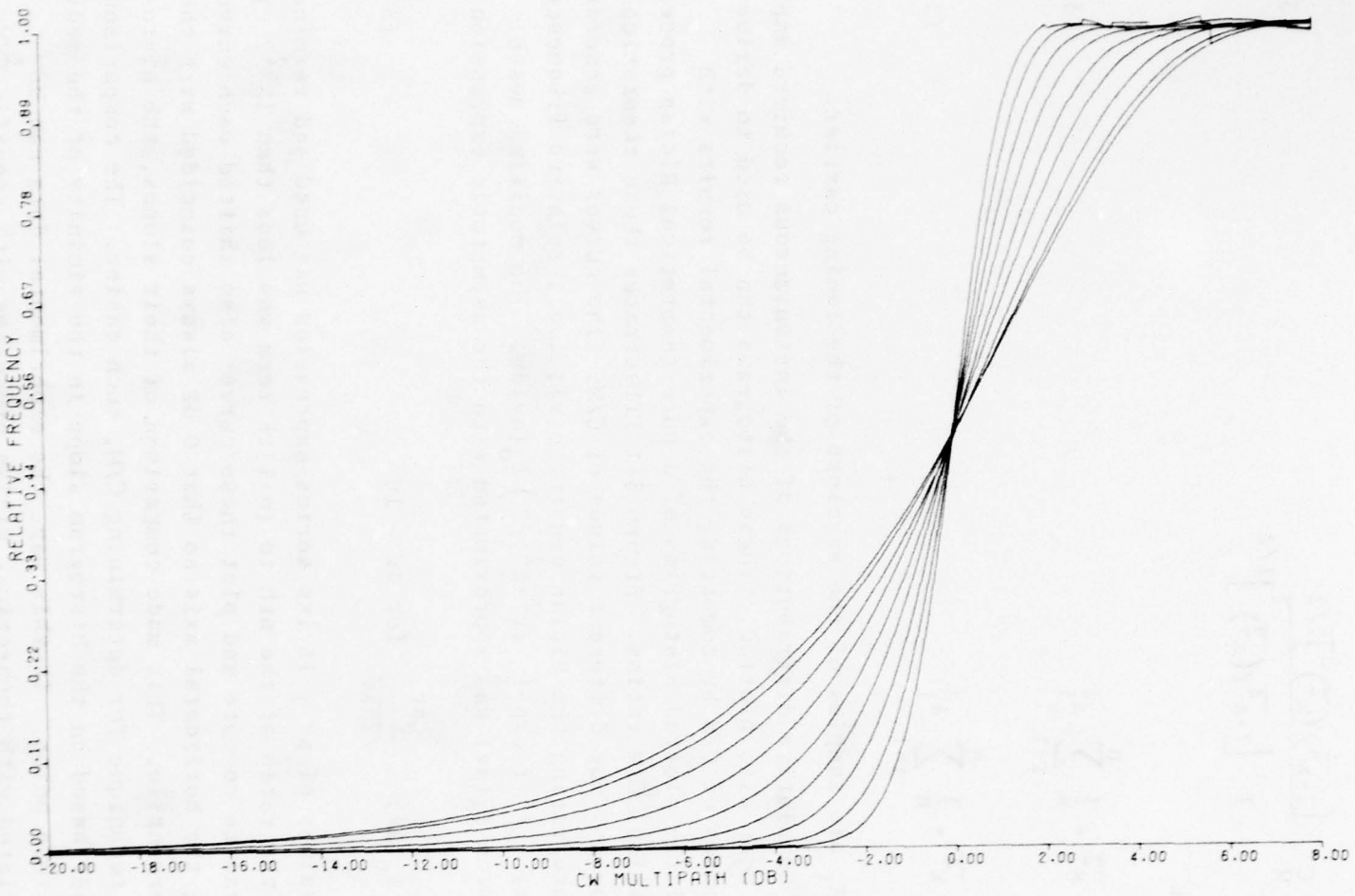

FIGURE 3-1. THEORETICAL HISTOGRAMS FOR VARIOUS C/M RATIOS

The experimental cumulative distributions are also used to determine the fade depths which correspond to the 90 percentile, the 50 percentile, the 10 percentile, and the 2 percentile of the distribution for various satellite-vessel geometries.

The I and Q samples are analyzed using a fast Fourier transform (FFT) to derive the baseband power spectrum of the received CW probing tone. The observed spectrum includes the direct path component and the multipath component, both of which may be Doppler shifted by the effect of ship's roll motion.

3.3.2 Wide-Band Data Analysis

The wide-band probing data was processed by a "quick look" computer analysis, which was implemented to provide the desired delay power spectra time histories. The analysis procedure also provided correlation bandwidth, Doppler spread, and delay Doppler scatter functions.

3.3.3 Voice Intelligibility Testing

The determination of voice intelligibility, as a function of C/N_o, via a satellite communications system, was one of the goals of the experiment. Three modems were used, two of which had the capability for the reception of a signal which contained both voice and digital data on the same carrier. (See section 2.2.4 for a description of the modems.) Thus, voice data were received in two modes: a simultaneous mode in which both voice and digital data were received at the same time and recorded for future analysis, and a voice-only mode in which voice signals were received by themselves and also recorded for future analysis

A single test consisted of recording the C/N_o ratio during the reception of a list of 400 phonetically balanced words. A DC voltage whose value was proportional to C/N_o was recorded simultaneously. Thus, by evaluation of the recorded data intelligibility versus C/N_o could be determined. The determination of intelligibility, which is simply the number of correctly interpreted words received, divided by the total number of words

received, and expressed as a percent, is done by a listener panel. This panel consists of a group of 10 persons trained to listen to the PB word lists. Thus, for any run an average intelligibility versus C/N_o can be determined (Milner and Golab, 1975).

Calibrations were made for the modems in which the C/N_o instrumentation voltage was plotted versus the C/N_o meter reading from each modem. Also, the meter C/N_o was plotted as a function of the actual C/N_o (see Figures 3-2 and 3-3). This was necessary to insure that discrepancies between meter readings and actual C/N_o's were accounted for. The actual C/N_o was calculated by measuring the carrier power in the channel and then measuring the noise power in the channel through a bandpass filter whose noise bandwidth was 40 kHz. Thus:

$$C/N_o = (P_C)_{dB} - (P_N)_{dB} + 46 \text{ dB-Hz} \qquad (3\text{-}13)$$

where P_C = carrier power

P_N = noise power in 40 kHz bandwidth.

The PB word lists along with C/N_o voltages as received at the demodulator outputs were recorded in real-time on 14-track tape for later analysis. Selected tapes were then reduced by re-recording onto 1/4 in high output, low noise tape. These tapes were sent to CBS Laboratories for intelligibility scoring.

3.4 DIGITAL MODEM DATA REDUCTION

This section discusses the data extraction and reduction procedures for digital modem data collected during the maritime-satellite tests. The form of the data is discussed first, followed by methods for determining probability of error versus signal-to-noise ratio, and block error statistics.

3.4.1 Data Formatting and Data Recovery

Digital modem performance is measured by transmitting a known PN sequence through the communication channel and observing errors

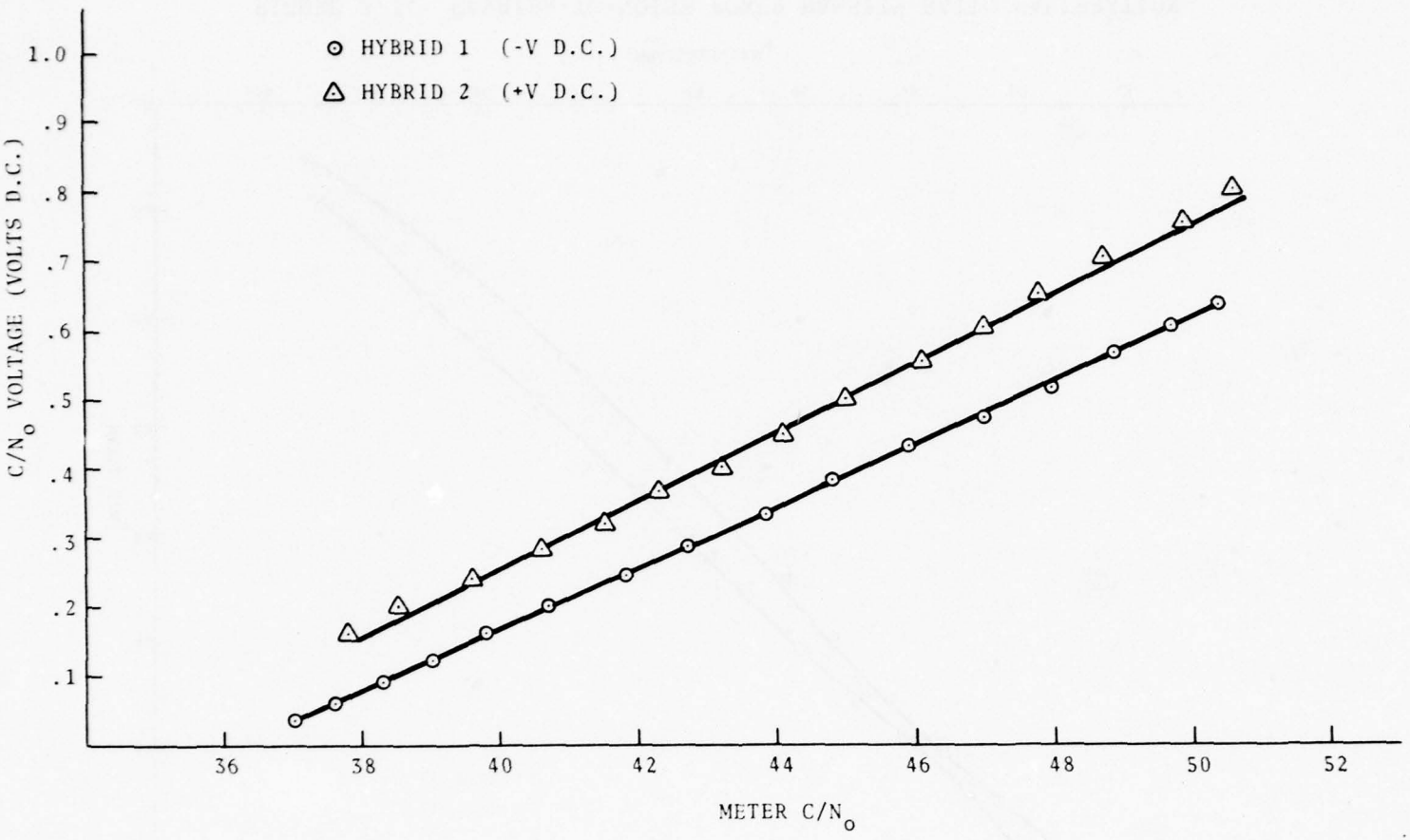

FIGURE 3-2. CARRIER-TO-NOISE POWER DENSITY RATIO CALIBRATION FOR THE VOICE INTELLIGIBILITY TESTS — INSTRUMENTATION VOLTAGE VS. METER READING

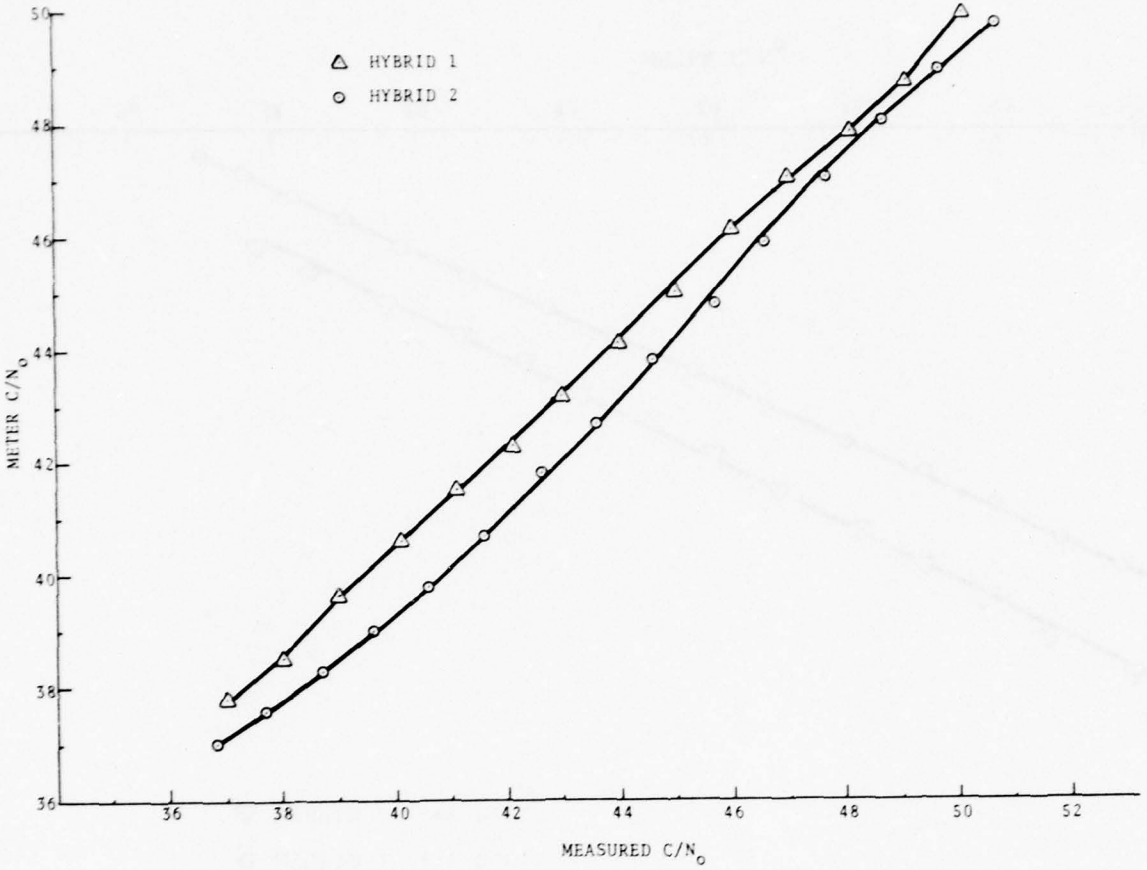

FIGURE 3-3. CARRIER-TO-NOISE POWER DENSITY RATIO CALIBRATION FOR THE VOICE INTELLIGIBILITY TESTS — METER VS. MEASURED C/N$_o$

in the received and demodulated PN sequence. This was done in real-time on board the Coast Guard ship in order to obtain preliminary system performance estimates. The received sequences were also recorded for later detailed analysis. Antenna pointing data and multipath data are also recorded during the modem tests and can be correlated with modem data in those cases where antenna pointing errors or multipath may have been of sufficient magnitude as to influence modem performance.

In order to facilitate recording of the received PN sequences on an instrumentation tape recorder using direct-mode equipment, the digital sequences were Manchester encoded. The received clock output of each modem under test was also recorded for future analysis. Three different modems were tested simultaneously using the same satellite down-link signal. Thus, six tape tracks were used to record the three Manchester encoded received PN sequences along with their associated clock signals. In addition, analog signals were recorded from C/N_o measuring circuitry on the two hybrid modems. Finally, a time code was recorded on all analog tapes.

Recovery of the Manchester encoded data is straightforward using the circuitry shown in Figure 3-4. For a single channel (modem) as shown, Manchester encoded data, clock, time code, and analog C/N_o signals are simultaneously reproduced by the instrumentation tape recorder. The data and clock signals are processed through comparator circuits for TTL compatibility in risetime and amplitude. The clock signal is then rephased to the data signal to compensate for differences in head skew in the recording and reproducing tape recorders. The rephased clock signal is then exclusive OR'd with the data signal and the result enters a Hewlett-Package 1645A data error analyser. The analyser compares the input PN data stream with an internally generated replica of the transmitted code and detects bit errors, block errors, clock slips, and carrier dropouts. This information is printed on paper tape in parallel with the time code information. The C/N_o signal is simultaneously recorded on a time coded strip chart recorder.

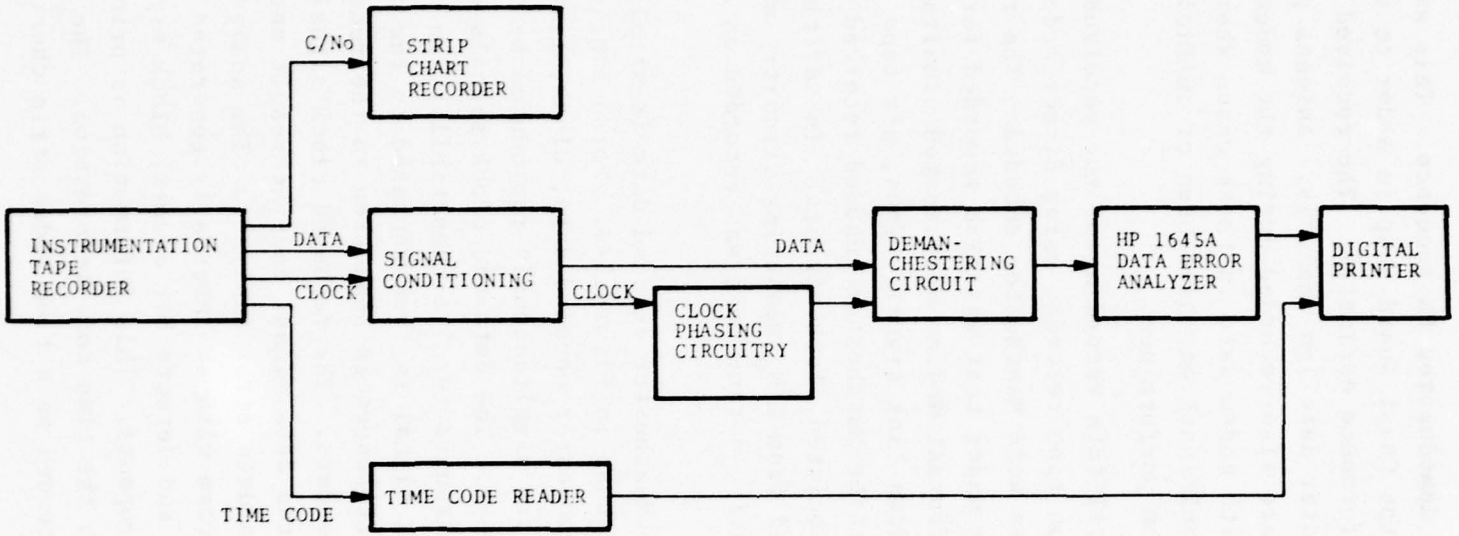

FIGURE 3-4. DIGITAL DATA REDUCTION (SINGLE CHANNEL SHOWN)

PN sequence transmission from the satellite was continuous for time intervals on the order of 20 min. and longer. However, test conditions were varied on board the vessel during these transmission intervals. In particular, the effective carrier-to-noise power density ratio was changed by the addition of a calibrated amount of noise to the received signal. The C/N_o ratio was thus set to 36, 38, 40, and 42 dB-Hz. Furthermore, the antenna and/or mode was selected to be either autotrack, slaved to ships gyrocompass, or low-gain antenna. Some of the data were recorded with the steerable antenna boresight intentionally reduced below the elevation angle to the satellite. Finally, some data were recorded with the ships heading changing through 360° with constant C/N_o. In the data extraction process, error rate, and block error rate performances for the various combinations of C/N_o, antenna configuration, and ship orientation are extracted. This is accomlished by reference to the test scenarios and test log to determine the test sequences carried out and by utilization of the time code which is recorded on the analog instrumentation tape. The block error and bit error statistics are used to estimate the error distribution statistics. However, the errors must be digitized and analyzed with the aid of a computer to determine complete error distribution statistics. This subject is discussed in more detail in Section 3.5.3.

3.4.2 Measurement of Bit Error Probability

The actual measurement of bit error rate, or equivalently, probability of error, is straightforward. In particular, the formatted PN sequence was analyzed by a Hewlett-Packard 1645A error analyzer. This device provides direct measurements of bit error rate, block error rate, carrier losses, and clock slips. The data reduction equipment as currently configured includes three error analyzers so that the performance of the three modems under test can be measured simultaneously. Furthermore, three data printers are used to record the results obtained at the end of each measurement interval. Normally, the measurement interval is chosen so that 100 or more errors are observed. Thus, when C/N_o is such

that $P_e \simeq 10^{-4}$, the time measurement interval, τ_m, should encompass 10^6 bits or

$$\tau_m = \frac{10^6}{BR} = \frac{10^6}{1200} = 833s, \qquad (3\text{-}14)$$

assuming a bit rate (BR) = 1200 bps. The error analyzer provides for such measurement intervals automatically. That is, it conveniently counts the number of errors in a fixed number of bits as an integer power of 10; i.e., 10^4 bits, 10^5 bits, etc. It should be noted that in order to reduce the percentage error to 1 percent, a prohibitive amount of time is required in some cases, particularly for error rates less than 10^{-6}. Such efforts are not justifiable in terms of the added insight derived.

3.4.3 Error Distribution Characteristics

Two types of error control procedures are envisioned for maritime-satellite links. First, one can employ the block retransmission approach. In that case, a block check sequence is transmitted at the end of each data block to enable error detection at the receiver. If an error is detected, a message is sent from the receiving end back to the transmitter via a return link requesting retransmission of the block which contained the error. The block is then retransmitted until it is received without error.

Alternatively, forward error correction procedures can be employed. In that case, the role and character of the block check sequence are expanded so that errors in a block can be detected and corrected at the receiving end. Convolutional coding techniques can be employed to provide continuous error detection and correction.

The selection of an appropriate error control procedure depends on the distriubtion and density of errors expected on the communication links. The interrelationship of these factors will be discussed next.

3.4.3.1 Block Error Statistics - Block error statistics are used to determine the error performance of a system in which block retransmission is employed. For example, consider a system which transmits BR b/s and which utilizes a data block of N_d bits. The total block size is $N = N_d + N_{bcs}$ where N_{bcs} is the number of bits in the block check sequence. The probability of block error is P_b. The probability of requiring two retransmissions is P_b^2, etc. Thus, assuming that no time is lost during the retransmission request, the time required to send N_d bits is

$$t_d = \frac{N}{BR} + \frac{N}{BR}\left(P_b + P_b^2 + P_b^3 \ldots\right) \tag{3-15}$$

or

$$t_d = \frac{N}{BR(1-P_b)} . \tag{3-16}$$

The effective throughput rate is then

$$(BR)_{eff} = \frac{N_d}{t_d} = \frac{N_d}{N_d+N_{bcs}} (BR)(1-P_b) \approx (BR)(1-P_b) \tag{3-17}$$

when $N_d >> N_{bcs}$. The block error rate could be derived directly from the bit error rate, P_e, provided that the bit errors were random and independent. In that case,

$$P_b = 1 - (1-P_e)^N \approx NP_e \tag{3-18}$$

Unfortunately, the bit errors are not always independent. First, it is noted that differential encoding techniques are employed by most of the modems being considered for the maritime-satellite application. This means that typically errors occur in pairs. Thus, the block error rate is lower than that predicted by Equation 3-18. In fact, the block error rate is approximated by

$$P_b \approx 1 - (1-P_e/2)^N \approx NP_e/2 \tag{3-19}$$

In some cases, channel fading causes the errors to occur in larger bursts. Assume for example that the channel or some other characteristic of the system causes errors to occur in bursts of k/bits; i.e., k errors occur over a short interval of say 2k or 3k bits. Then the block error rate can be approximated by

$$P_b \simeq 1 - (1-P_e/k)^N \simeq N P_e/k, \; N >> k \qquad (3\text{-}20)$$

A reasonable estimate of the value of the effective error burst length, k, can be obtained emphericallly from bit error and block error data. Figure 3-5 shows the relationship between bit error rate and block error rate in a land-mobile 2400 b/s data communication system. Each point plotted in the figure represents the bit error rate and block error rate observed in a single run of 10^5 bits. The block length was set at 1000 bits. The solid curve is a plot of Equation 3-19 with k = 1 and N = 1000; the dashed curve is the same except k = 5. The figure shows us that at lower error rates, e.g., $P_e = 10^{-5}$, the errors are occurring randomly and independently. On the other hand, as error rate increases, e.g., $10^{-4} < P_e < 10^{-3}$, the effective burst length increases to say k = 2.5. At higher error rates k continues to increase.

The printed outputs of the HP1645A error analyzer were used to generate graphs of the form shown in Figure 3-5. The resulting graphs yielded reasonable estimates of the error burst length, k, as a function of bit error rate, satellite elevation angle, sea-state, and other environmental factors.

The estimates obtained in this way were improved and confirmed by reconfiguring the error analyzer to measure the block error rate for 100 bit blocks. (The block length is determined by internal strapping connections in the error analyzer.) These data can be used directly to evaluate the potential improvements obtained by the implementation of more sophisticated forward error correction coding techniques.

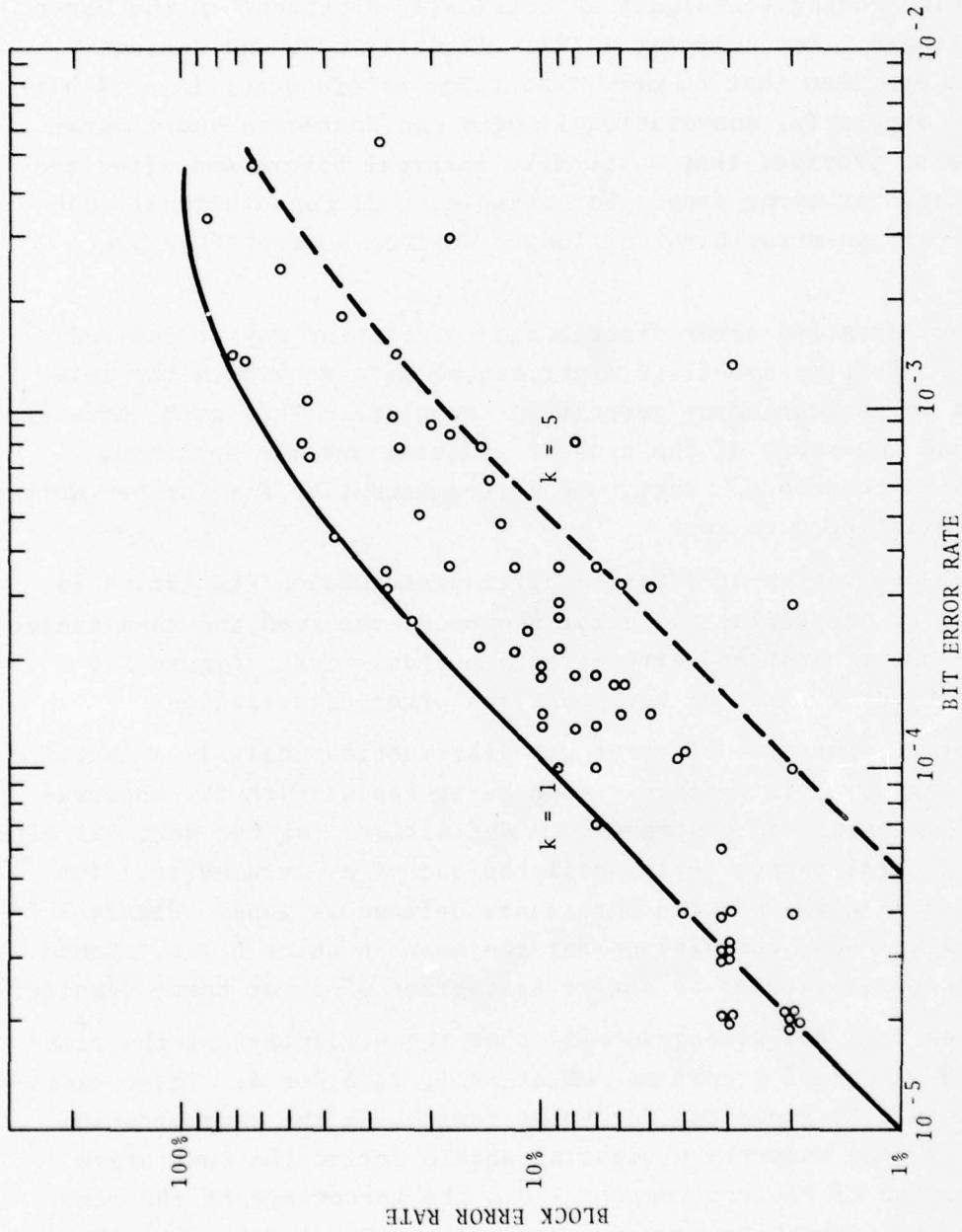

FIGURE 3-5. BLOCK ERROR RATE ANALYSIS OF FIELD TEST DATA

3.4.3.2 Error Distribution Statistics - The block error statistics yield rough estimates of the error burst length as a function of environmental conditions. The applicability of various error correcting coding techniques is critically dependent on the burst error length. For example, a (24, 12) Golay code can correct errors, provided that no more than three errors occur in a 24-bit block. Similarly, convolutional codes can correct a short burst of errors, provided that a specific interval before and after the error burst is error free. For example, a B1 convolutional code can correct an error burst of length 4 given a error-free gap of 15.

More detailed error distribution statistics may be derived from the maritime-satellite experimental data to aid in the selection of an optimum error correction technique. This work, however, is beyond the scope of the present program, and the following paragraphs therefore constitute a recommendation for further work on the existing data base.

The derivation of detailed error distriubtion statistics is achieved by digitizing the error sequences observed and then analyzing the error burst and error-free gap statistics. Figure 3-6 shows a block diagram of equipment for error digitization.

For the purposes of error gap distriubtion analysis a specific burst length, b, is defined. Each burst begins with the observation of an error and continues, by definition, for the next b-1 bits. The next burst cannot begin until the end of a given burst. The error-free regions between bursts are defined as gaps. Figure 3-7 illustrates these definitions for the case in which b = 4. Computer processing is used to derive histograms of error burst density.

When b=4, the histogram will show the percentage of the time that the number of errors per burst is 1, 2, 3, or 4. These histograms should be generated for burst lengths in the range $1<b<10$. Similarly, the computer processing should derive the cumulative distribution of the gap length; i.e., the percentage of the time that the gap length exceeds a given value. Gap length distributions should also be derived for burst length in the range $1<b>10$.

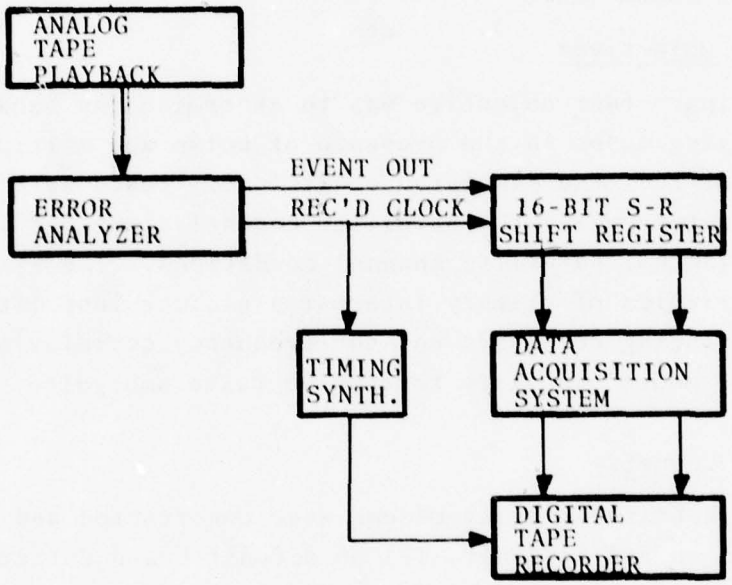

FIGURE 3-6. BLOCK DIAGRAM FOR AN ERROR DIGITIZATION SCHEME

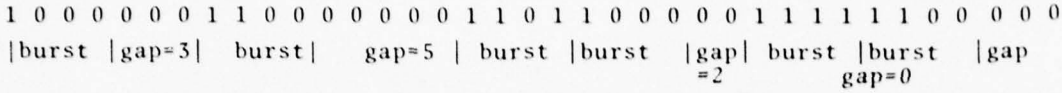

FIGURE 3-7. BURST AND GAP ILLUSTRATION

The error burst and gap distribution statistics can be used to evaluate candidate error correction coding techniques for maritime-satellite applications.

3.5 RANGING MODEM TESTS

3.5.1 Test Objectives

The primary test objective was to determine the behavior of a digital ranging modem in the presence of noise and multipath interference under real and simulated conditions. Tests were performed in the laboratory using the satellite channel simulator and in the field under actual satellite channel conditions. The system performance variables of primary interest are clock loop jitter, which represents ranging accuracy; and sub-frequency correlation error, which is the modem's ability to resolve range ambiguity.

3.5.2 Test Geometry

Three identical ranging modems were constructed and installed, (1) on board an FAA aircraft, (2) on a Coast Guard Cutter, (3) at the ground station at Rosman, North Carolina. This configuration allows a comparison of data collected at two locations, the aircraft and cutter.

The ranging code is generated at the ground station, modulated on a carrier, up-converted, received at the satellite, and retransmitted back to earth. The down-link is received at the cutter and the aircraft simultaneously to allow comparison of data samples at both locations.

3.5.3 Test Procedure

The test procedure was to transmit code from the ground station and receive it aboard the Coast Guard cutter under controlled carrier-to-noise power density ratios.

For each ranging experiment day, range data were accummulated, using both narrow- and wide-band codes, at several carrier-to-noise power density ratios. Approximately 10 min. of data was taken at each test condition. The sequence varied from day-to-day, depending on the scenario. The C/N_o parameter was varied over the range from 48 dB-Hz to 36 dB-Hz. Each ranging experiment, however, always included both wideband and narrow-band code formats. Wideband code has a clock frequency of 156.250 kHz and narrow-band code has a clock frequency of 19.53125 kHz.

Since the clock-tracking loop determines the overall performance of the modem, experiments were conducted with increased power in the clock component of the code, comparing equally weighted code components against a code in which the power in the clock component was doubled. The different code formats are defined as follows: format 1 - equally weighted narrow-band code; format 2 - equally weighted wide-band code; format 3 - narrow-band clock power doubled; format 4 - wide-band clock power doubled.

The carrier-to-noise power density ratio was determined by first feeding signal followed by noise through a calibrated filter and then measuring the power of each each independently to calculate C/N_o.

3.5.4 Data Formatting

The recorded ranging data consists of a serial 40-bit word clocked out at a rate of 4/s. This serial bit stream appears at two connectors on the front panel as NRZ (Non-return-to-zero) data Manchester encoded for recording on the analog tape. NRZ data allows the observation (on an oscilloscope) of the correct functioning of the ranging modem with a word sync also provided on the front panel. The 40-bit word is composed of the following: The first 7-bits are a preamble sequence, representing a flag. The next 5-bits are status information to indicate lock of the

various loops and functions in this order: Bit 8 indicates the 70 MHz loop is locked in phase; bit 9 indicates the 70 MHz loop is locked out of phase; bit 10 indicates the clock loop is locked; bit 11 indicates correct correlations have been made; and bit 12 is not used. Bits 13 through 20 indicate the code format. Bits 20 through 40 represent the range reading in binary; the least significant bit is the last bit of the data word and is equivalent to a 25 ns quantization in the range measurement process.

3.5.5 Data Reduction

Ranging data were collected on magnetic tape and stored for future reduction and processing. In order to strip data off the magnetic tape, a special data reducer was designed and constructed. It contains a clock tracking loop which phase-locks to the 305 Hz data clock and tracks it through any tape speed fluctuations. A new clock is generated which is phase-locked to the transitions of data contained on the tape. It is then possible to reverse the Manchester encoding procedure to extract NRZ data. There is circuitry which recognizes the preamble sequence and primes registers to accept the range data in binary and the status bits. Range data in binary is converted to decimal and printed out along with the status bits on paper tape. Range data in the form of serial pulses, each one equal to 25 ns time intervals, appear at a front panel connector. This is then sent to a computer for processing and computation.

3.5.6 Data Reduction Processing Technique

The recorded data must be processed to remove the trends caused by oscillator drift and vessel motion. This is achieved by carrying out a least-squares fit to the data.

The steady-state trend in the data can be expressed by the form

$$r = a + bt \qquad (3\text{-}21)$$

where r is range and a and b are constants. We desire to determine optimum values for a and b such that the difference between the range r and the actual measurements of range, r_k, made at time t_k is minimum in the mean-square sense.

The solution to this problem is well known. Specifically, assuming that r_k and t_k are random variables and that there are n measurements, then,

$$a = \frac{\left(\sum t_i^2 \sum r_i - \sum t_i \sum (t_i r_i)\right)}{n\sum t_i^2 - \left(\sum t_i\right)^2} \tag{3-22}$$

and

$$b = \frac{n\sum (t_i r_i) - \sum t_i \sum r_i}{n\sum t_i^2 - \left(\sum t_i\right)^2} \tag{3-23}$$

For the case under consideration here, t_i is not random. In fact, t_i is of the form

$$t_i = i\,\Delta T \quad i = 0, 1, \cdots k \cdots n-1 \tag{3-24}$$

where $t_o = 0$ defines the start of the data run. Equations 3-23 and 3-24 can be simplified in that case by making the following substitutions:

$$\sum_{i=0}^{n-1} i\,\Delta T = \frac{(n)(n-1)\Delta T}{2} \simeq \frac{n^2 \Delta T}{2} \tag{3-25}$$

and

$$\sum_{i=0}^{n-1} (i\Delta T)^2 = \frac{(n-1)(n)(2n-1)\,\Delta T^2}{6} \simeq \frac{n^3 \Delta T^2}{3} \tag{3-26}$$

$$a \simeq \frac{4}{n} \sum_{1}^{n} r_i - \frac{6}{n^2} \sum_{1}^{n} i\, r_i \tag{3-27}$$

and

$$b \simeq \frac{12}{n^3 \Delta T} \sum_{i}^{n} i \cdot r_i - \frac{6}{n^2 \Delta T} \sum_{i}^{n} r_i \qquad (3\text{-}28)$$

Finally, the least-squares estimate of the range at the k measurement time is given by

$$r_{ok} \simeq \left(\frac{4n - 6k}{n^2}\right) \sum_{i}^{n} r_i + \left(\frac{12k - 6n}{n^3}\right) \sum_{i}^{n} i\, r_i \qquad (3\text{-}29)$$

Let us now define the detrended range estimate $\rho_k = r_k - r_{ok}$. (ρ_k is a zero mean random variable). The root-mean-square ranging error is found in the usual way by solving for

$$\Delta\rho_{RMS} = \frac{1}{n} \sum_{i}^{n} \rho_i^2 - \left(\frac{1}{n} \sum_{i}^{n} \rho_i\right)^2 \qquad (3\text{-}30)$$

The choice of the number of data points, n, to use in a single computation of Equation 3-30 is not clear. The channel statistics are probably stationary over a few seconds; i.e., n on the order of 10 - 20. A large measurement error should be expected with n so small. However, cyclical range fluctuations due to vessel pitch and roll may be detectable with averaging times less than a few seconds.

Alternatively, several thousand samples can be averaged in Equation 3-30. This seems to be the better choice because the results will be directly applicable to the analysis of error of satellite based navigation systems for maritime applications. This latter alternative was selected for the ranging data reduction process.

4. USCG DEMONSTRATIONS

4.1 INTRODUCTION

Communications satellites for maritime use promise many advantages in terms of safety, reliability, communications time, communications quality, and cost savings. The systems being contemplated require the satellite to serve a large number of highly mobile, globally dispersed vessels. It is therefore necessary to efficiently manage the utilization of communications channels in order to obtain reliable performance at a reasonable cost. The resultant system should be compatable with ship-to-shore, ship-to-air, ground-to-ground, and ship-to-ship voice/data/facsimile systems.

Experiments were planned to demonstrate equipment use in an operational system. The experimental equipment usage was predicated on previous studies which identified access control techniques and sytem management procedures best suited to accommodate the communication requirements of maritime vehicles.

4.2 SELCAL DEMONSTRATION

The United States has proposed a digital selective calling system be adapted for maritime use in MF, HF, and VHF terrestrial communications. Such a system may be suitable for L-band signaling and its utility must be tested. The selective calling (SELCAL) system to be evaluated was a narrow-band digital scheme for which prototype HF/MF equipment has been tested.

The SELCAL unit was designed to enable the transmission and reception of selectively addressed digital transmissions (GTE, 1973 A,B). The terminal tested by the Transportation Systems Center consists of a keyboard, a 32-character alphanumeric display, microprocessor controlled digital circuitry, and FSK modems for interface with voice communication channels. The operating functions are programmed into a read-only memory, and thus the SELCAL can be reprogrammed if new operating functions are desired.

The SELCAL terminals were installed at the NASA/Rosman Earth Station at Rosman, North Carolina, and on the WHEC GALLATIN. Figure 4-1 shows the equipment installation on the GALLATIN. The units transmitted signals over an FM voice channel with the characteristics given in Table 4-1.

The test consisted of sending a series of selectively addressed messages from Rosman to the GALLATIN and receiving the automatic replies from the GALLATIN. The sequence of messages was repeated at different values to signal-to-noise injection on the GALLATIN. No noise was injected on the return link to Rosman. The test results are tabulated in Table 4-2.

The errors in test 4 of the January 21 series and test 5 of the January 28 series did not affect message reliability. The errors on test 6 of January 28 resulted in unreadable messages. Thus, the SELCAL performed well in the NBFM channel at all carrier-to-noise power density ratios from 42 dB-Hz to the system maximum of approximately 62 dB-Hz.

4.3 RADIOTELETYPE DEMONSTRATION

Typical communication equipment interfaces with the satellite system were planned for demonstration of radioteletype equipment. Part of the demonstration consisted of a radioteletype test set, using General Electric TermiNet 300 teleprinters, which were installed on the GALLATIN and at the Rosman Earth Station. The TermiNet units were equipped with the 1200 baud option and tape cassette accessory units. Each unit was interfaced to a 1200 b/s data modem through an interface module. This equipment allowed message transmission from a prerecorded tape at the 1200 b/s rate necessary on the DECPSK channel.

The objective of the demonstration was to evaluate radioteletype communication at 1200 b/s on the ATS-6 DECPSK channel. For this purpose, a test tape was prepared containing a stream of 10^4 identical characters. The data stream was transmitted from the tape at Rosman to the GALLATIN with successively greater amounts of noise injected at the receiver to vary the signal-to-noise ratio. Table 4-3 summarizes the tests.

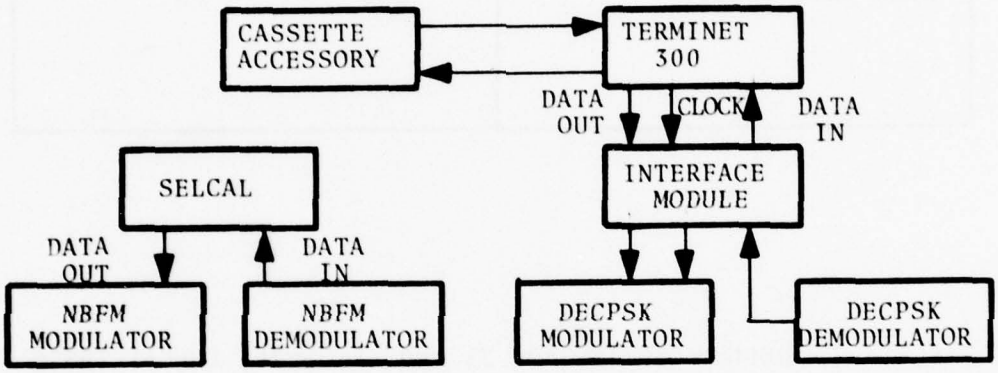

FIGURE 4-1. BLOCK DIAGRAM OF THE SELCAL/TERMINET 300 INSTALLATION ON THE WHEC GALLATIN

TABLE 4-1 NBFM CHARACTERISTICS OF THE SELCAL UNIT

PARAMETER	VALUE
Center Frequency (Hz)	1900
Frequency Shift (Hz)	± 425
Data Rate (baud)	600

TABLE 4-2 SUMMARY OF JANUARY 21 AND 28, 1975, SELCAL TESTS

DATE	TEST #	C/N_o (dB-Hz)	# MESSAGES SENT	# MESSAGES RECEIVED	ERRORS
Jan. 21 1975	1	Max.	50	50	0
	2	51	50	50	0
	3	47	25	25	0
	4	44	25	25	2
Jan. 28 1975	1	Max.	50	50	0
	2	48	50	50	0
	3	46	50	50	0
	4	44	50	50	0
	5	42	20	20	4
	6	40	20	20	11

TABLE 4-3 SUMMARY OF JANUARY 28 AND 29, 1975, TERMINET DEMONSTRATIONS

DATE	C/N_o (dB-Hz)	COMMENTS
January 28, 1975	Max.	The test was terminated due to lack of time. The data has not yet been reduced.
	42	
	38	
January 29, 1975	45	Received error free.
	42	Received error free.
	40	Received error free.
	37	Character error rate of approximately 7 %. The 45 dB-Hz (error free) tape was then retransmitted from the GALLATIN to Rosman and received error free.

This test sequence has demonstrated the transmission of digital data at 1200 b/s over a DECPSK channel using commerically available data communication equipment. The link was found acceptable at carrier-to-noise power density ratios of 40 dB-Hz and higher. Automatic control of the receiving data terminal was also demonstrated.

4.4 SEARCH-AND-RESCUE DEMONSTRATIONS

The ATS-6 Satellite Maritime Safety Equipment demonstrated the search-and-rescue (SAR) applications of satellite communications. On March 21 and 26, 1975, USCG search-and-rescue demonstrations were performed using the ATS-6 satellite. The purpose was to demonstrate the advantages of search-and-rescue coordination using satellite communications. A search-and-rescue incident was staged for these demonstrations which involved the following U.S. Department of Transportation agencies: USCG, FAA, and OST. The European Space Agency also participated. Figure 4-2 illustrates the scenario for the satellite safety demonstration configuration (Gutwein et al., 1975).

ESA utilized an L-band Emergency Position Indicating Radio Beacon (EPIRB) buoy, developed by the Federal Republic of Germany (Goebel, 1975 A,B). The EPIRB is a distress alerting device capable of transmitting the distressed vessel's call sign via the L-band satellite link and providing a homing beacon at the international distress frequency (2182 kHz) for direction finding and final vectoring of search units. The EPIRB is designed to become energized upon immersion in the sea, or it may be manually energized. A photograph of the buoy is shown in Figure 4-3.

The search-and-rescue demonstration was initiated by deploying the buoy, equipped with an EPIRB device, in the general area of the Azores Islands. The EPIRB transmission was initiated upon buoy deployment; receipt via satellite of the EPIRB distress alert signal at the NASA/Rosman Earth Station initiated the search-and-rescue coordination. This provided the vital first step in the search-and-rescue effort through indication that a distress incident had occurred.

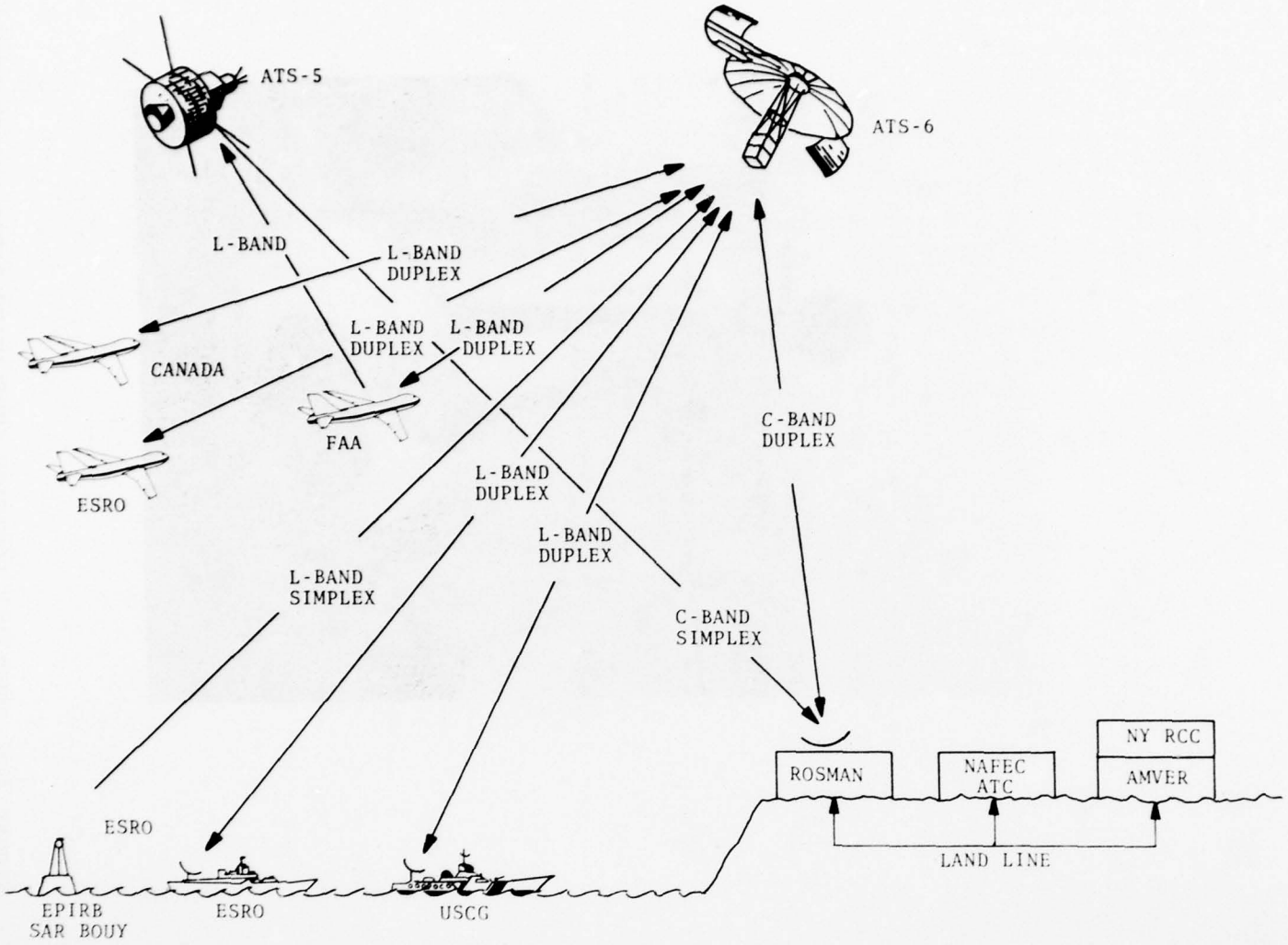

FIGURE 4-2. DIAGRAM OF THE ATS-6 USCG SEARCH-AND-RESCUE DEMONSTRATION CONFIGURATION

FIGURE 4-3. EMERGENCY POSITION INDICATING RADIO BEACON BUOY

Personnel at the NASA/Rosman Earth Station relayed the distress alert and ship call letters, via land line, to the U.S. Coast Guard Rescue Coordination Center (RCC) in New York City. The computer at the Automated Mutual - Assistance Vessel Rescue System (AMVER) determined the identity and the most probable position of the distressed unit and locations of the nearest available vessels of opportunity, which were the GALLATIN or the OTTO HAHN. The Rescue Coordination Center established immediate communications with both vessels via the ATS-6 satellite, determined their positions, initiated direction finding, and assigned search areas to each mobile.

The New York City Rescue Coordination Center (RCC) then took action to determine whether any aircraft were in the vicinity of the distress position. RCC contacted via land line the National Aviation Facilities Experimental Center (NAFEC), which was participating as a simulated Oceanic Air Traffic Control Center with the ATS-6 spacecraft. NAFEC informed RCC about the aircraft of opportunity in the area of the distress.

The two airplanes under NAFEC air traffic control were the FAA KC-135 and the ESA Comet. Since part of the avionics aboard the FAA and ESA aircraft consisted of automatic aircraft position data transmission equipment, a situation display of the aircraft in the distress area was available to the air traffic controller. All mobiles were transmitting and receiving full duplex on a common emergency L-band channel. This allowed full duplex L-band communications among all mobiles and ground facilities in a conference configuration. The mobiles interconnected in this manner were: GALLATIN, OTTO HAHN, FAA KC-135, ESA Comet, NAFEC, and NASA/Rosman, with RCC directing the entire operation. RCC requested both aircraft to direction find on the buoy homing signal. The direction finding information and aircraft positions were relayed back to the RCC. This provided a more accurate fix than that available from the AMVER predictions.

The KC-135, because of aircraft low altitude restrictions, could not do any low altitude visual searching but was able to direction find at nominal aircraft altitude. The Comet tried a low altitude visual search, but though the electronic search indicated the buoy position, the visual search was in vain. In actual conditions commercial aircraft of opportunity will, in general, assist by providing direction finding services but will maintain assigned altitude and course. Position information and situation reports were immediately available at the RCC who was able to converge the OTTO HAHN and the GALLATIN to the distress site and successfully recover the buoy.

The entire demonstration took place in a period of time of about 3 hours. While it is recognized that in a typical situation not all mobiles will be coordinated a priori, the tests were extremely successful in demonstrating the rapid access of satellite emergency communications, the ability to have all mobiles communicate with each other, the ability to minimize confusion through such communication, and finally, the ability to direct a search-and-rescue emergency of all participating vessels over a large area, thousands of miles distant from an RCC and an ATC center.

The ATS-6 search-and-rescue simulation became the "real thing" on the night of March 20, 1975, when a non-participating vessel in distress, the NORTHERN WORKER, suffered rudder and engine problems during a storm. In addition, the signal sideband radio aboard the NORTHERN WORKER was inoperative. The following day, the WHEC GALLATIN, in the vicinity, radioed the New York City Rescue Coordination Center via the L-band ATS-6 spacecraft link that it was escorting the distressed vessel and informed the RCC of the nature of the problems, current status, and position information. The GALLATIN also sent a teletype message via high frequency to the NYC RCC. The information gave the RCC the required data necessary to proceed with a rescue if necessary. RCC kept a vigil on this distress problem along with the GALLATIN during the conduct of the ATS-6 search-and-rescue demonstration. The NORTHERN WORKER made it safely to port in the Azores under USCG cognizance.

The ATS-6 Satellite Maritime-Safety Experiments demonstrated the search-and-rescue applications of satellite communications. The entire satellite experiment and actual search-and-rescue operations, involving AMVER and an operational rescue coordination facility, were without precedent and, moreover, were highly successful. The results of the maritime safety tests have confirmed that safety of life at sea may be significantly enhanced when future aeronautical and maritime satellite systems become operational.

Another significant precedent was the establishment of direct satellite communications among several mobiles separated by large distances well beyond radio line-of-sight. Conference networks were provided at the recently designated L-band frequency of 1600 MHz. These networks permitted instantaneous access, two-way simultaneous (full duplex) communications among several ships, several aircraft and various ground station coordination and control centers.

In exercises utilizing an emergency position indicating radio beacon (EPIRB), the ability of a satellite system to provide a world wide distress alerting capability was demonstrated. The EPIRB promises to be a low-cost distress alerting device. A worldwide service such as this is not currently available to ships in the present maritime radio distress system.

Another unique accomplishment of the aeronautical and maritime satellite experiments with the ATS-6 spacecraft involved rescue coordination of AMVER predictions with flyover air traffic identified by a Simulated Oceanic Air Traffic Control Center at the NAFEC. The Oceanic Air Traffic Control Center was able to remotely command and control the flyover air traffic while several thousand miles out over the ocean. Future aeronautical and maritime satellite systems could provide substantial benefits to the safety of transoceanic ship or air transportation. Moreover, radio position determination systems, based on trilateration to several orbiting satellites, could greatly improve the position prediction capabilities of AMVER, which are currently derived from sail plans and routine position reporting. Time for area search

is a direct function of knowledge of position. Commensurate advantages will accrue to saving lives by virtue of the precision inherent in satellite position determination.

With regard to technical performance, the satellite search-and-rescue utilized voice communications for coordination. The quality of the L-band satellite voice from all mobiles exceeded the quality of typical high frequency systems and was comparable with a high quality maritime line-of-sight VHF-FM voice link. The constancy and reliability of the L-band satellite voice communications also exceeds the performance of high frequency voice. In future maritime satellite systems the predominance of transmissions will be via teleprinters. High speed data transmission, at kilobit rates, is also possible with L-band satellite systems but not with high frequency because of the inherent limitations in data transmission rate via high frequency.

5. RESULTS OF EXPERIMENTS

5.1 INTRODUCTION

This section presents the results achieved during the ATS-6 maritime-satellite tests. First, medium-gain antenna performance is described and discussed. It is shown that the antenna provided better performance in the slave mode than in the autotrack mode in most cases.

The characteristics of multipath on the maritime-satellite test link are presented. The collected data indicate that the multipath reflection coefficient is typically around -8 dB, with slight dependence on sea-state and other conditions. The data also indicate that the multipath is not specular. In particular, it is shown that the majority of the multipath energy comes from angles just below the horizon rather than from the multipath specular point.

The voice and data performances of several modems are reported. In general, the modem designated Hybird 1 provides the best performance in the voice mode, the data mode, and the voice plus data mode. Voice intelligibility was better than 80 percent for all test conditions for this modem. It was observed that multipath had little effect on intelligibility, an expected result based on laboratory simulation results. The data performance of Hybrid 1 was superior. It provided a bit error rate of 1×10^{-5} at 43 dB-Hz when carrier-to-multipath ratios were in excess of 15 dB. Data performance was effected by the present of multipath. In particular, it is extrapolated that when carrier-to-multipath is on the order of 11 dB, a carrier-to-noise power density ratio in excess of 48 dB-Hz is required to provide 1×10^{-5} bit error rate performance.

The ranging modem tests reported in this section demonstrated that measurement precision in the order of 100 m is achievable at 40 dB-Hz using the DOT/TSC digital ranging system in its wide-band mode.

5.2 ANTENNA POINTING ERROR

One of the objectives of the ATS-6 measurements was to evaluate the performance of a medium gain antenna and to compare two methods (slave and autotrack) of antenna stabilization. Antenna performance was evaluated by computing the total pointing error and its components in azimuth and in elevation. Comparisons of slave and autotrack performance were made using a figure of merit. Figures of merit are calculated separately for pointing in azimuth and in elevation and are defined as the ratios of the standard deviations of the corresponding pointing errors in the absence of stabilization (simulated remote operation) to those achieved with stabilization (slave or autotrack). In addition, the received carrier-to multipath ratio (C/M) was calculated for each test, so that C/M represents another parameter against which antenna performance can be judged. Figures 5-1 through 5-18 show representative examples of antenna performance in the slave and autotrack operating modes. Figures 5-1 through 5-3 are time history plots of the total pointing error (TPERR), elevation error (ELERR), and azimuth error (AZERR) in slave operation. These data, collected on March 27, 1975, are representative of a medium sea state condition; i.e., 6-ft seas were reported. The time history of the ship's motion is illustration in Figures 5-4 through 5-6. Figure 5-4 indicates that the ship changed course from approximately 344° to 290° during the test segment. This occurred about 600 s into the run. In Figure 5-1, it can be seen that the slave mode tracked out the change in ship's heading; in the simulated remote mode, the antenna's total pointing error and azimuth error increased considerably, as shown in Figures 5-7 and 5-8, although the elevation error, Figure 5-9, increased only moderately.

If we restrict our attention to the first 9 min. of the run (i.e., prior to the turn) the corresponding figures of merit are $F_{AZ} = 2.2$ and $F_{EL} = 2.3$.

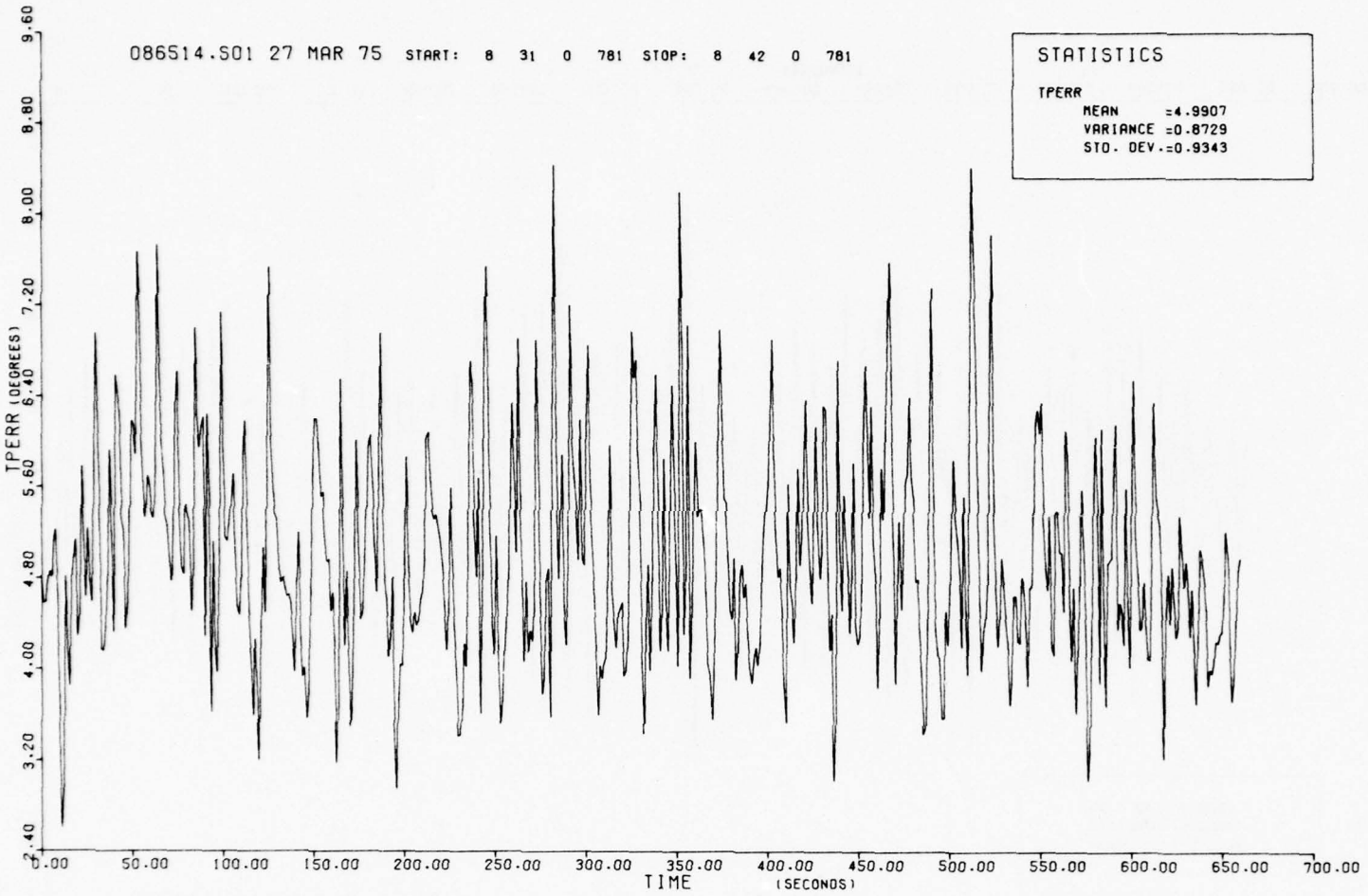

FIGURE 5-1. TIME PLOT OF THE TOTAL POINTING ERROR WITH THE ANTENNA IN THE SLAVE MODE

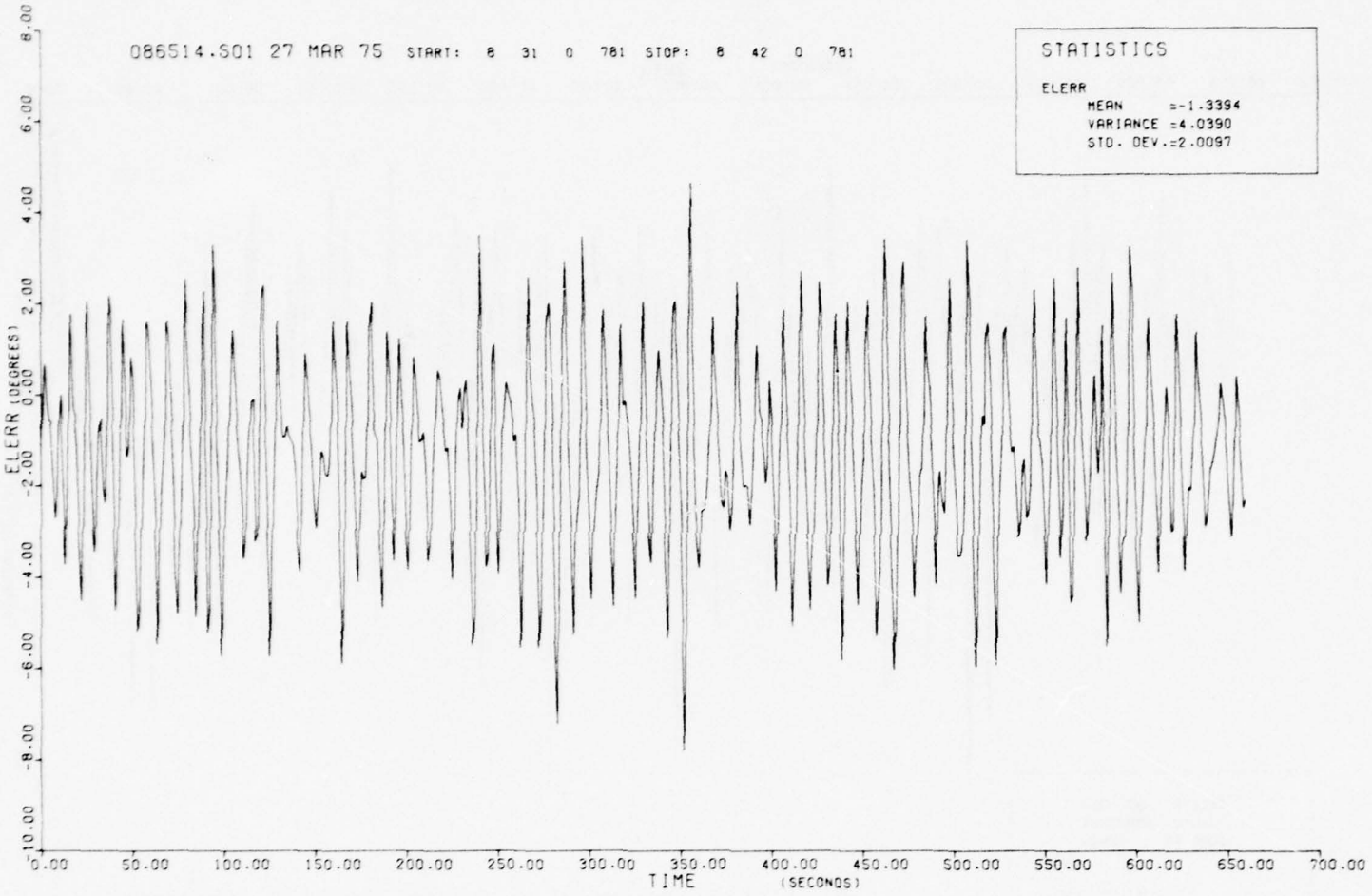

FIGURE 5-2. TIME PLOT OF THE ELEVATION ERROR WITH THE ANTENNA IN THE SLAVE MODE

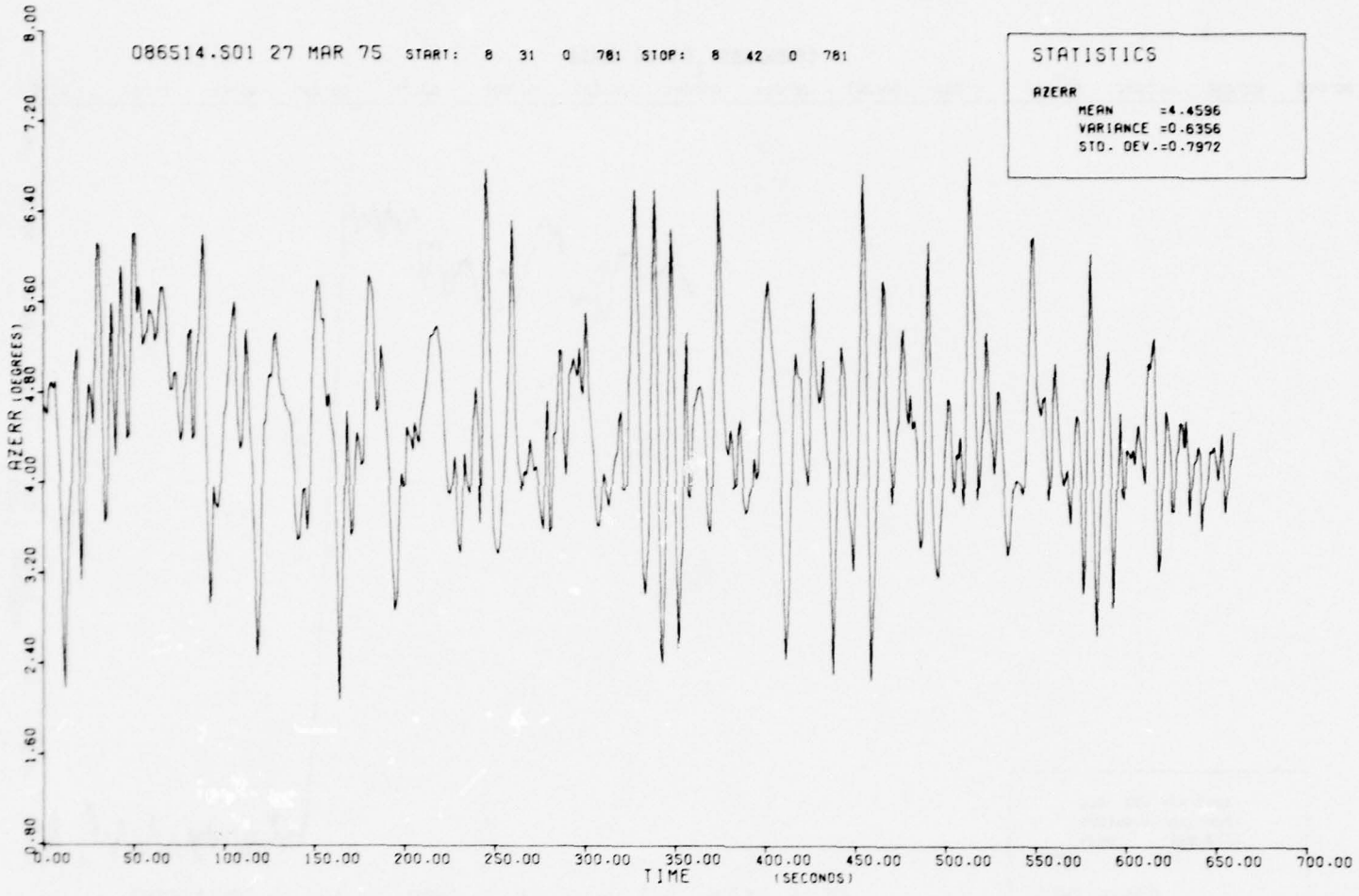

FIGURE 5-3. TIME PLOT OF THE AZIMUTH ERROR WITH THE ANTENNA IN THE SLAVE MODE

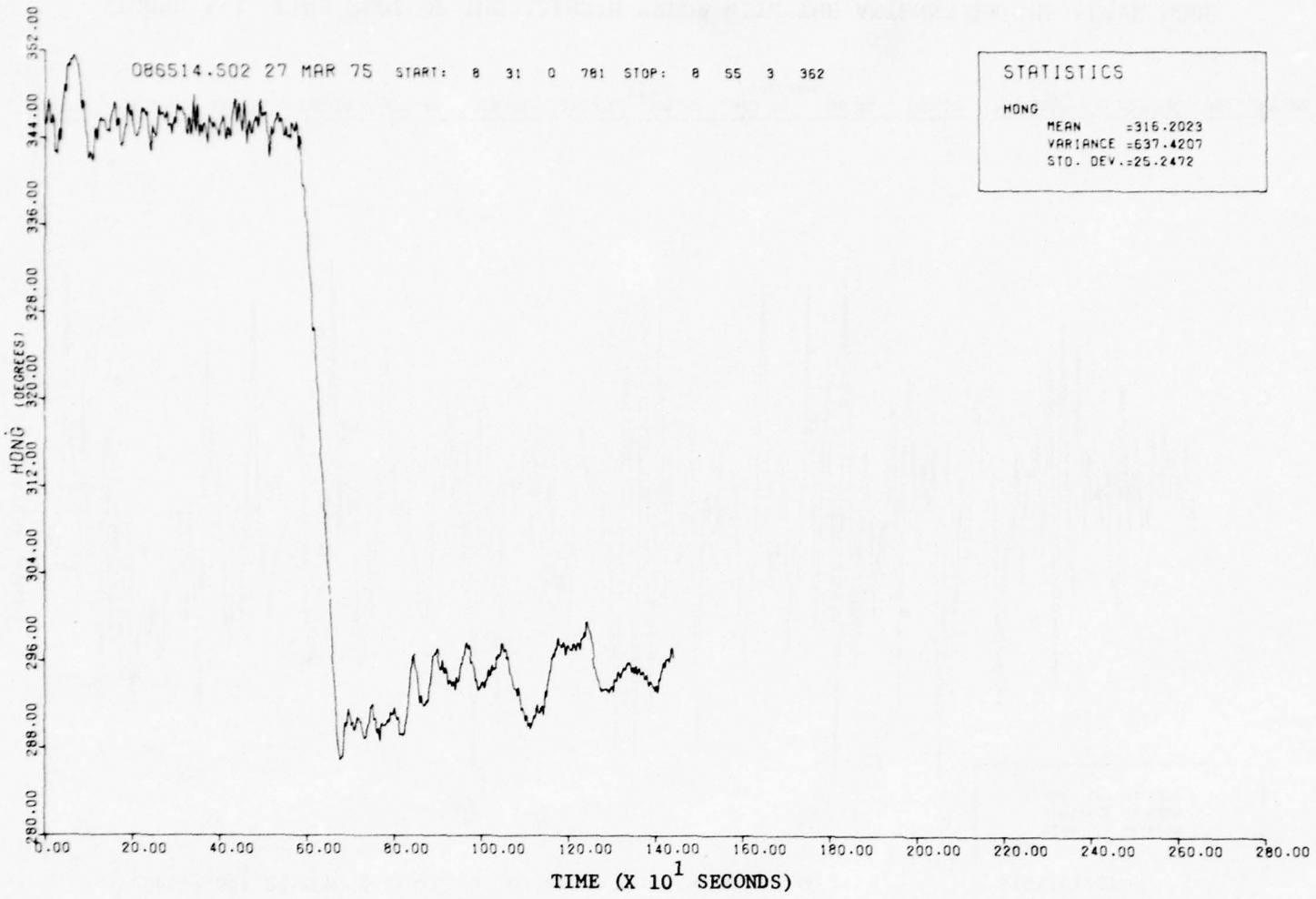

FIGURE 5-4. TIME PLOT OF SHIP'S HEADING

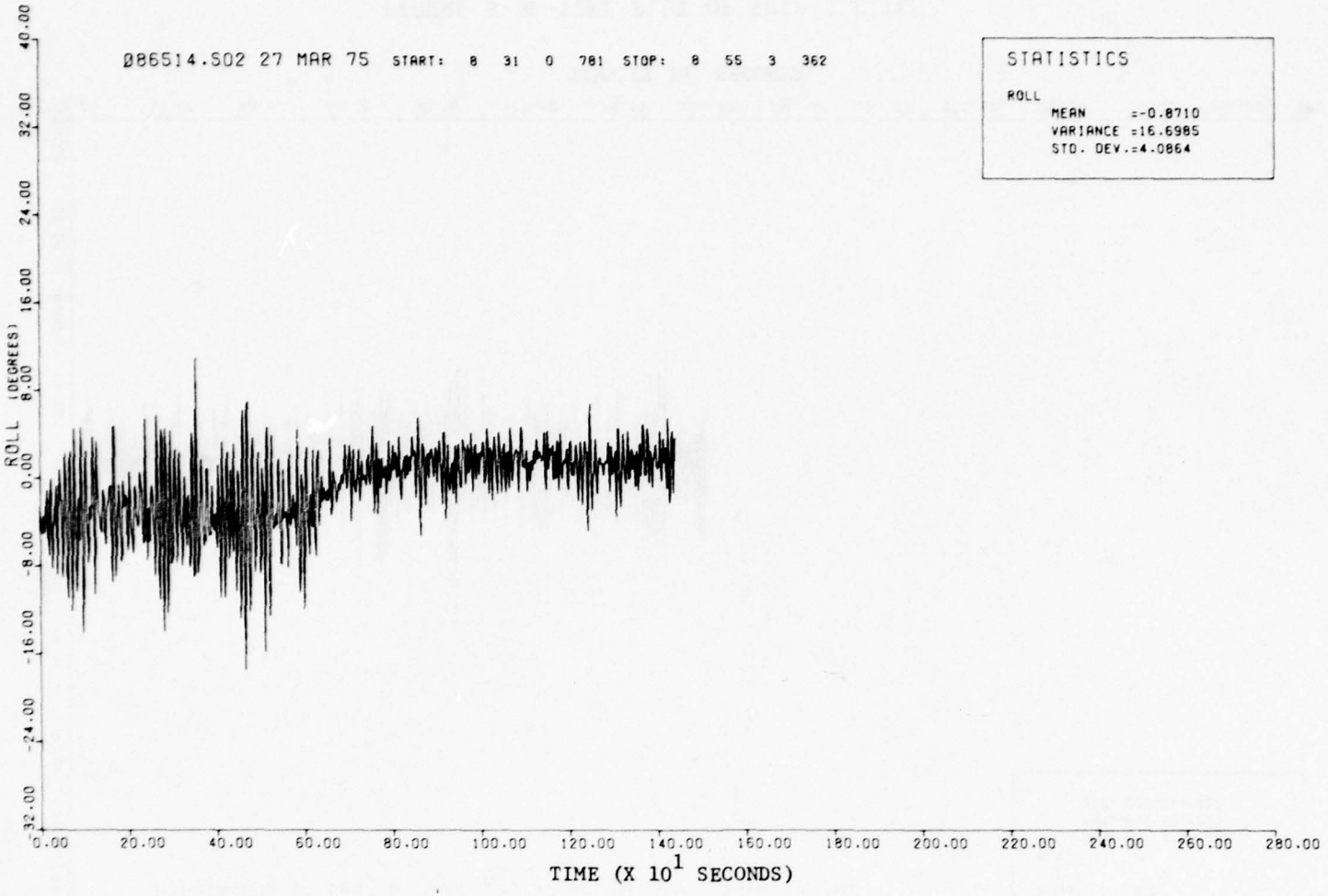

FIGURE 5-5. TIME PLOT OF SHIP'S ROLL

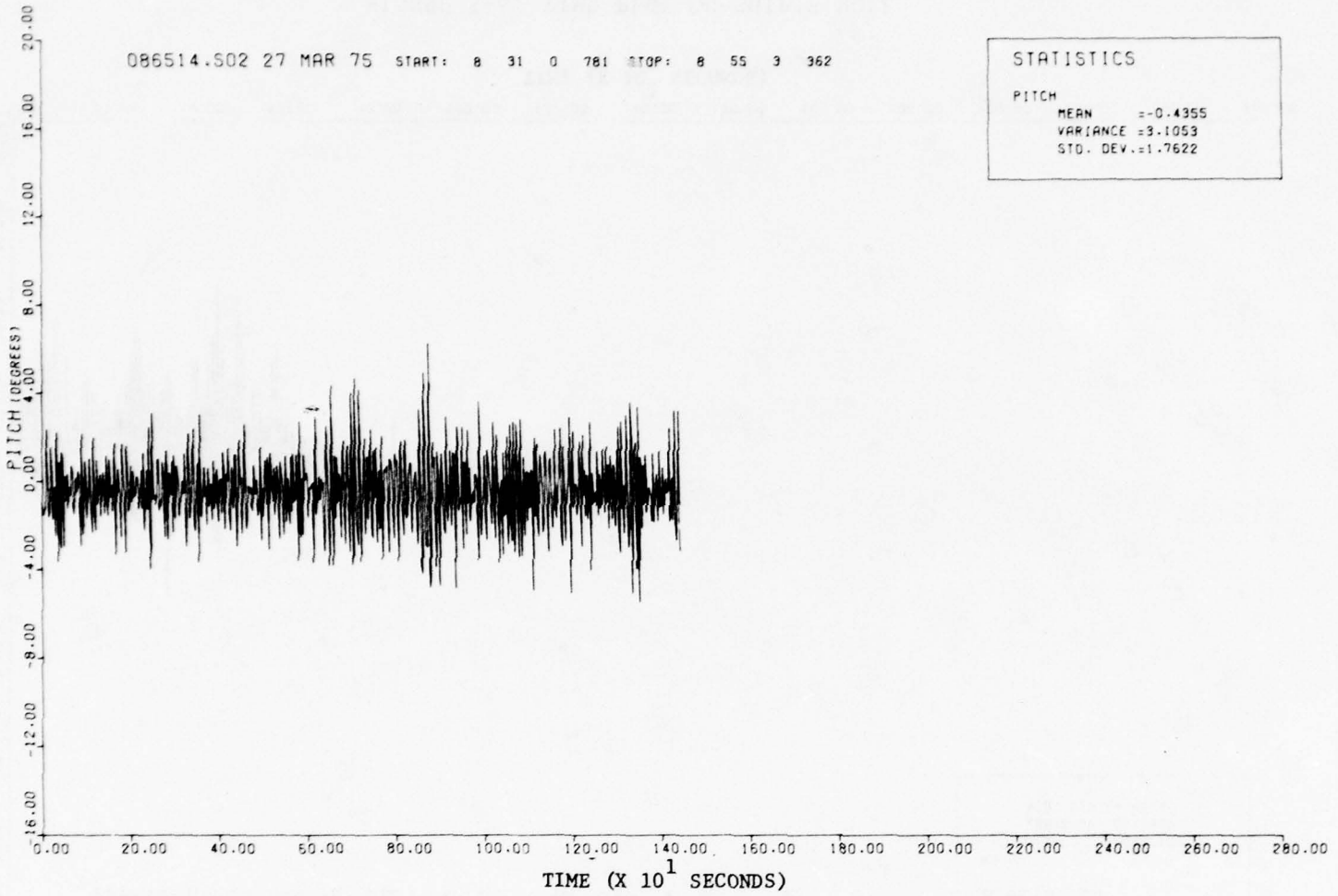

FIGURE 5-6. TIME PLOT OF SHIP'S PITCH

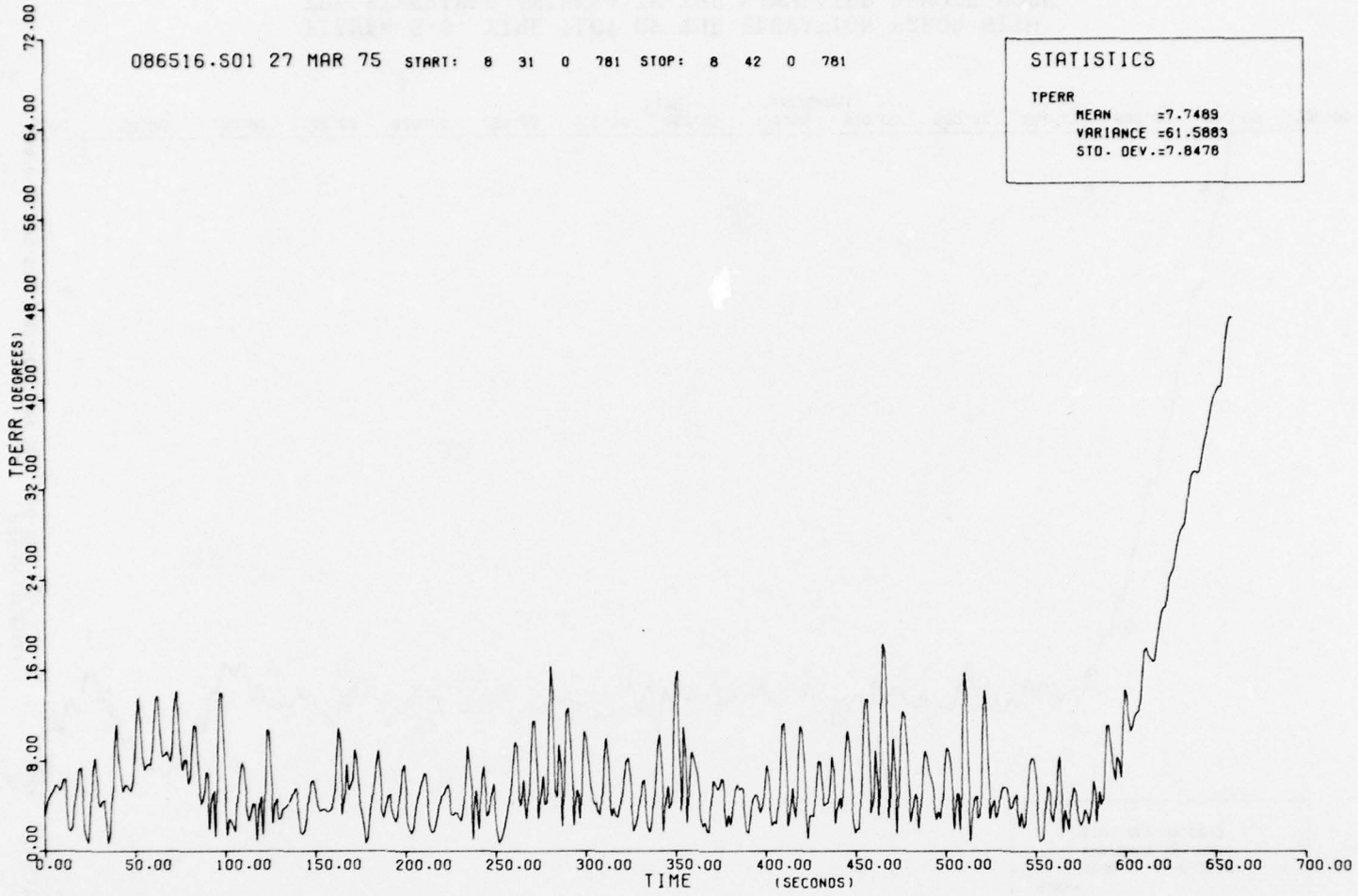

FIGURE 5-7. TIME PLOT OF THE TOTAL POINTING ERROR WITH THE STEERABLE ANTENNA IN A SIMULATED REMOTE MODE

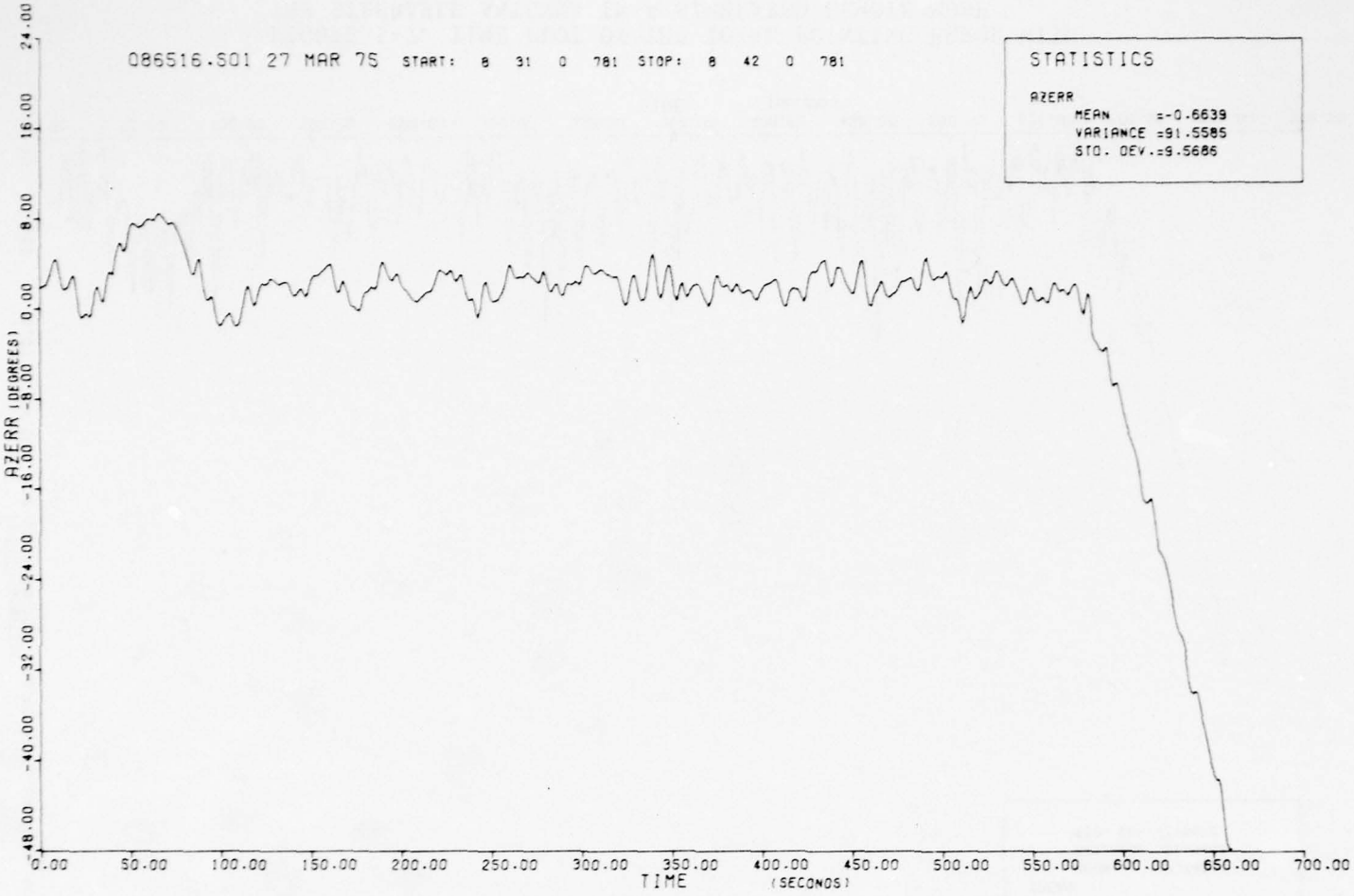

FIGURE 5-8. TIME PLOT OF THE ELEVATION ERROR WITH THE STEERABLE ANTENNA IN THE SIMULATED REMOTE MODE

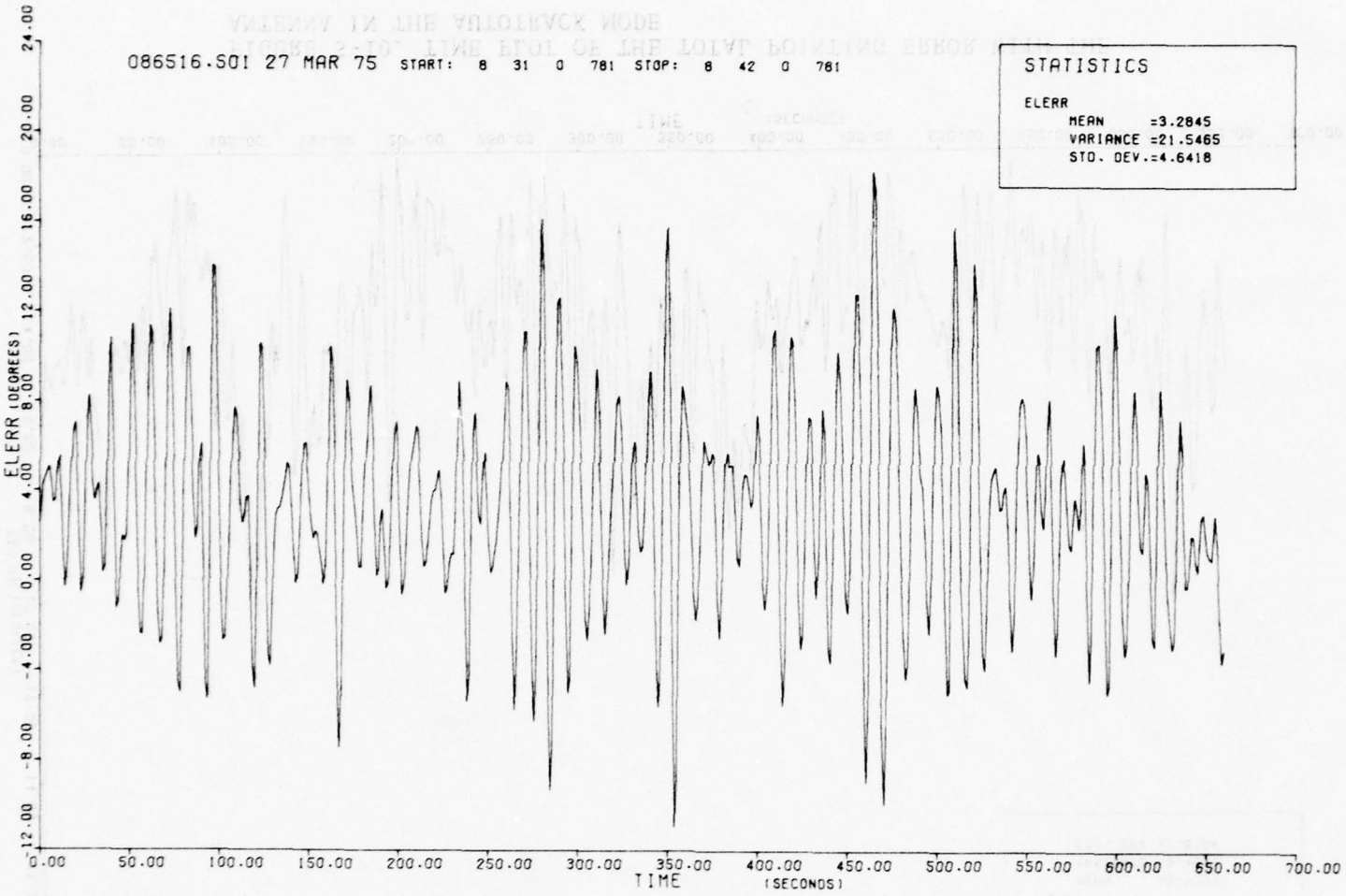

FIGURE 5-9. TIME PLOT OF THE AZIMUTH ERROR WITH THE STEERABLE ANTENNA IN THE SIMULATED REMOTE MODE

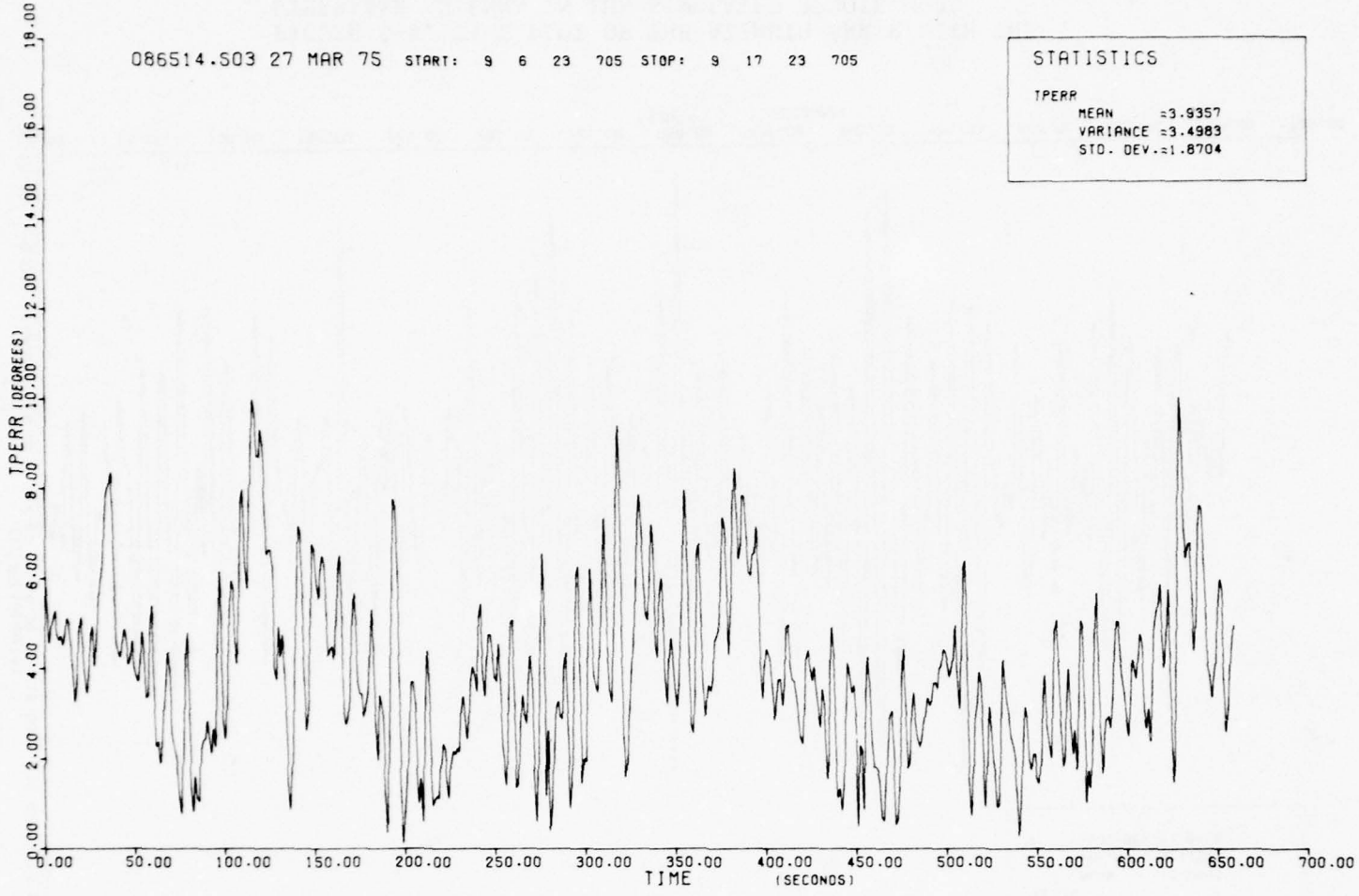

FIGURE 5-10. TIME PLOT OF THE TOTAL POINTING ERROR WITH THE ANTENNA IN THE AUTOTRACK MODE

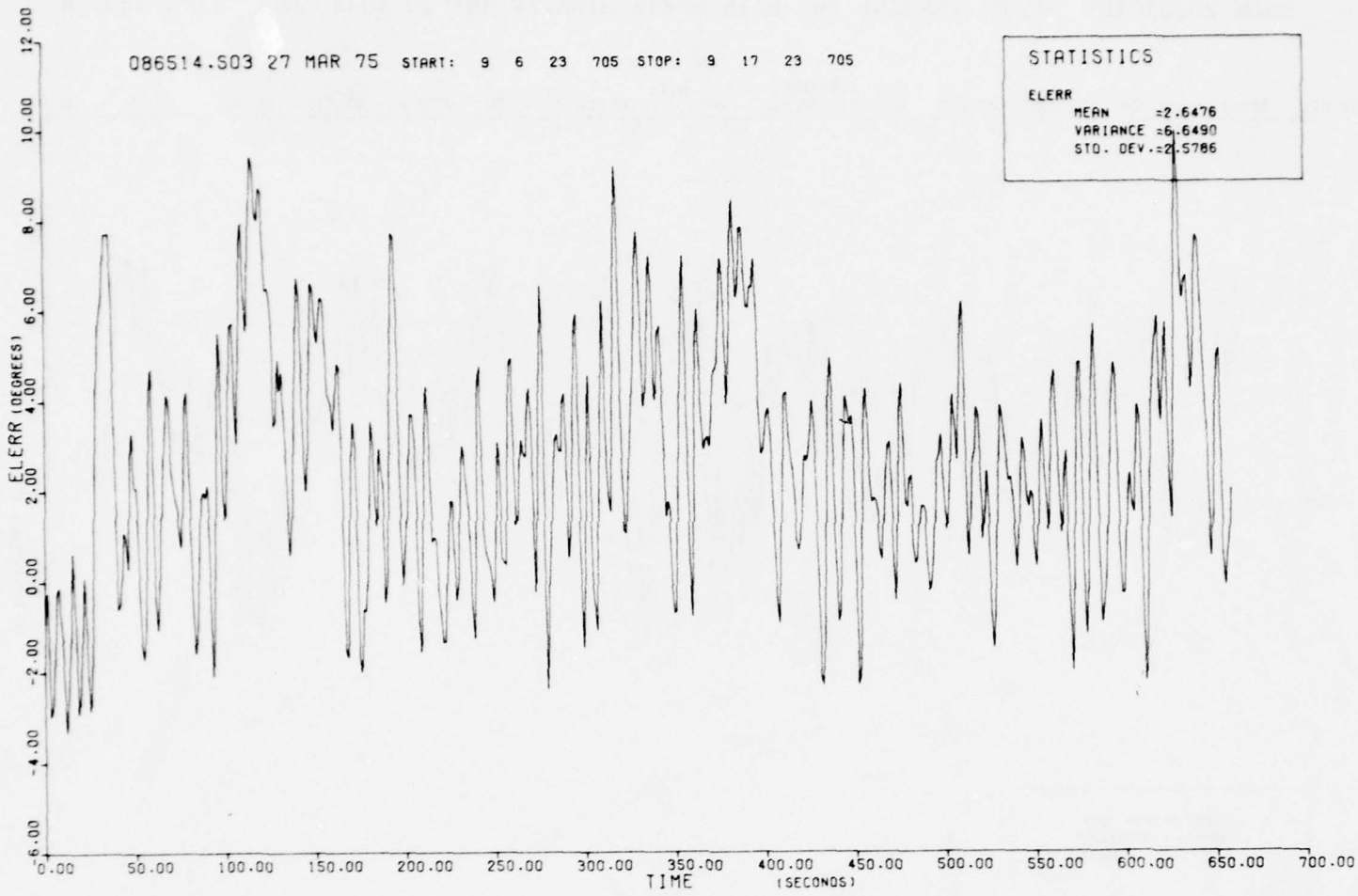

FIGURE 5-11. TIME PLOT OF THE ELEVATION ANGLE POINTING ERROR WITH THE ANTENNA IN THE AUTOTRACK MODE

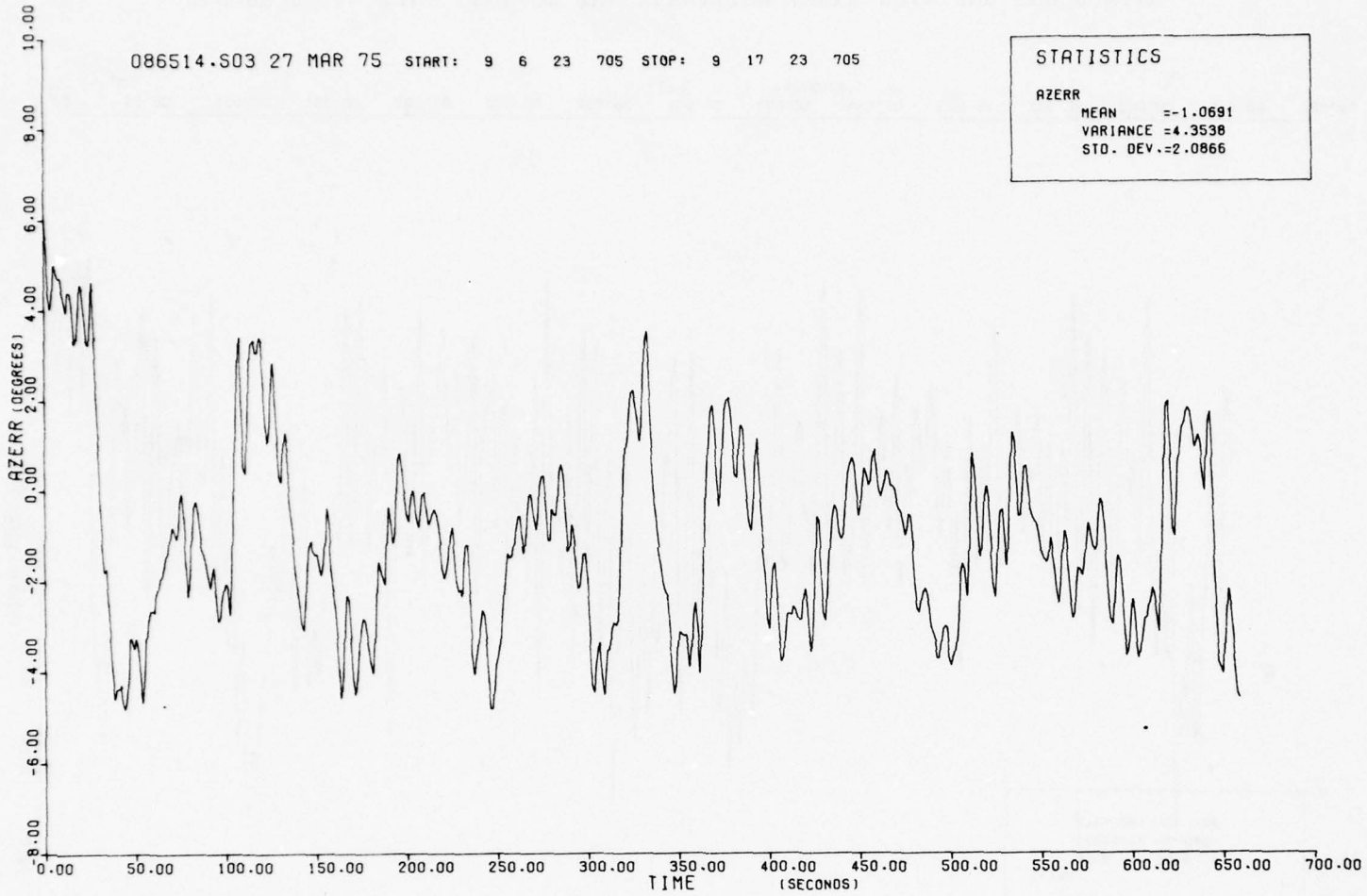

FIGURE 5-12. TIME PLOT OF THE AZIMUTH ERROR WITH THE ANTENNA IN THE AUTOTRACK MODE

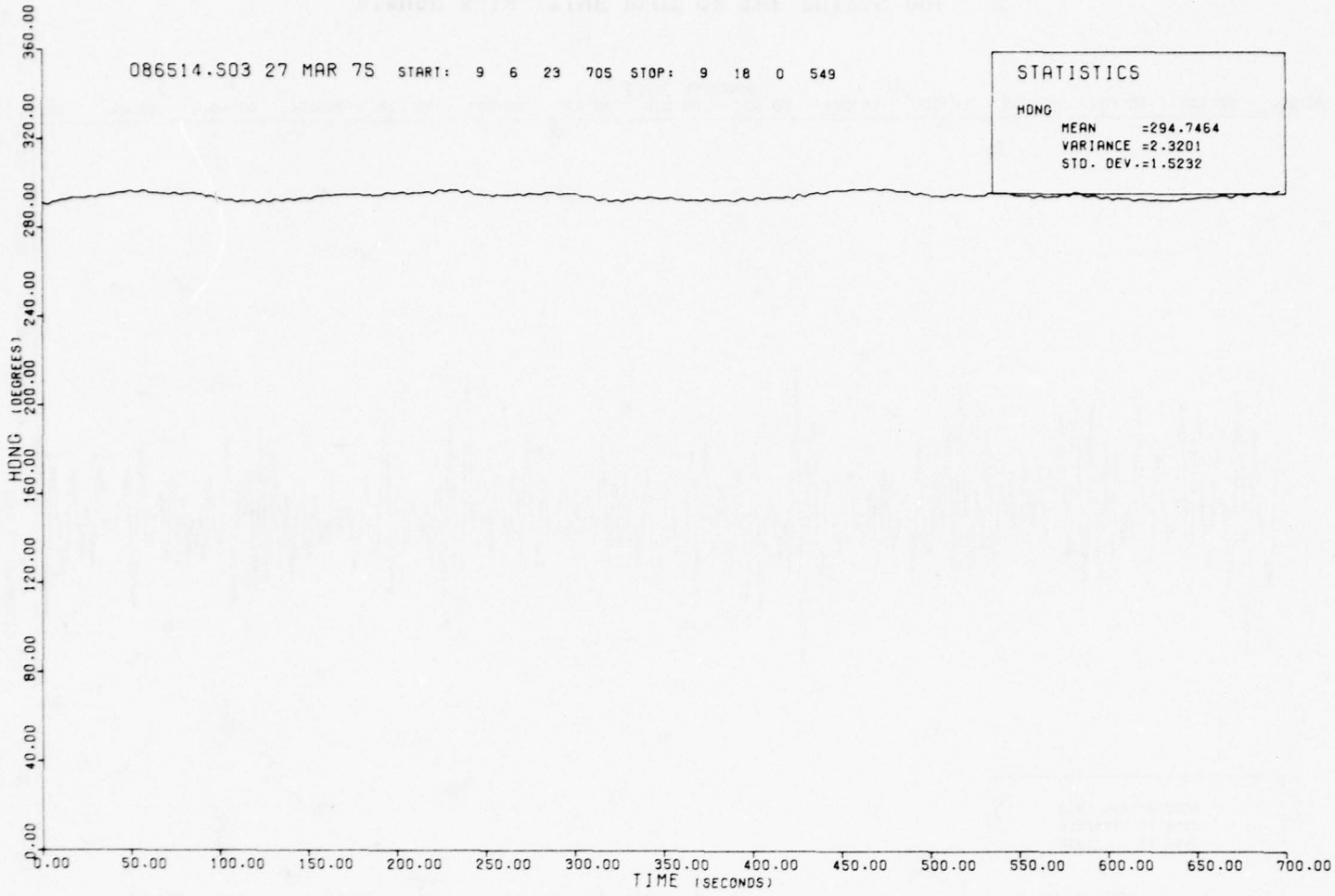

FIGURE 5-13. TIME PLOT OF THE SHIP'S HEADING

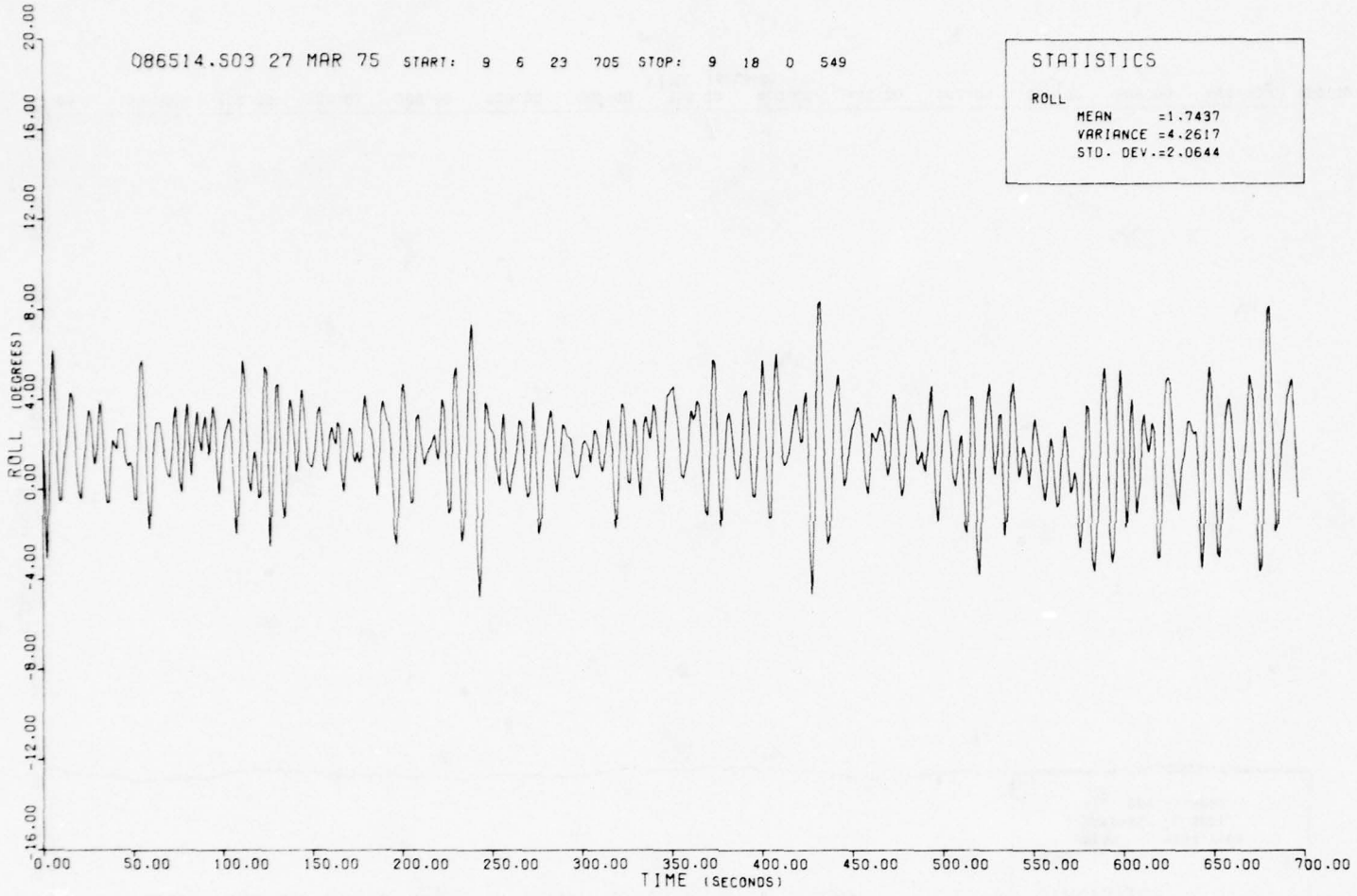

FIGURE 5-14. TIME PLOT OF THE SHIP'S ROLL

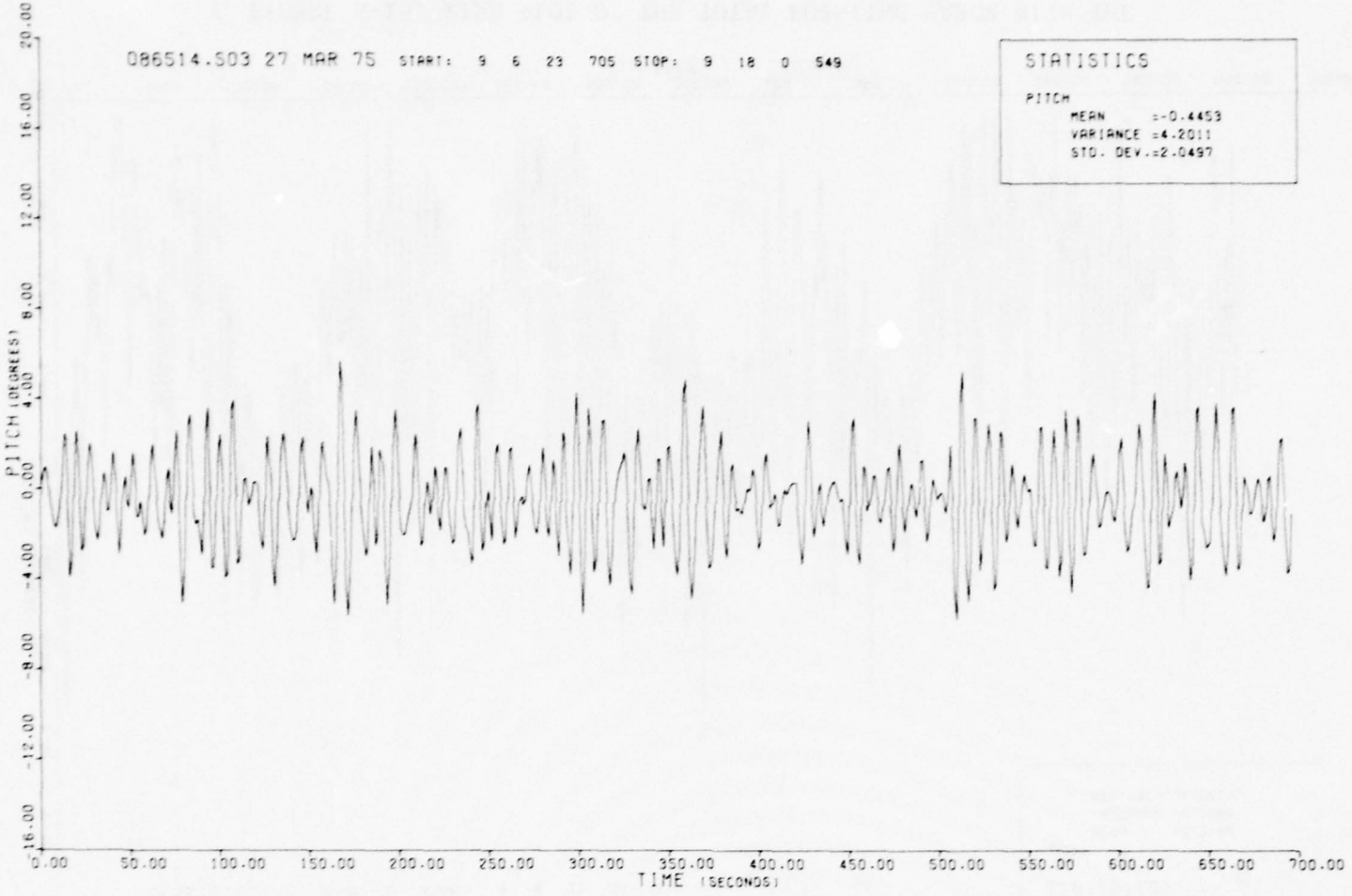

FIGURE 5-15. TIME PLOT OF THE SHIP'S PITCH

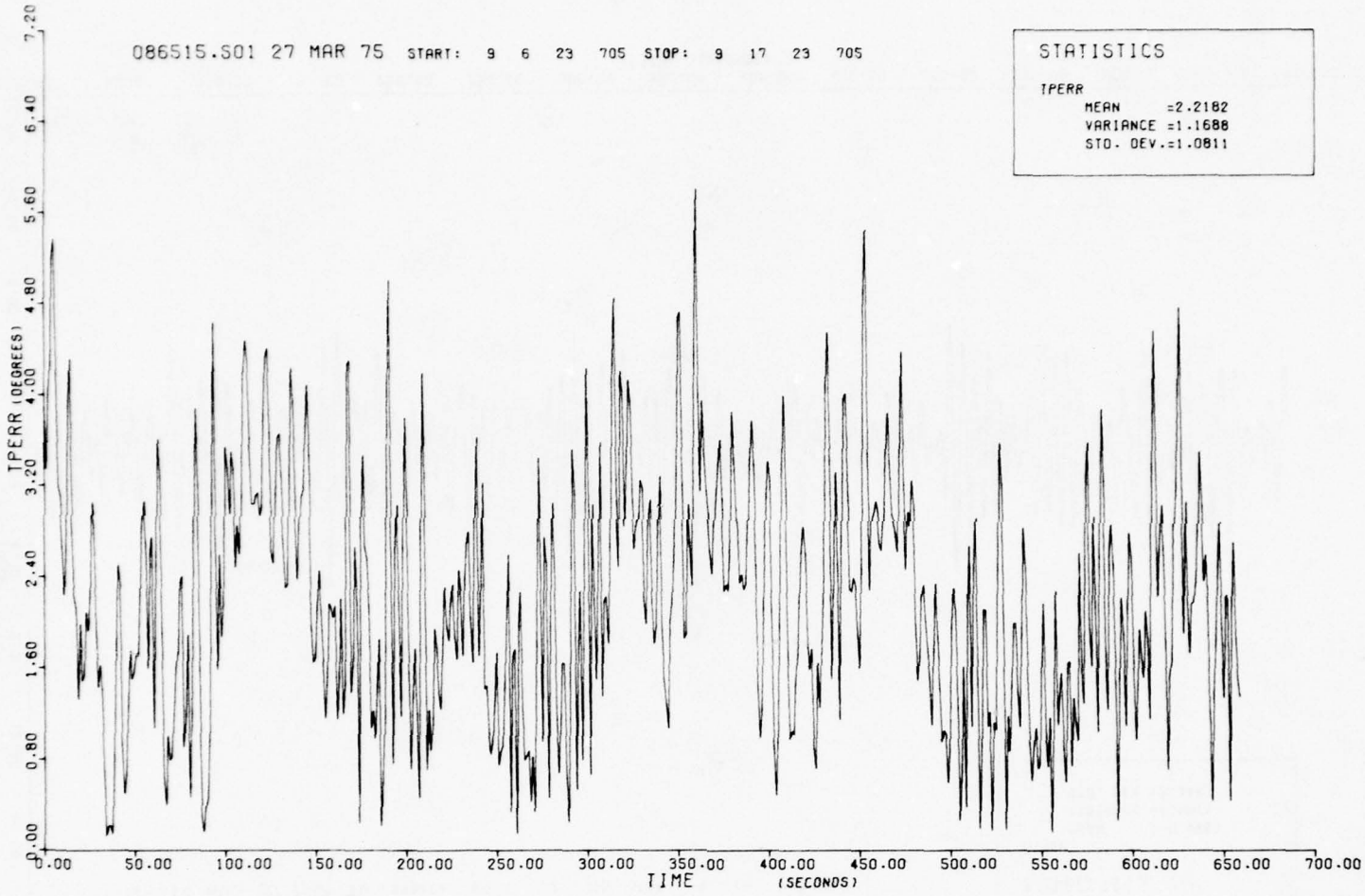

FIGURE 5-16. TIME PLOT OF THE TOTAL POINTING ERROR WITH THE STEERABLE ANTENNA IN THE SIMULATED REMOTE MODE

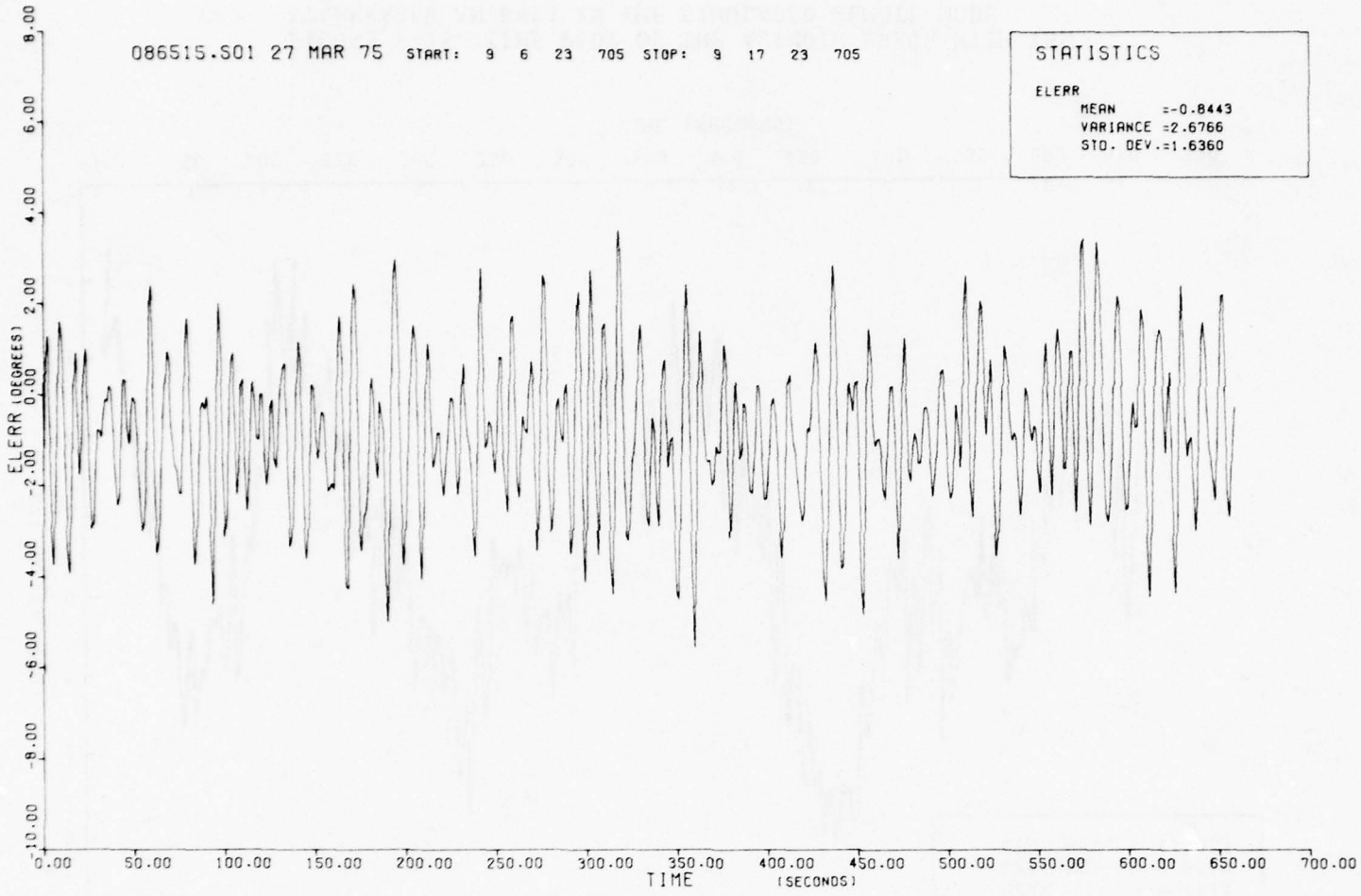

FIGURE 5-17. TIME PLOT OF THE ELEVATION ANGLE ERROR WITH THE STEERABLE ANTENNA IN THE SIMULATED REMOTE MODE

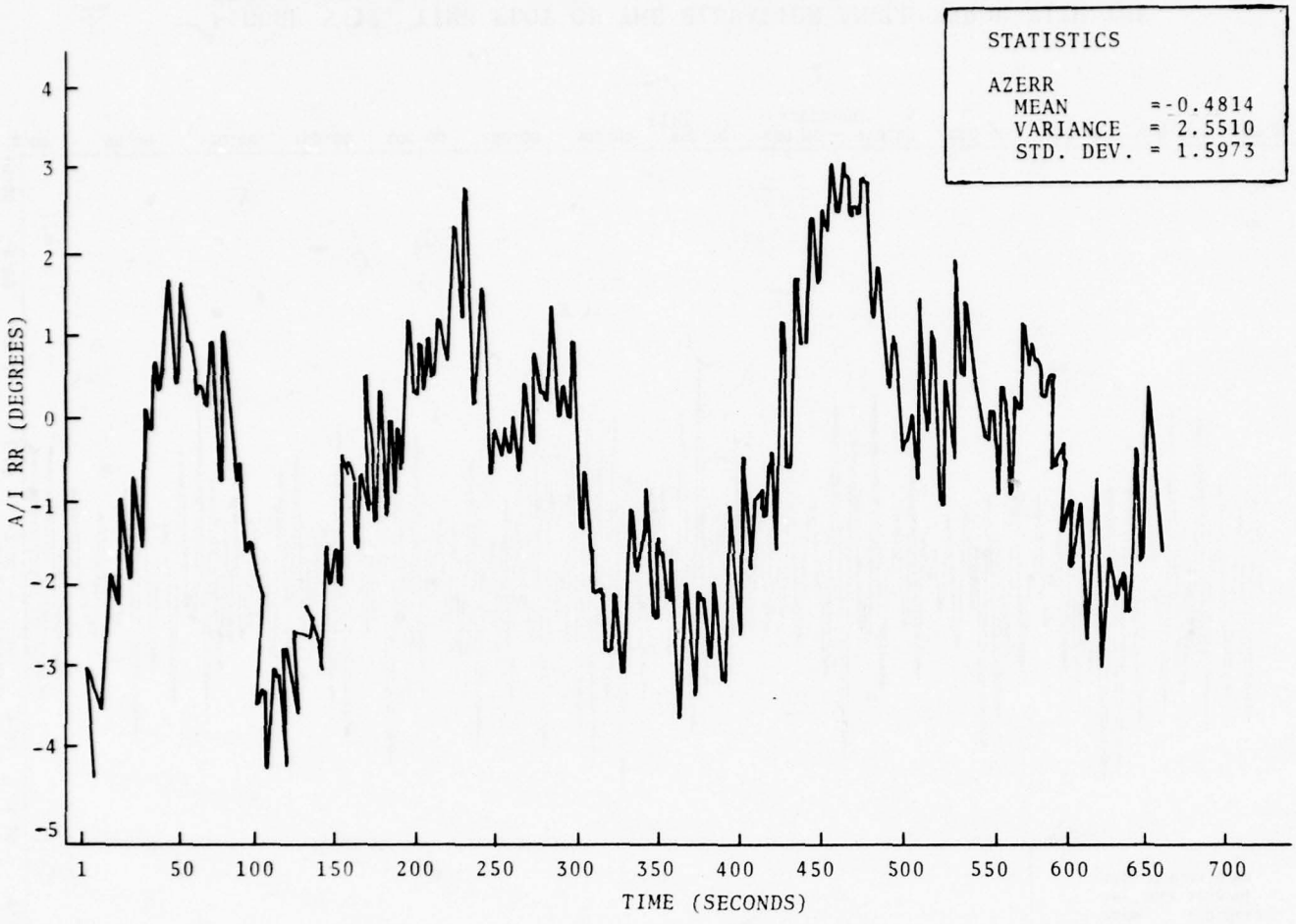

FIGURE 5-18. TIME PLOT OF THE AZIMUTH ERROR WITH THE STREERABLE ANTENNA IN THE SIMULATED REMOTE MODE

The autotrack mode was used on the same day, March 27. The performance of this mode is illustrated in Figures 5-10 to 5-12. The corresponding ship's motion is shown in Figures 5-13 through 5-15. The ship's course was approximately fixed at 290° during this test run. Figures 5-16 through 5-18 show antenna pointing errors under simulated remote conditions. The corresponding figures of merit for the autotrack run are $F_{AZ} = 0.76$ and $F_{EL} = 0.64$. We note that under the conditions of low elevation angle (9.5°) and medium sea state (6-ft wave height) the slave mode was more effective in providing antenna stabilization than was autotrack. In this particular case, the multipath was relatively severe with little antenna discrimination against the multipath and with the specular point occurring within approximately 1 dB of the peak of the difference pattern (see Figure 2-14). The C/M ratio measured during this run was 11 dB.

Table 5-1 summarizes the antenna data obtained during the spring tests. (Reduced data are not available for the fall test series because of a nonlinearity in the roll amplifier used to provide gyrocompass signals to the antenna during those tests.) Data for tests during which the ship was following a circular course are presented separately for time intervals during which the relative bearing to the satellite was within $\pm$ 45° of the bow. This test provided signal levels and multipath data when the view of the satellite was obstructed by the ship's superstructure. In addition, signal reflections from the ship's superstructure were expected to be present in this test. The antenna was located near the stern of the ship with an unobstructed view of the satellite in all directions except forward. The geometry was such that the elevation angle from the antenna to the top of the air search radar located at the top of the aft mast was 28° and the elevation angle to the top of the exhaust stacks was 8°. Looking forward into the ships superstructure, the view in azimuth below 8° elevation was limited by the exhaust stacks, which subtended an angle of $\pm$ 10-1/2° from the bow. Consequently, for satellite elevation angles below 8° and with relative bearings of $\pm$ 45°, scattering from the exhaust stacks would originate at approximately 35° off boresight, which is at least -15

TABLE 5-1. SUMMARY OF ANTENNA POINTING PERFORMANCE - SPRING 1975

WAVE HEIGHTS	1 FT to 20 FT
SATELLITE ELEVATION ANGLES:	8.7° to 39°
C/M RATIOS:	6.9 dB to 21.2 dB*
HEADING σ:	0.6° to 3.6°
ROLL σ :	1.1° to 5.2° (PEAK ROLL=17.5°)
PITCH σ :	0.5° to 2.0°

FIGURE OF MERIT	SLAVE	AUTOTRACK
F (AZIMUTH)	1.0° to 8.5°, Av.=3.5°	0.5° to 1.4°, Av.=1.0°
F (ELEVATION)	1.3° to 5.3°, Av.=2.1°	0.5° to 0.8°, Av.=0.6°
MAXIMUM POINTING ERROR WHILE LOCKED	3.3° to 8.4°, Av.=5.2°	9.9° to 14.8°, Av.=11.9°

*C/M ranged from 10.3 dB to 13.1 dB during autotrack measurements.

dB down on the antenna sum pattern and outside of the peaks of the difference pattern. Specific comments for data taken with the relative bearing to the satellite within ± 45° of the bow are presented separately in Section 5.2.2. The following general observations may be made from an examination of the data presented in Table 5-1:

1. The slave mode of antenna stabilization generally gave superior performance to that of the autotrack mode. Figures of merit were always greater than unity for slave while they averaged only 1.0 (azimuth) and never exceeded 0.8 (elevation) when the antenna was operated in the autotrack mode.

2. The maximum total pointing error never exceed 8.4° in slave versus 14.8° in autotrack. Thus the slave mode of operation was capable of maintaining the satellite within the -1 dB contour of the sum pattern (approximately 11° off boresight). The maximum

pointing error in the autotrack mode ranged from 9.9° to 14.8° over 13 runs of approximately 10 min duration each. The average value of the 13 peak pointing errors (i.e., maximum values for each run) was 11.9°. This corresponds very closely to the -1 dB contour of the antenna pattern.

5.2.1 Spring 1975 Test Program

This section presents a more detailed summary of the antenna data collected during the spring 1975 tests. Data are presented for 6 days representing low, intermediate, and high satellite elevation angles and covering a wide range of sea conditions. In certain instances in the slave mode the antenna was intentionally pointed at double (2θ), half ($\theta/2$), and one-quarter ($\theta/4$) of the satellite elevation angle. These tests allowed us either to reject multipath (2θ) or enhance ($\theta/2$ and $\theta/4$) the effect of multipath scattering from the ocean surface. The tests were generally run with the ship either following a circular course (360° in approximately 10 minutes) or steaming with the relative bearing of the satellite approximately $\pm$ 90° from the bow. In certain tests, however, the ship maintained a constant heading with the relative bearing of the satellite significantly different from $\pm$ 90°. These runs are denoted "constant heading" in Tables 5-2 through 5-7. Specific comments with respect to individual test days are given below.

5.2.1.1 February 26, 1975 (Table 5-2) - The 17- to 20-ft wave encountered on February 26th were substantially greater than those experienced during the other test days for which valid antenna data are available. The standard deviation of the ship's roll generally ranged from 1° to 3° during the March and April tests, while two of the three runs on February 26th were made with roll standard deviation of 5° or greater, with peak rolls exceeding 14°. Correspondingly, the standard deviation of the elevation error in the slave mode was greatest during the February tests. Antenna performance was plotted during 1-minute time segments centered on the times at which maximum roll amplitudes were encountered during the February

TABLE 5-2. DATA SUMMARY FOR FEBRUARY 26, 1975

SATELLITE ELEVATION ENGLE: 39°

SATELLITE AZIMUTH: 212°

WAVE HEIGHT: 17 FT - 20 FT

SHIP'S COURSE	ANTENNA MODE	C/M (dB)	HEADING		ROLL	PITCH	TPERR		AZERR		ELERR		F_{AZ}	F_{EL}	MAX TPERR	TEST DURATION (MIN: SEC)
			MEAN	σ	σ	σ	MEAN	σ	MEAN	σ	MEAN	σ				
⊥	SLAVE/θ	-	123.2°	2.3°	5.0°	1.1°	2.4°	1.3°	-1.1°	1.2°	0.4°	2.3°	2.1	2.1	6.9°	10:00
		21.2	124.1°	1.9°	3.4	1.2	2.1	1.1	-0.9	1.3	0.5	2.0	1.7	1.7	5.3	
			103.0°	3.2°	5.2	1.0	2.8	1.2	-2.1	1.2	0.6	2.3			6.2	

tests. The plots for one of these time segments are presented in Section 5.1.3 and correspond to the first entry in Table 5-2. In this case, the maximum roll amplitude was 14.3° versus a standard deviation of 5.0° for the entire 10-minute run. While the roll amplitude was only about half of the maximum (30°) set forth in the antenna design goals, the roll velocity reached 9.2°/s and the roll acceleration reached 7.8°/s^2 versus design goals of 15°/s and 7.5°/s^2, respectively. Consequently, the antenna data presented in Table 5-2 are representative of a reasonably severe test of the antenna's slave stabilization system. Although operation of the antenna in the autotrack mode was attempted on February 26, successful tracking could not be achieved. The reason for failure of the autotrack system to track under the favorable multipath conditions (C/M = 20 dB) created by the high satellite elevation angle of 30° is unknown at the present time.

5.2.1.2 March 24, 1975 (Table 5-3) - The data for March 24 are primarily representative of autotrack operation at a low satellite elevation angle (8.7°) under smooth sea conditions (1 to 2 ft wave heights). Ship motion was very limited, with standard deviations of the ship's heading, roll, and pitch of only 1.1° to 2.7°, 2.1° to 1.5° and 0.5°, respectively. Under these conditions, the autotrack system was able to maintain reasonably good antenna stability with standard deviations of the antenna error in azimuth and elevation ranging from 1.1° to 2.3° and 2.1° to 2.5°. These values are, however, inferior to the 0.5° and 1.2° values achieved in slave operation, and the figures of merit are approximately half of the corresponding values for slave operation. Note that the mean total pointing errors in autotrack are approximately three times the slave value, primarily due to the mean elevation error of approximately 5" on autotrack. This error appears consistent with the mean elevation error values of approximately + 3° for the autotrack data on March 27 (Table 5-4) and 4.6° on April 3 (Table 5-7). It is believed to be due to a combination of mechanical misalignment and electrical biases producing an offset between the null of the antenna difference pattern and the antenna elevation

TABLE 5-3. DATA SUMMARY FOR MARCH 24, 1975

SATELLITE ELEVATION ANGLE: 8.7°

SATELLITE AZIMUTH: 254.3°

WAVE HEIGHT: 1 FT-2 FT

SHIP'S COURSE	ANTENNA MODE	C/M (dB)	HEADING		ROLL	PITCH	TPERR		AZERR		ELERR		F_{AZ}	F_{EL}	MAX. TPERR	TEST DURATION (MIN: SEC)
			MEAN	σ	σ	σ	MEAN	σ	MEAN	σ	MEAN	σ				
⊥	SLAVE/θ		344°	-	1.6°	0.5°	2.2°	0.6°	-1.8°	0.5°	0.2°	1.2°	2.4	1.3	4.1°	9:09
↓	AUTOTRACK	13.1	344.7	1.1	1.5	0.5	6.4	2.2	-1.5	1.3	6.0	2.4	0.9	0.6	13.0	10:00
	↓	12.9	345.1	1.7	1.4	0.5	6.0	2.1	-1.5	2.3	5.2	2.5	0.8	0.6	11.9	↓
		11.0	343.8	1.4	1.3	0.5	5.3	1.9	-1.3	1.3	4.9	2.1	1.1	0.6	11.3	
		10.8	343.9	1.3	1.2	0.5	5.2	1.9	-0.8	1.1	5.0	2.1	1.2	0.6	11.5	
		10.7	344.3	1.7	1.2	0.5	5.3	1.8	-1.7	1.3	4.7	2.1	1.3	0.6	11.9	
↓	↓	10.3	345.5	2.7	1.4	0.5	5.7	2.1	-2.0	2.1	5.0	2.4	1.3	0.6	12.4	

based upon the ship's gyrocompass and the antenna syncho outputs. Such biases are not considered to be of particular interest because they are easily calibrated out and are neglected in the computations of the figures of merit, which involve only the standard deviations of the azimuth and elevation errors wherein the mean values are subtracted out. Operation of the autotrack system represented in Table 5-3 is considered quite adequate for maintaining the satellite within the -1 dB antenna pattern contour. Note that C/M was approximately 11 dB during these runs. This is a rather moderate carrier-to-multipath ratio and does not represent particularly severe multipath conditions.

5.2.1.3 March 27, 1975 (Table 5-4) - The data from March 27 provide an interesting comparison to the autotrack data of March 24. The satellite elevation angle was fairly low, 9.5° versus 8.7° on March 24, but the sea was considerably rougher, with wave heights of 6 ft reported from the bridge and a wind speed of 30 knots versus 20 knots reported on March 24. Note that C/M was approximately 11 dB as on March 24, but that the standard deviations of the pointing errors in azimuth and in elevation were somewhat greater, averaging 2.2° and 2.9° versus 1.6° and 2.3° for azimuth and elevation, respectively. While the values are adequate to meet the -1 dB antenna pattern requirements, we note that again slave stabilization provided lower pointing error standard deviations by approximately a factor of two.

5.2.1.4 March 31, 1975 (Table 5-5) - The tests represented by the data of Table 5-5 were run at a moderate satellite elevation angle, 17°, and with relatively calm sea conditions. All these were run with the antenna operating in the slave mode. The first six tests were conducted with the ship steaming on a circular course. In the first test, the antenna was pointing at twice the satellite elevation angle, 2θ. This placed the satellite on the -3 dB contour of the antenna pattern and provided significant (greater than 14 dB) discrimination against multipath scattering from the ocean surface. The second and third tests were run with the antenna pointing at

TABLE 5-4. DATA SUMMARY FOR MARCH 27, 1975

SATELLITE ELEVATION ANGLE: 9.5°

SATELLITE AZIMUTH: 253.9°

WAVE HEIGHT: 6 FT

SHIP'S COURSE	ANTENNA MODE	C/M (dB)	HEADING MEAN	HEADING σ	ROLL σ	PITCH σ	TPERR MEAN	TPERR σ	AZERR MEAN	AZERR σ	ELERR MEAN	ELERR σ	F_{AZ}	F_{EL}	MAX. TPERR	TEST DURATION (MIN: SEC)
⊥	SLAVE/θ	-	345.6°	1.8°	4.8°	1.4°	5.1°	1.0°	4.5°	0.8°	-1.3°	2.1°	2.2	2.3	8.4°	9:00
CONST. HDNG	"	10.3	294.8	2.2	2.1	1.7	3.7	0.6	3.3	0.6	-1.5	0.9	3.8	1.7	5.5	10:00
↓	AUTOTRACK	11.0	294.7	1.5	2.1	2.0	3.9	1.9	-2.6	2.6	1.1	2.1	0.6	0.8	10.0	11:37
↓	↓	11.1	294.5	2.4	2.5	2.0	4.6	2.1	-1.8	2.0	3.2	2.9	1.3	0.7	13.2	10:00
↓	↓	11.1	295.0	2.2	2.0	1.9	4.3	1.9	-1.7	1.6	3.2	2.5	1.4	0.6	9.9	6:15
↓	↓	-	295.3	1.3	2.4	1.7	4.8	1.6	0.8	3.1	-1.2	3.8	0.5	0.5	12.0	10:00
↓	↓	-	293.6	1.4	2.9	1.8	5.4	2.1	-2.1	1.6	4.2	2.9	0.9	0.7	12.2	↓
↓	↓	-	294.9	2.5	2.6	1.5	5.1	2.3	-1.8	2.0	3.9	3.1	1.3	0.6	14.8	↓

TABLE 5-5. DATA SUMMARY FOR MARCH 31, 1975

SATELLITE ELEVATION ANGLE: 17°

SATELLITE AXIMUTH: 245°

WAVE HEIGHT: 2 FT

SHIP'S COURSE	ANTENNA MODE	C/M (dB)	HEADING MEAN	HEADING σ	ROLL σ	PITCH σ	TPERR MEAN	TPERR σ	AZERR MEAN	AZERR σ	ELERR MEAN	ELERR σ	F_{AZ}	F_{EL}	MAX. TPERR	TEST DURATION (MIN: SEC)
		12.8														
CIRCU-LAR	SLAVE 2θ	15.5	-	-	1.7°	0.7°	2.0°	0.9°	-1.5°	1.3°	0.7°	1.2°	N/A	N/A	5.5°	6:00
↓	SLAVE θ	16.4	-	-	2.1	0.8	3.7	1.0	-1.4	1.1	3.2	1.2	↓	↓	6.6	6:14
	"	14.9*	-	-	1.1	0.9	3.2	0.8	-1.1	0.5	3.0	0.8			5.2	2:06
	SLAVE θ/2	11.1	-	-	2.1	0.8	1.9	0.8	-0.9	1.0	1.3	1.0			4.2	4:06
	SLAVE θ/4	6.9*	-	-	1.9	0.8	2.5	0.7	-1.4	0.5	-2.0	0.9			5.0	2:07
	"	9.8	-	-	2.1	0.6	3.5	1.1	-2.0	0.8	-2.7	1.1			6.7	3:51
↓	SALVE θ/2	11.5	344.2	3.3	1.7	0.7	1.5	1.0	0.2	0.4	-1.3	1.2	8.5	1.4	4.1	9:05
	↓	11.7	345.5	2.4	1.8	0.8	1.1	0.7	0.2	0.4	0.1	1.2	6.0	1.5	3.3	10:00
		11.3	347.6	2.4	3.1	0.8	1.3	0.8	0.2	0.5	0.1	1.5	4.8	2.0	5.1	8:12

the satellite elevation angle, θ, which placed the horizon on the -3 dB antenna pattern contour. The fourth test was run with the antenna elevation angle set to one-half of the satellite elevation angle. The fifth and sixth tests were run with the antenna elevation angle set to only one-quarter of the satellite elevation angle, thereby enhancing the effect of multipath scattering from the ocean surface. The increased effect of the multipath is evidenced in the lower values of C/M measured at the lower antenna elevation angles. The lower value of C/M associated with operation at twice the satellite elevation angle is believed to be due to the increased change in antenna gain in the direction of the satellite as a function of pointing error resulting from operation off the center of the antenna pattern. (See Figure 2-14.) In none of the tests reported in Table 5-5 did the standard deviation of the antenna pointing error in azimuth or in elevation exceed 1.5° under the relatively smooth sea conditions on March 31. Table 5-5 also contains data from runs where the relative bearing of the satellite is within $\pm$ 45° of the bow (indicated with an asterisk). Specific comments concerning the effect of satellite blockage by the superstructure are given in Section 5.2.2, and the effect of operating off the antenna pattern boresight is discussed in Section 5.3.1.

5.2.1.5 April 2, 1975 (Table 5-6) - The data presented in Table 5-6 were gathered at a moderate (20.4°) satellite elevation angle, but under somewhat rougher sea conditions (wave height of 5 ft versus 2 ft) than that presented in Table 5-5. As with the March 31 data, the antenna was operated in the slave mode; however, in this instance, the ship was following a straight-line course and the antenna was boresighted on the satellite elevation angle. As can be seen from the table, C/M values were quite high (18 to 20 dB) and antenna stabilization was quite adequate. Again, the standard deviations of the antenna pointing errors in azimuth and in elevation did not exceed 1.5°, nor did the maximum total pointing error exceed 5°.

TABLE 5-6. DATA SUMMARY FOR APRIL 2, 1975

SATELLITE ELEVATION ANGLE: 20.4°

SATELLITE AZIMUTH: 242.1°

WAVE HEIGHT: 5 FT

SHIP'S COURSE	ANTENNA MODE	C/M (dB)	HEADING		ROLL	PITCH	TPERR		AZERR		ELERR		F_{AZ}	F_{EL}	MAX. TPERR	TEST DURATION (MIN: SEC)
			MEAN	σ	σ	σ	MEAN	σ	MEAN	σ	MEAN	σ				
⊥	SLAVE θ	18.7	323.6°	1.8°	2.4°	0.7°	2.0°	0.7°	-1.2°	0.7°	1.2°	1.4°	2.7	1.7	4.8°	9.59
↓	↓	20.2	322.3	1.0	2.9	1.1	1.8	0.9	1.0	0.7	-0.6	1.5	1.4	5.3	4.8	10:00
↓	↓	-	322.8	0.7	3.4	1.1	1.9	1.1	1.0	0.8	-0.6	1.5	1.0	2.3	4.9	↓
CONST. HDGS	↓	18.3	300.0	2.6	3.0	1.1	1.5	1.1	1.0	0.8	-0.7	0.9	3.1	3.0	3.9	↓
↓	↓	17.9	265.0	3.2	3.0	1.3	1.6	0.8	1.0	0.8	-1.0	1.0	3.7	1.7	1.7	↓
↓	↓	18.5	266.0	3.6	2.7	1.1	1.6	0.8	1.0	0.7	-1.0	0.9	4.9	1.7	1.7	↓

5.2.1.6 April 3, 1975 (Table 5-7) - Table 5-7 presents data for autotrack operation at a somewhat higher satellite elevation angle (27.5°) under moderately calm sea conditions (wave height = 2-1/2 feet). Although the figures of merit were only 0.6 and 0.5 for azimuth and elevation, respectively, the autotrack system maintained the satellite within the -1 dB antenna pattern contour throughout the test, and the standard deviation of the pointing errors in both azimuth and elevation remained less then 2°. Unfortunately, no carrier-to-multipath measurement was made on this run. Little multipath scattering into the antenna aperture would be expected at this relatively high elevation angle, and consequently, this test cannot be considered a severe test of the autotrack system.

5.2.2 Circular Course Antenna Data

The signal level or envelope of the CW signal was recorded along with antenna pointing data as the ship traveled through a circular course. These data were recorded to illustrate the effect of the ship's superstructure on the received signal level and to determine the antenna performance as it passes through the critical keyhole position. On March 31, the WHEC GALLATIN traveled in a circular path and recorded antenna and CW data. The antenna tracked the satellite, which was at a 17° elevation angle and was operating in its slave mode. Sea state conditions on March 31 were moderate, with 2-ft waves. The 17° elevation angle positioned the antenna boresight approximately half way up the radar mast when the antenna was pointed directly above the bow. Therefore, it is reasonable to assume that any fading in signal level while in this position was due to the radar mast. At 9:08:22.5 and 9:16:46, the ship's heading coincided with the satellite's azimuth, as shown in Figure 5-19. At these times, there appears to have been significant fades in the received signal envelope. Since the ship took only a few seconds to pass through the mast, the resolution of Figure 5-19, one sample per second, was not sufficient to measure the exact signal fade. Figures 5-20 and 5-21 show the same fading with 10 samples per second resolution. Both plots indicate a maximum fade depth of about 8 dB. A fade of this magnitude could

TABLE 5-7. DATA SUMMARY FOR APRIL 3, 1975

SATELLITE ELEVATION ANGLE: 27.5°

SATELLITE AZIMUTH: 233.9°

WAVE HEIGHT: 2-1/2 FT

SHIP'S COURSE	ANTENNA MODE	C/M (dB)	HEADING		ROLL	PITCH	TPERR		AZERR		ELERR		F_{AZ}	F_{EL}	MAX. TPERR	TEST DURATION (MIN: SEC)
			MEAN	σ	σ	σ	MEAN	σ	MEAN	σ	MEAN	σ				
CONST. HDNG.	AUTOTRACK	-	271.6°	0.6°	2.6°	1.0°	4.9°	1.8°	-0.8°	1.5°	4.6°	1.9°	0.6°	0.5°	10.7°	8:20

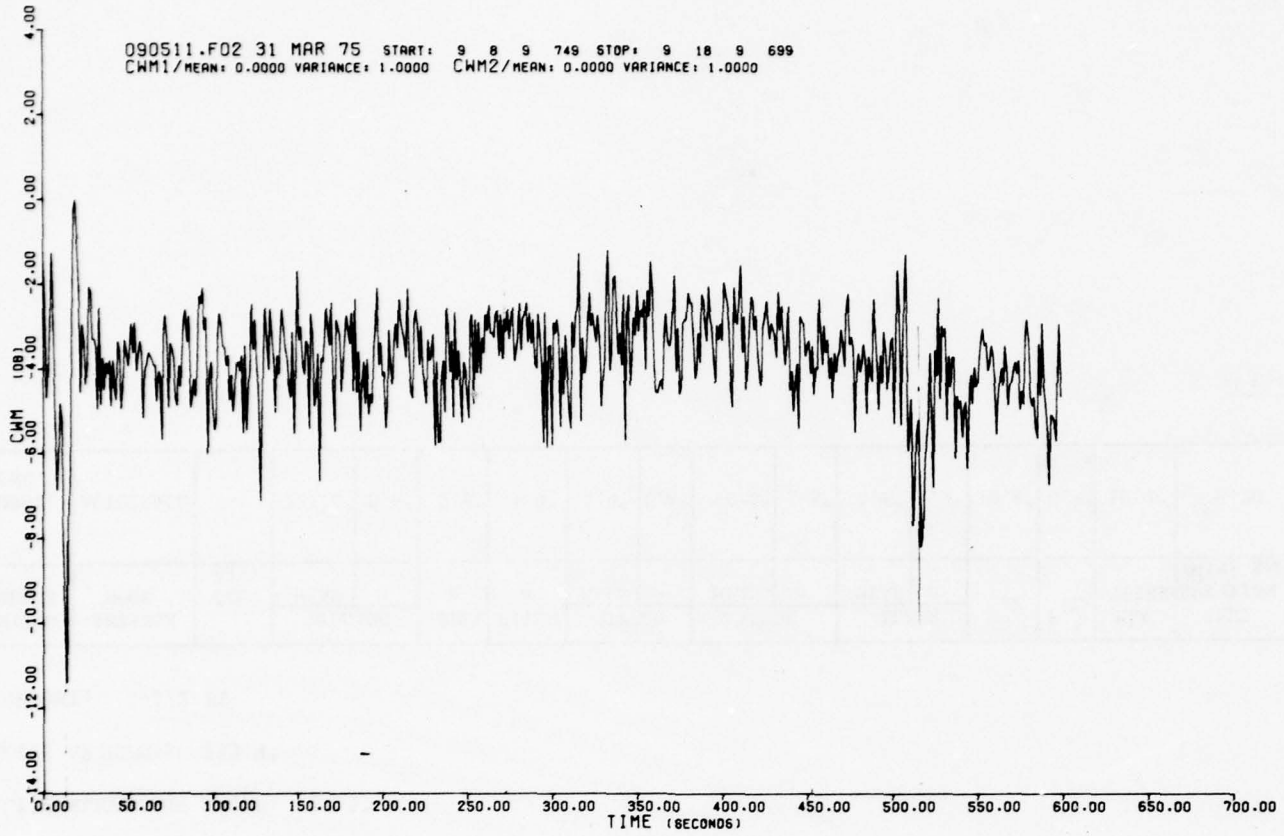

FIGURE 5-19. CIRCULAR COURSE ANTENNA DATA (31 MARCH 75). CW MULTIPATH

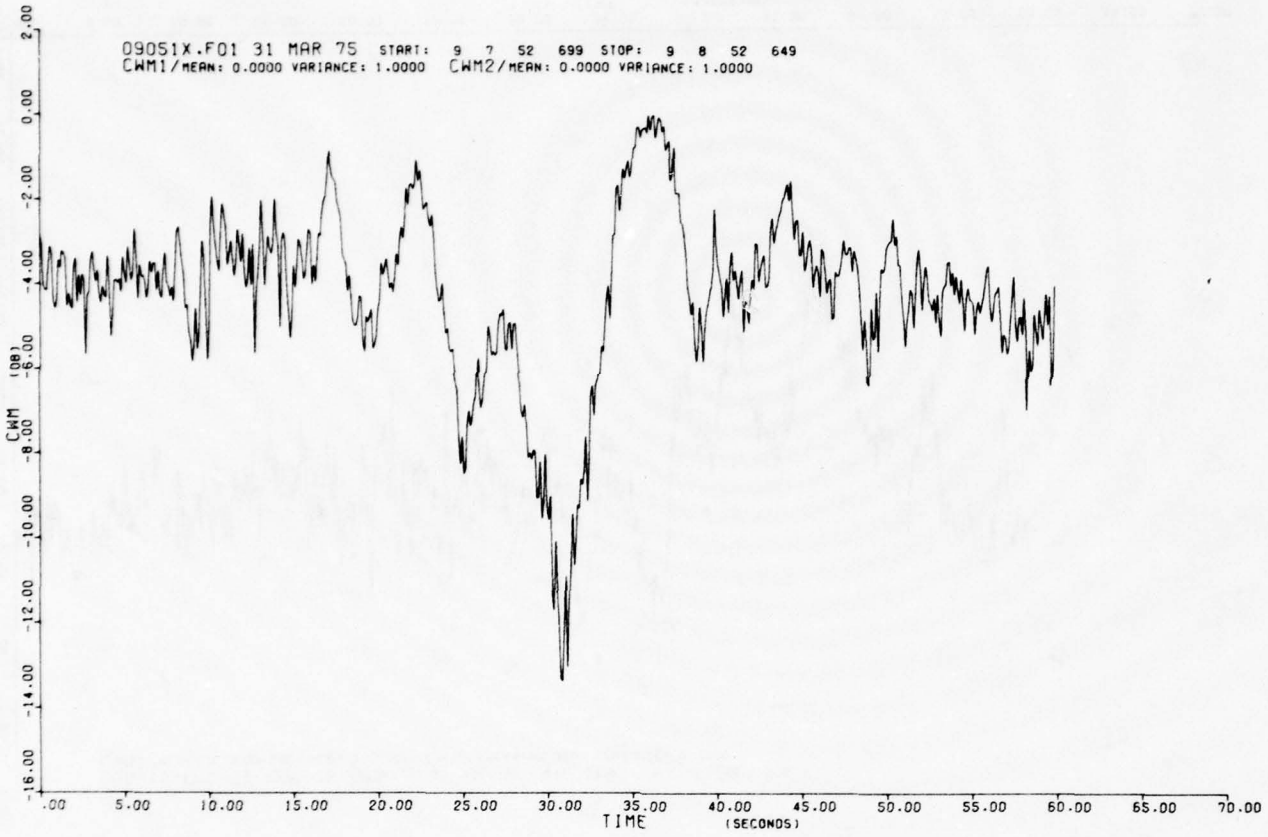

FIGURE 5-20. CIRCULAR COURSE ANTENNA DATA (31 MARCH 75), CW MULTIPATH

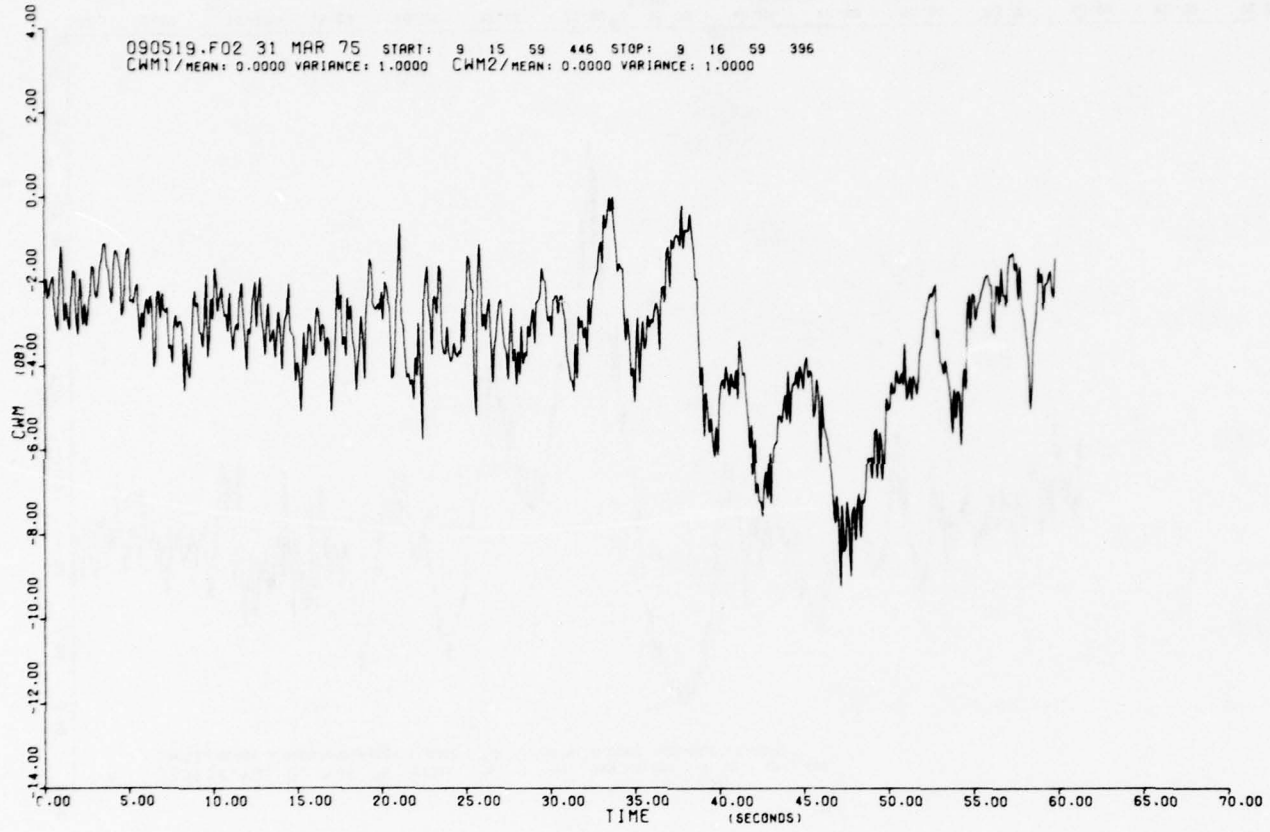

FIGURE 5-21. CIRCULAR COURSE ANTENNA DATA (31 MARCH 75). CW MULTIPATH

cause serious degradation performance of a satellite-to-ship communication link. Since deeper faded should occur at lower elevation angles, it appears that minimum elevation to the satellite should not go below 17° if satisfactory modem or autotrack performance is desired when the antenna is pointed at the ship's superstructure.

Figures 5-22 and 5-23 show the azimuth and elevation pointing errors over the time segment shown in Figure 5-19. Although there appears to be no significant variation on the elevation error as the antenna passes through the superstructure, the azimuth error has a noticeable shift in its mean value. Both the azimuth and elevation errors were sufficiently small such that the boresight error was always well within the required performance specifications. Since the antenna mount Z-axis was parallel to the ship's longitudinal axis a "keyhole" discontinuity in tracking accuracy is also expected, as the relative bearing of the antenna passes the ship's bow. Accordingly, we conclude from this test that the keyhole effect was not significant at these elevation angles.

5.2.3 Severe Roll Data

On February 26, the combination of rough seas and the ship's course resulted in the ship experiencing significant rolling. The log reported heavy rolls at approximately 7:53. A short segment of time (1 min) centered about 7:55:30 was examined to determine how well the antenna system performed. Figures 5-24 through 5-31 include the ship's dynamics and the antenna pointing errors. It can be seen that the antenna's total pointing error is well within the 11° requirement. During the given time interval, the ship experienced a maximum roll amplitude of approximately 14.3°. This was accompanied by a roll velocity and acceleration of approximately 9.2°/s and $7.8s^2$, respectively. Since the antenna was pointing off the starboard side, the X-axis had to undergo identical motion to maintain the small antenna pointing error. For sea state conditions that approach the maximum antenna performance specifications (roll velocity of 15°/s and roll acceleration of $7.5°/s^2$, the antenna in its slave mode stayed well within the design specifications.

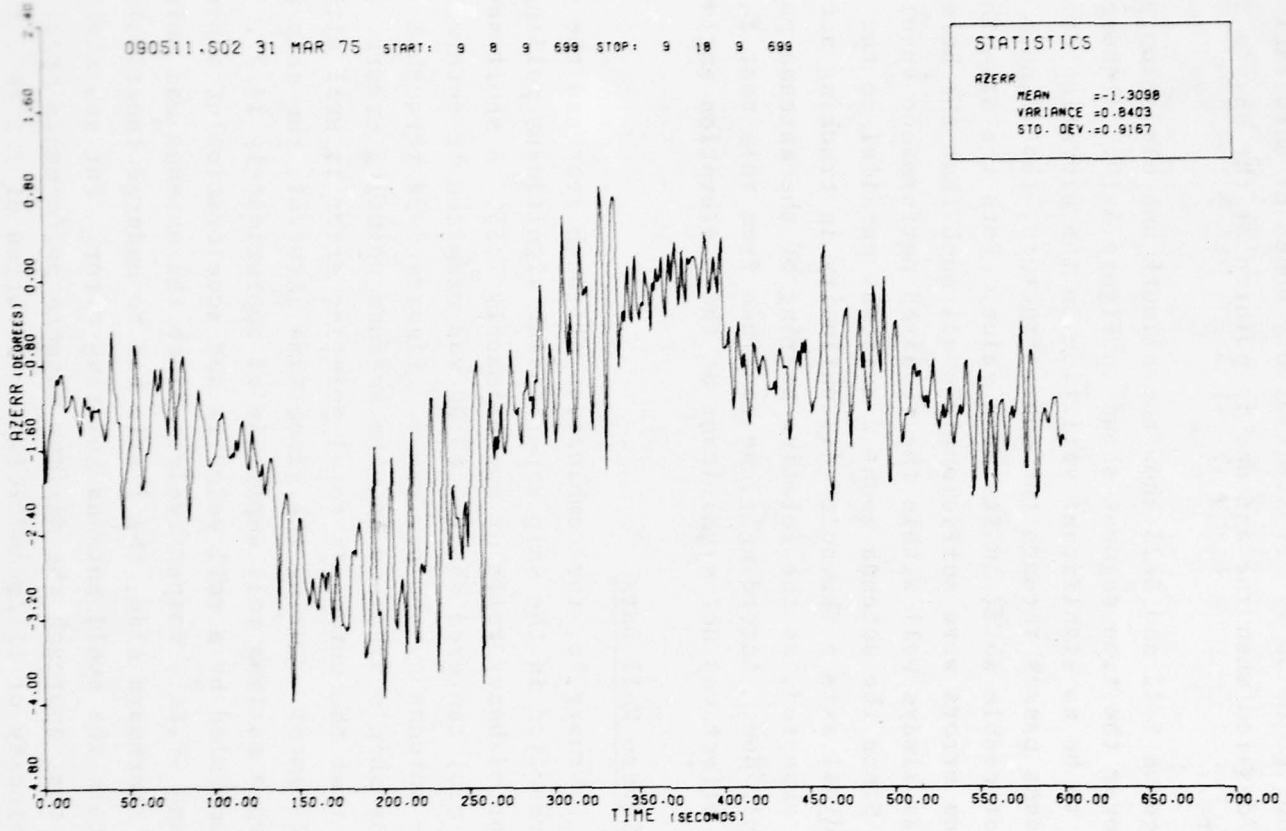

FIGURE 5-22. CIRCULAR COURSE ANTENNA DATA (31 MARCH 75). AZIMUTH ERROR

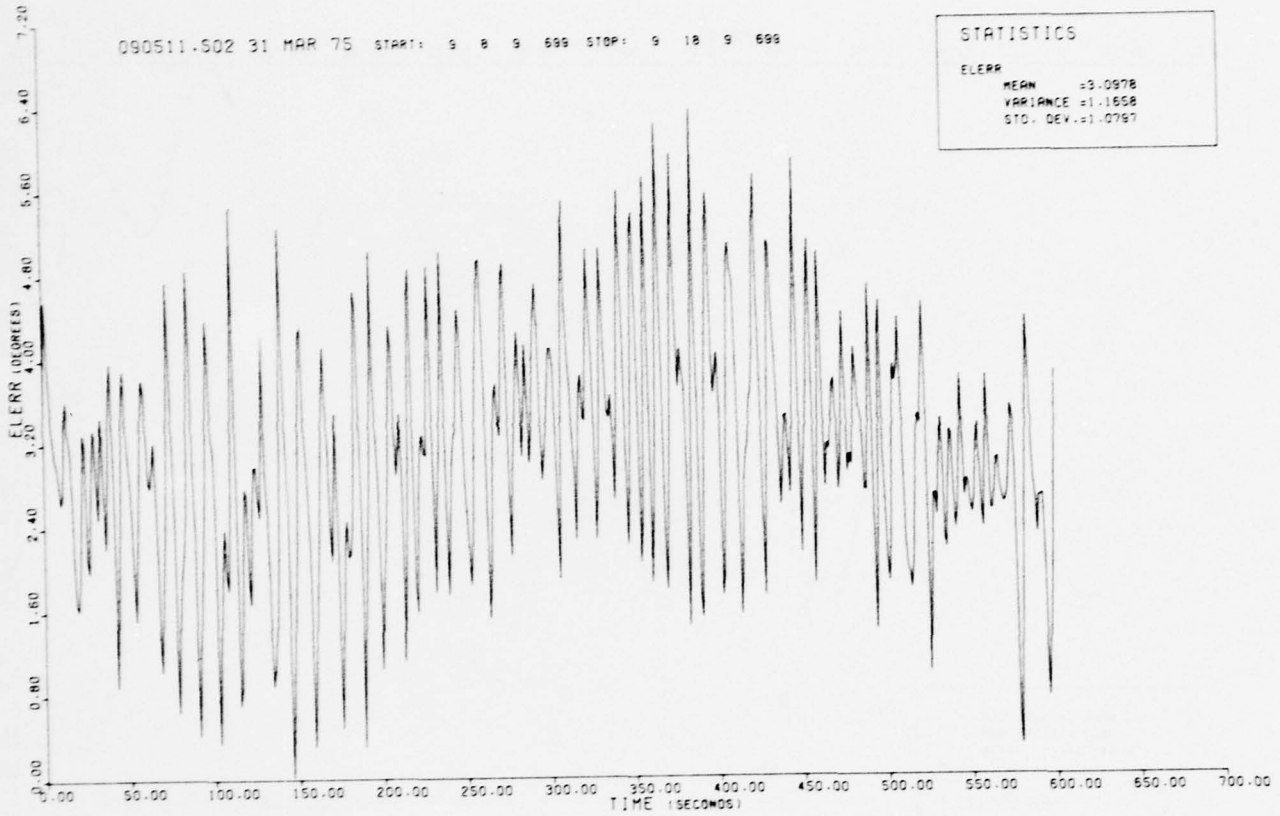

FIGURE 5-23. CIRCULAR COURSE ANTENNA DATA (31 MARCH 75), ELEVATION ERROR

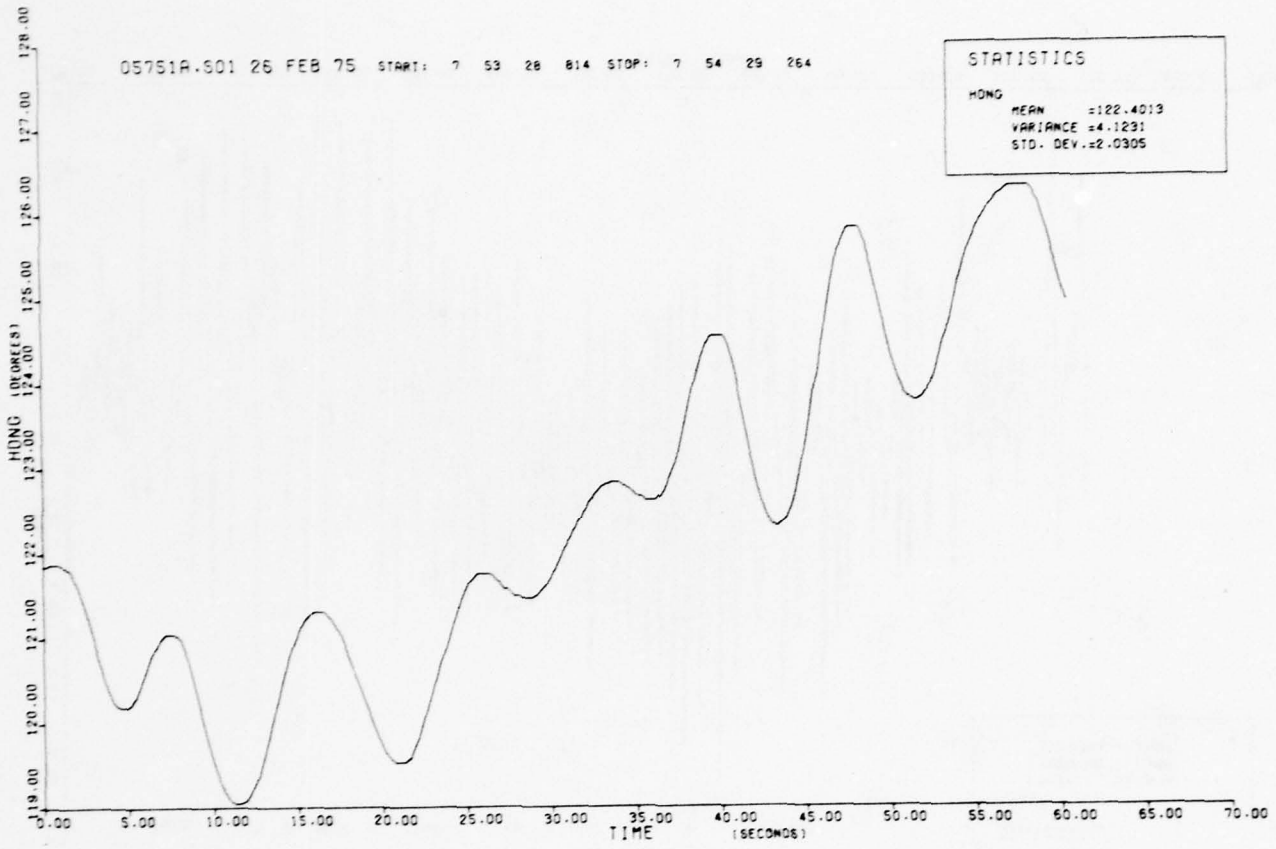

FIGURE 5-24. SEVERE ROLL DATA (26 FEBRUARY 75), HEADING

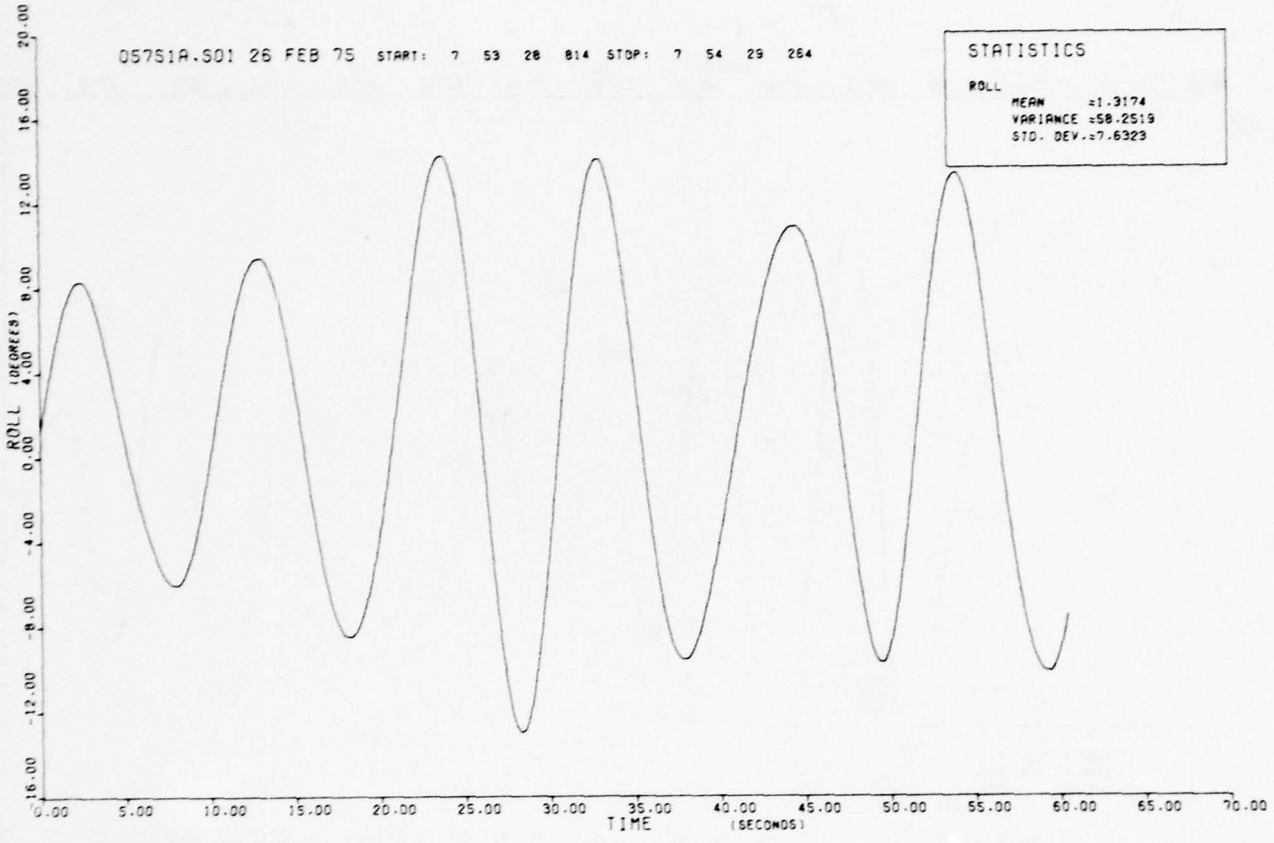

FIGURE 5-25. SEVERE ROLL DATA (26 FEBRUARY 75), ROLL

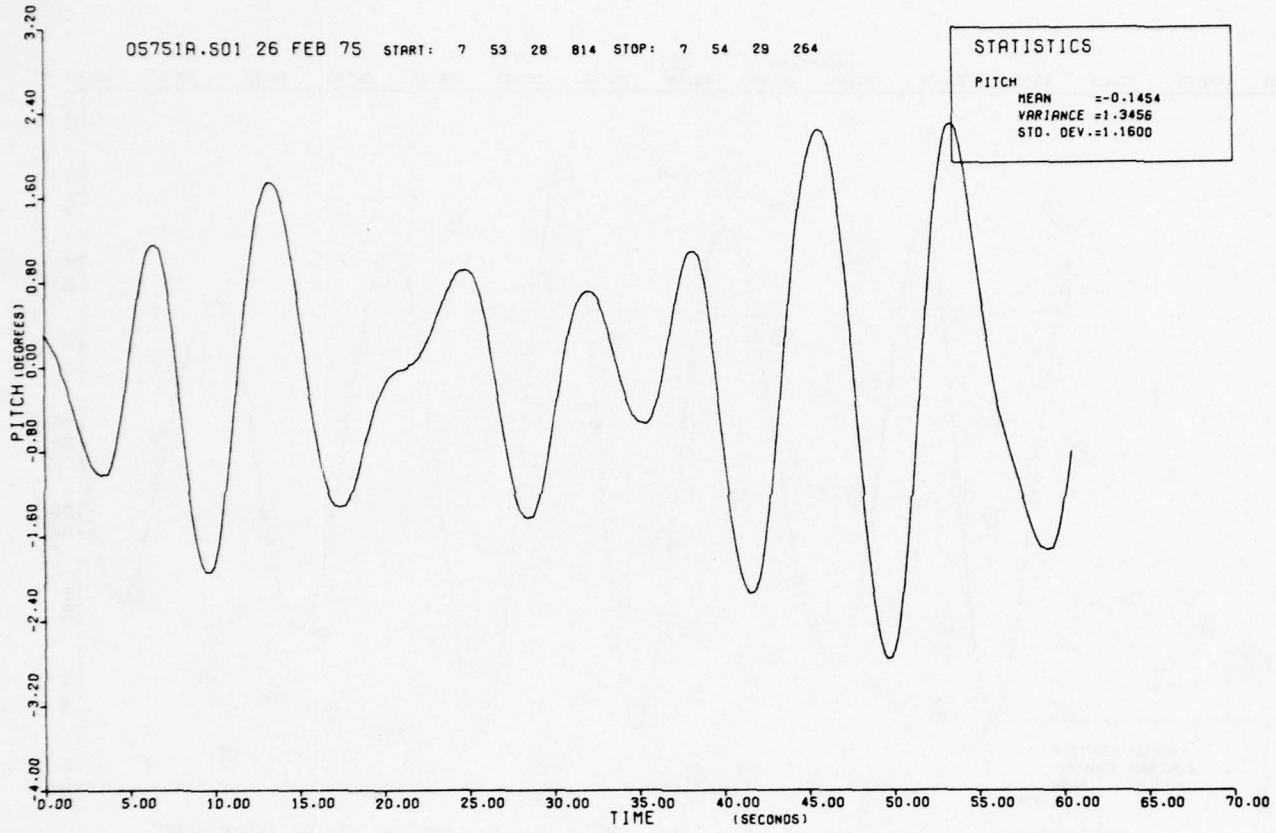

FIGURE 5-26. SEVERE ROLL DATA (26 FEBRUARY 75), PITCH

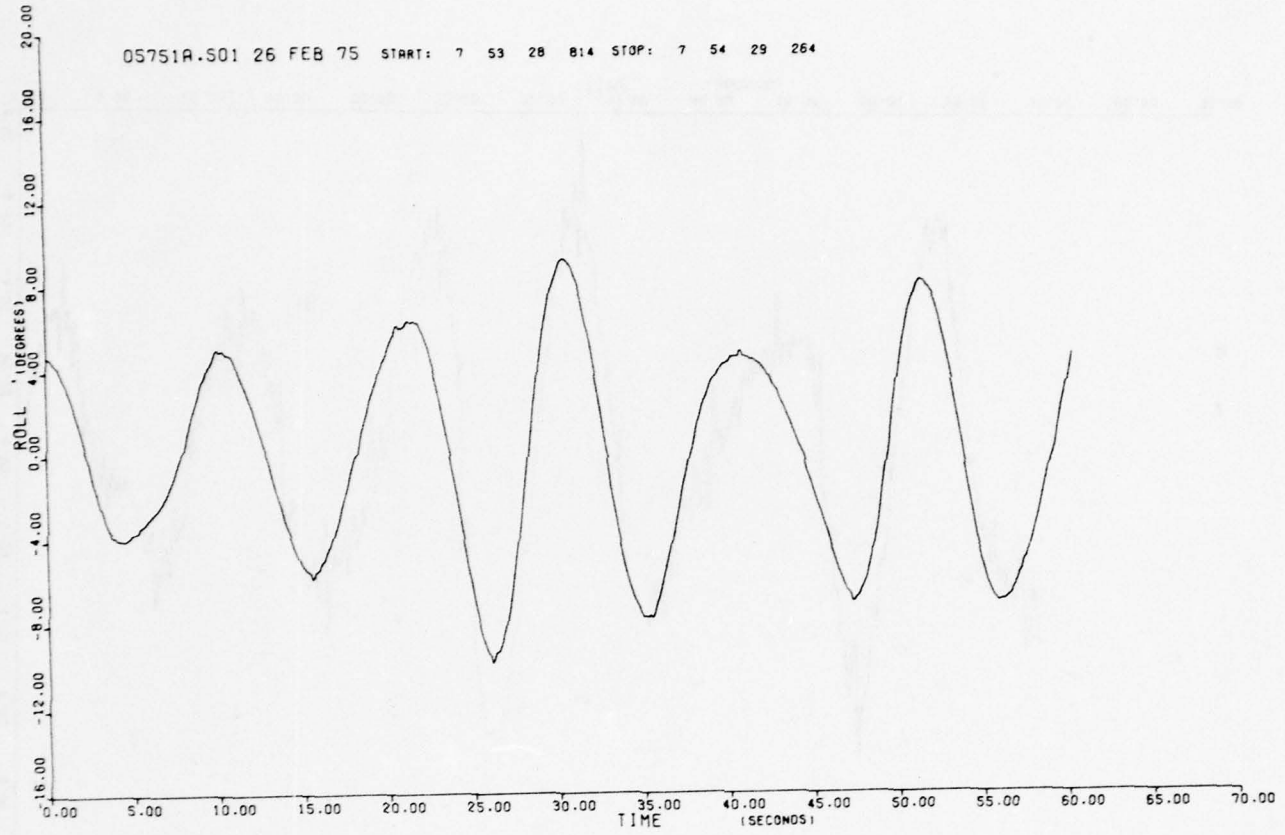

FIGURE 5-27. SEVERE ROLL DATA (26 FEBRUARY 75). FIRST DERIVATIVE OF THE ROLL

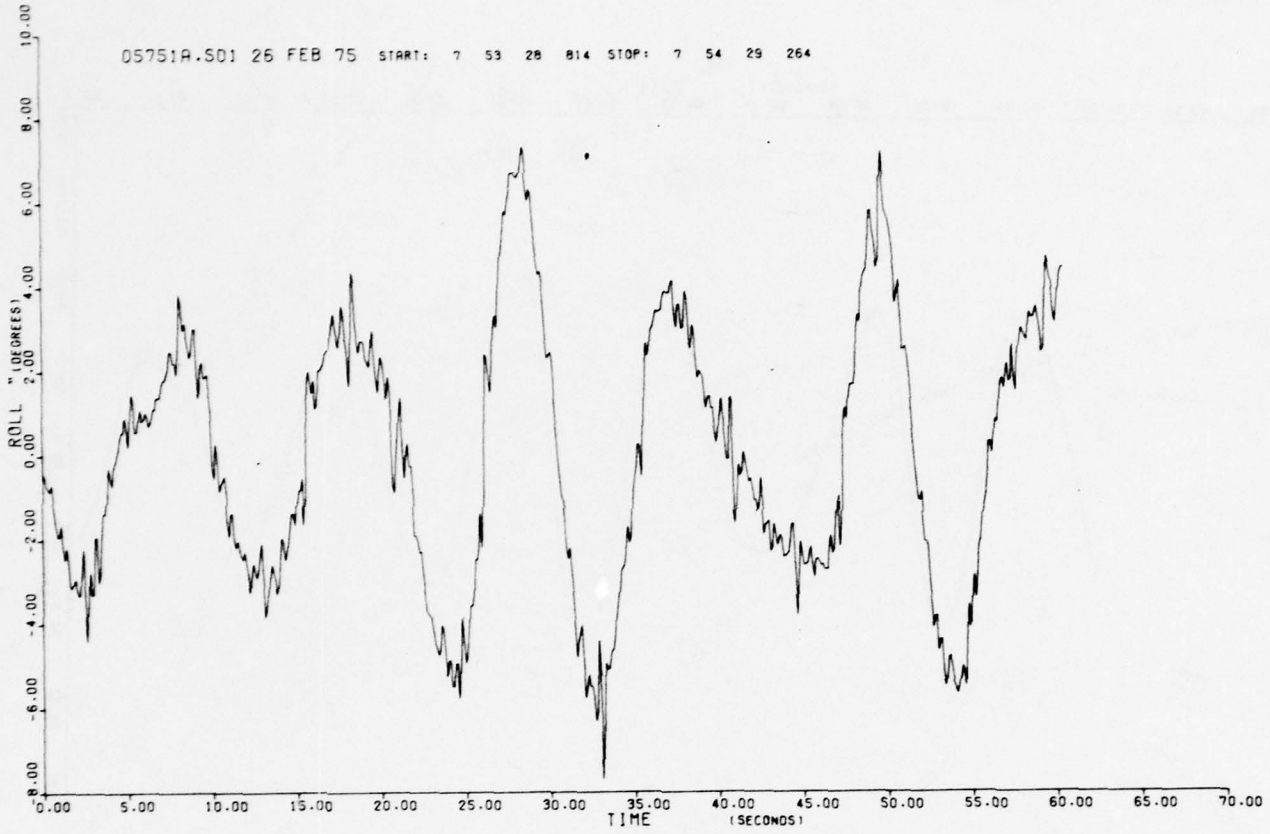

FIGURE 5-28. SEVERE ROLL DATA (26 FEBRUARY 75), SECOND DERIVATIVE OF THE ROLL

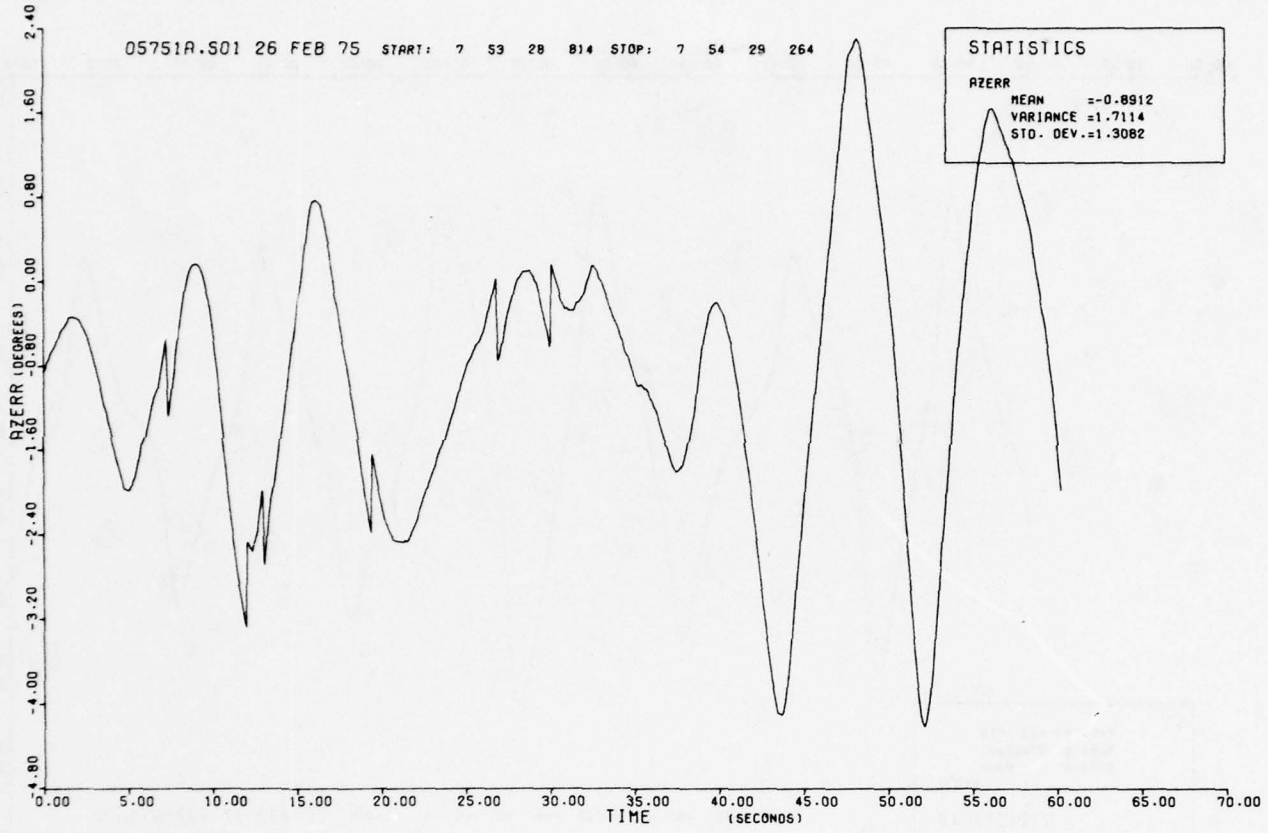

FIGURE 5-29. SEVERE ROLL DATA (26 FEBRUARY 75), AZIMUTH ERROR

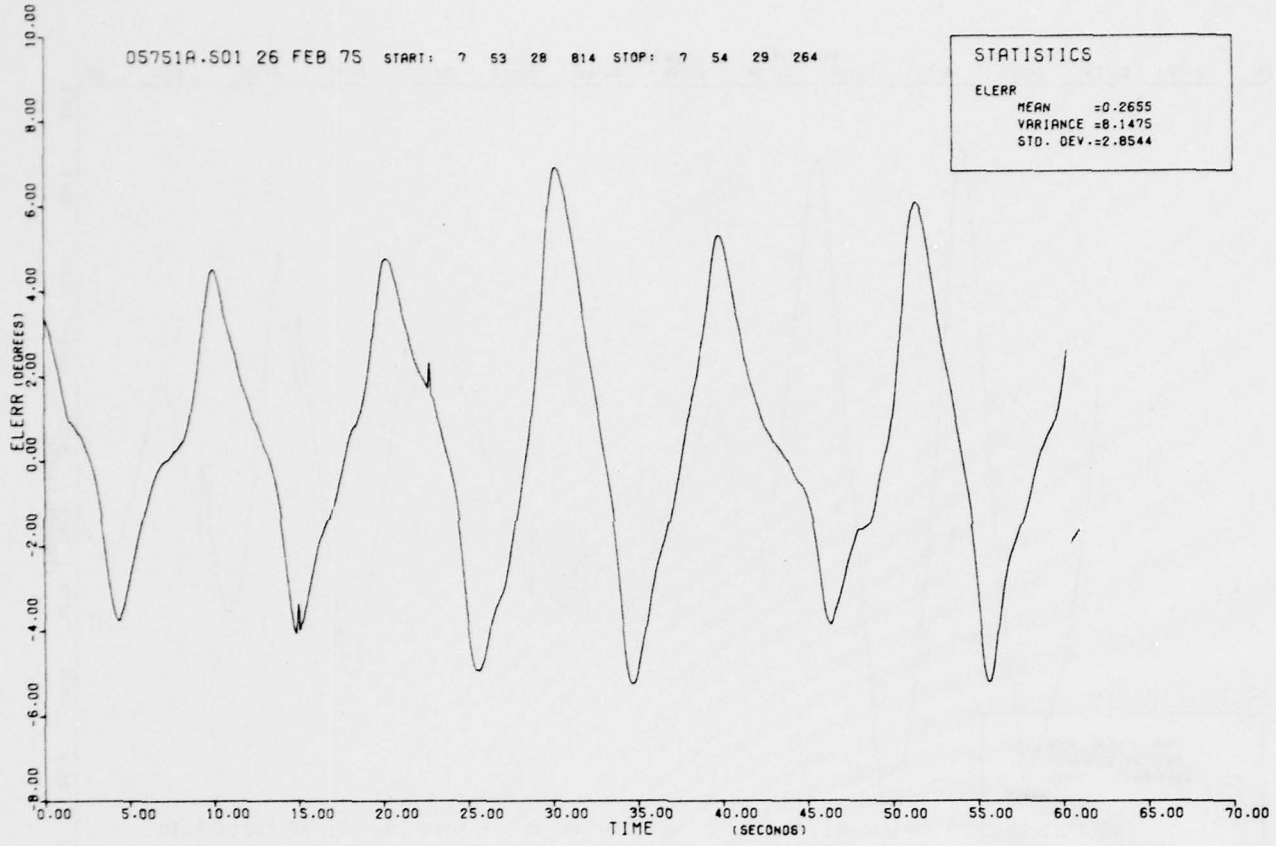

FIGURE 5-30. SEVERE ROLL DATA (26 FEBRUARY 75). ELEVATION ERROR

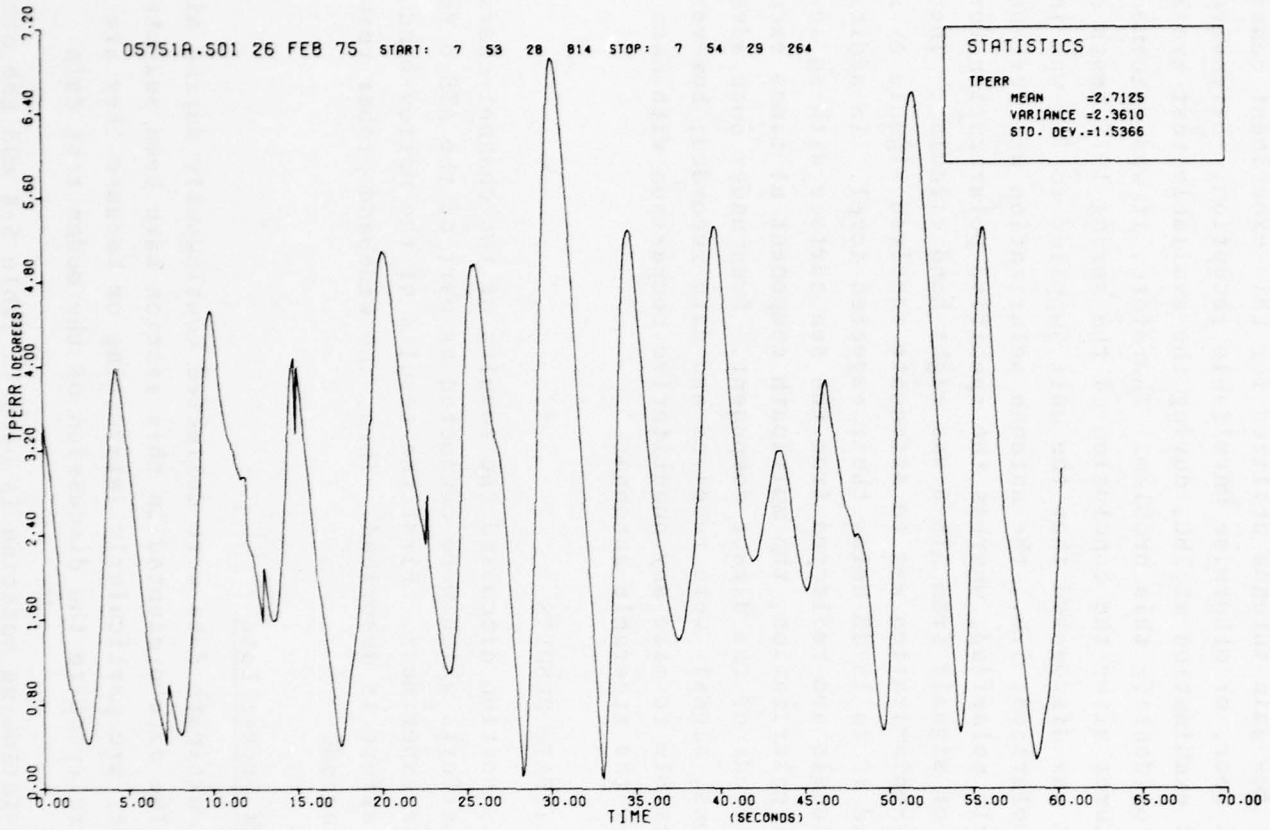

FIGURE 5-31. SEVERE ROLL DATA (26 FEBRUARY 75), TOTAL POINTING ERROR

5.2.4 Low-Gain Antenna

The low-gain antenna utilized for this experiment consistently provided poor, or otherwise unreliable reception. Extensive analysis and examination at TSC, during the available test breaks, failed to identify this problem. Therefore, it was returned to the manufacturer after the conclusion of the spring 1975 tests series. There it was discovered that the unit supplied to TSC was incorrectly polarized; i.e., the antenna polarization was left-hand circularly polarized, whereas the specified polarization for reception of signals from ATS-6 was right-hand circular. The effect of cross-polarization was to attenuate received signals by an estimated 10 to 15 dB below their expected level. In addition, since signals are reflected from the sea surface with an inverted sense of polarization, the multipath component at times exceeded the amplitude of the direct component. Even under such adverse conditions, signals were received and data recorded; however, it is impossible to make any quantitative comparison with data received by the steerable antenna.

5.3 MULTIPATH RESULTS

This section discussed the results of two channel characterization efforts which were conducted as part of the ATS-6 Maritime Satellite experiment. First the results of the narrow-band (CW) probing effort is described. Then, the wideband prober results are discussed.

5.3.1 CW Prober Data

CW multipath data were collected continuously during all modem tests. The data presented in this section have been selected because they are particularly interesting or because they are particularly relevant to the discussion of the modem test data.

The following notation is used in Table 5-8 and the other CW multipath tables. The antenna and/or mode is either slaved (denoted by S), autotrack) (denoted by A), or low-gain antenna (denoted by 0). In the slave mode, the antenna was not necessarily

pointed directly at the satellite. Thus, S35 indicates that the antenna is in the slaved mode and at an elevation angle of 35°. The ship heading for these tests was usually either perpendicular to the boresight to the satellite-denoted by P, or the ship steamed in a circle-denoted by C. The modems under test at the time of the CW multipath measurement are indicated under "test conditions." V + D = voice + data, D = data only, R = ranging, and PN = wideband multipath probing. The number following the modem designation is the carrier-to-noise ratio setting during the multipath measurement.

TABLE 5-8. CW MULTIPATH DATA FOR SEPTEMBER 24, 1974
(5 FT SEAS - 35° SATELLITE ELEVATION)

Antenna Mode	Heading	Test Conditions	C/M_m	C/M_h	Fade Depth 2%	Bandwidth
S35	P	V + D 43	20.4	>16 dB	-1.7	6.3 Hz
A	P	D 38	18.5	>16 dB	-1.8	5.5 Hz
A	P	D42	17.4	>16 dB	-1.9	6.3 Hz

The tables show two estimates of the signal-to-multipath ratio. The first, C/M_m, is derived by the method of moments described in Section 4. The second, C/M_h, is derived emperically based on the slope of the multipath fading histogram for the interval under consideration. A typical histogram is shown in Figure 5-32. The tables also show the fade depth which is exceeded less than 2 percent of the time. Finally, the bandwidth of the received CS multipath probing is given. This value is derived by inspection of the spectrum of the received tone. A typical power spectrum is shown in Figure 5-33.

It is reasonable to expect very little multipath when the elevation angle to the satellite is high. For example, consider

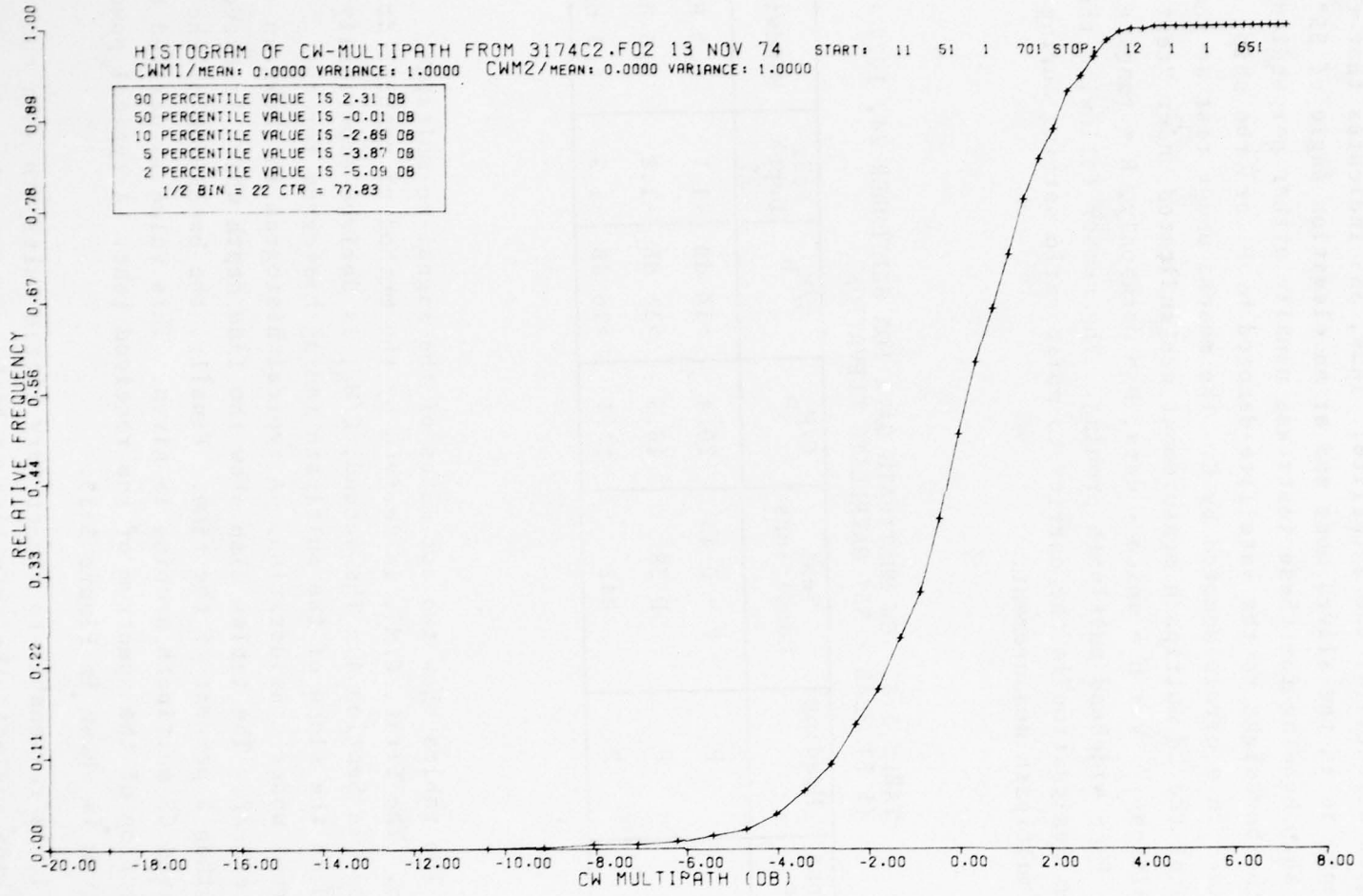

FIGURE 5-32. HISTOGRAM OF MULTIPATH DATA

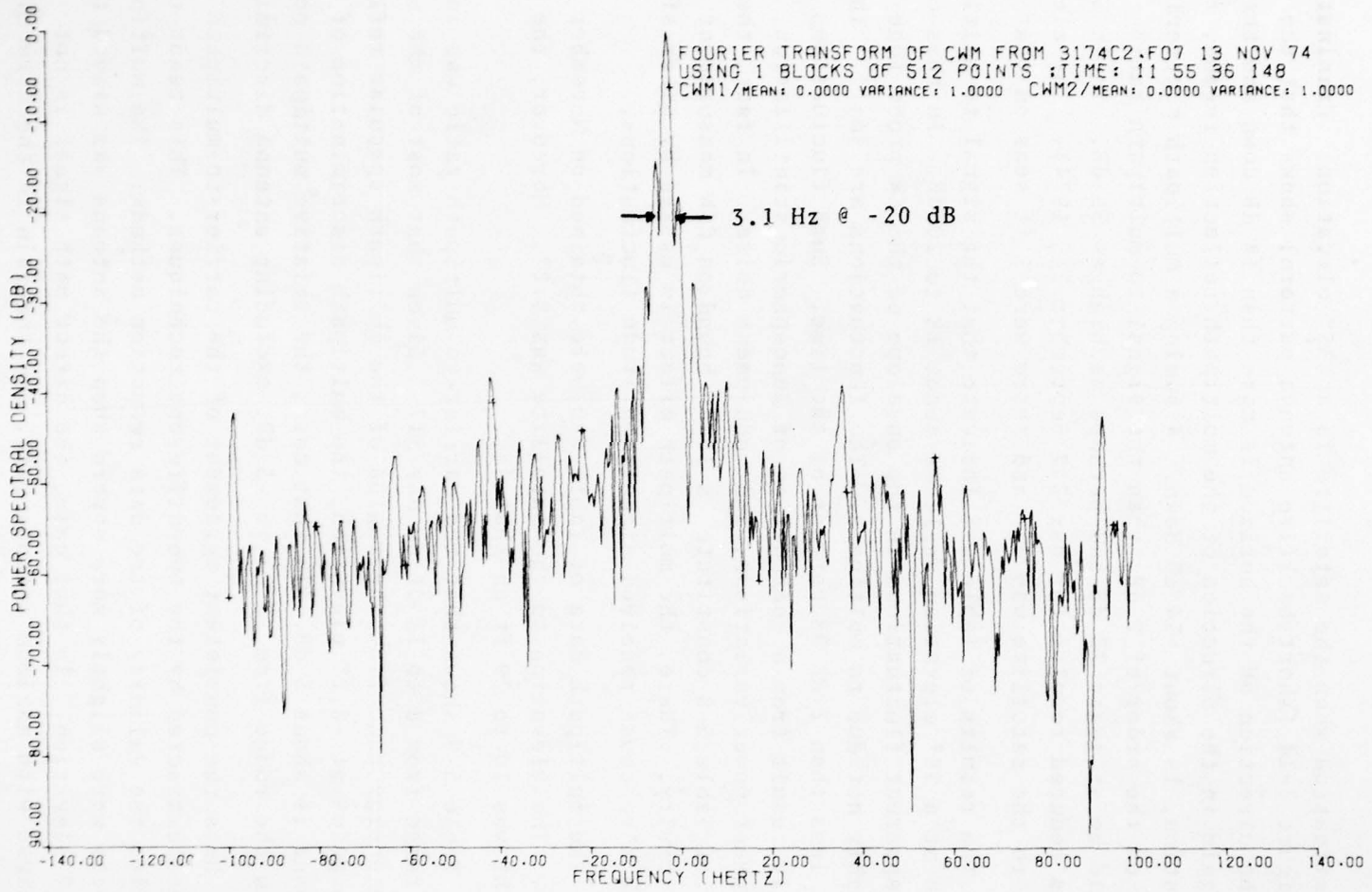

FIGURE 5-33. A TYPICAL POWER SPECTRUM OF CW MULTIPATH DATA